Sara Sofia Gonçalves Sousa Félix

Licenciada em Bioquímica

Formation of membraneless organelles by liquid-liquid phase separation of intrinsically disordered proteins

Dissertação para obtenção do Grau de Mestre em Bioquímica

Orientador: Prof. Doutor Eurico José da Silva Cabrita, Professor Associado com Agregação, Faculdade de Ciências e Tecnologia, Universidade Nova de Lisboa

Júri:

Presidente: Prof. Doutor Pedro António Brito Tavares
Arguente: Prof. Doutor Douglas Vinson Laurents

FACULDADE DE CIÊNCIAS E TECNOLOGIA
UNIVERSIDADE NOVA DE LISBOA

Setembro 2018

Sara Sofia Gonçalves Sousa Félix

Licenciada em Bioquímica

Formation of membraneless organelles by liquid-liquid phase separation of intrinsically disordered proteins

Dissertação para obtenção do Grau de Mestre em Bioquímica

Orientador: Prof. Doutor Eurico José da Silva Cabrita, Professor Associado com Agregação, Faculdade de Ciências e Tecnologia, Universidade Nova de Lisboa

Júri:

Presidente: Prof. Doutor Pedro António Brito Tavares
Arguente: Prof. Doutor Douglas Vinson Laurents

FACULDADE DE CIÊNCIAS E TECNOLOGIA
UNIVERSIDADE NOVA DE LISBOA

Setembro 2018

Formation of membraneless organelles by liquid-liquid phase separation of intrinsically disordered proteins

Agradecimentos

O trabalho desenvolvido ao longo desta tese não teria sido possível sem a ajuda direta e indireta de várias pessoas, as quais quero deixar o meu enorme agradecimento.

Em primeiro lugar, gostaria de agradecer ao meu orientador, Professor Doutor Eurico Cabrita, por toda a confiança que depositou em mim e por acreditar que iria conseguir desenvolver este projeto desafiante. Quero agradecer pelo enorme apoio ao longo deste trabalho, pela constante disponibilidade e paciência, e por exigir sempre o melhor de mim. Gostaria também de agradecer por todo o conhecimento transmitido e por me ter proporcionado várias oportunidades de aprendizagem e crescimento profissional ao longo deste ano. A sua dedicação e vasto conhecimento científico foram uma enorme fonte de motivação.

Um agradecimento especial aos meus colegas de laboratório, Ana Diniz, Carmen Montoya, Helena Coelho, Micael Silva e Wagner Silva, por toda a ajuda e companheirismo, e pela extraordinária boa disposição diariamente. Obrigada por me terem aturado ao longo desse ano!

Gostaria de agradecer à Dra. Ana Sofia, Dra. Filipa Marcelo, Dr. Jorge Dias e Dr. Aldino Viegas, pelos indispensáveis esclarecimentos e por estarem sempre disponíveis a ajudar. Um obrigado especial ao Dr. Aldino Viegas pela ajuda essencial na parte do RMN. Obrigada ao Dr. Jorge Dias pelos esclarecimentos na parte da biologia molecular e por me fazer sempre rir quando estava "agarrada" ao AKTA!

Quero agradecer ao Professor Doutor Nicolas Fawzi, pela ajuda indispensável na parte de expressão e purificação da proteína, que se revelou bastante desafiante.

Um agradecimento ao Professor Doutor Mário Diniz pela incansável disponibilidade e auxílio na realização dos ensaios com microplacas.

Gostaria também de agradecer ao Professor Doutor Jaime Mota e à Doutora Irina Franco, pela disponibilidade e por toda a ajuda crucial na realização dos ensaios de microscopia.

Muito obrigada ao Professor Doutor Pedro Viana Baptista por me ter disponibilizado o RNA, que foi fundamental no desenvolvimento deste trabalho.

A toda a minha família, amigos e colegas que me acompanharam e apoiaram nesta jornada, um grande obrigado. Aos meus pais, que são uma fonte inesgotável de inspiração e motivação. Obrigada por todos os esforços e sacrifícios que fazem por mim, por acreditarem sempre no meu melhor, e por acreditarem que um dia vou ganhar um Prémio Nobel!

Ao meu pai, que me conhece melhor do que eu me conheço a mim própria, que sem ele nem sequer estava onde estou, muito obrigada. Obrigada pelo carinho, apoio inabalável e por todos os ensinamentos. Obrigada por lutares sempre por mim. Foste e és a minha maior motivação.

À minha mãe, por ter imenso orgulho em mim, e por estar sempre interessada em falar sobre organelos! Obrigada por todo o carinho e amor que me dás, e por, apesar de seres mãe galinha, saberes sempre o que é melhor para mim. A tua dedicação a tudo o que te é importante é uma enorme inspiração.

Ao meu irmão Gui, por ser o melhor irmão que podia pedir. Obrigada por me teres feito sempre rir mesmo quando estava em baixo, por todas as noitadas a jogar

playstation depois de um dia longo de trabalho, e por todas as viagens de carro a dançar com a música aos altos berros. O facto de adorares ciência por causa de mim e do meu trabalho, deixa-me extremamente orgulhosa. Fico à espera de um dia ler a tua tese de mestrado! Ao Lobo, por ser uma fonte constante de conforto, diversão e alegria.

Obrigada também aos meus avós, por serem as pessoas maravilhosas que são e por serem um exemplo para mim. Obrigada pela compreensão ao longo deste ano, por me desculparem por todas as vezes que faltei a almoços devido ao trabalho!

Ao Tomás, que me apoiou incansavelmente ao longo destes anos e que motivou mesmo nas piores alturas. Pelo amor e amizade inesgotáveis. Pelas discussões intelectuais, pelas aventuras e pelas constantes gargalhadas. Sem ti, teria sido impossível. Obrigada por tudo.

Resumo

A compartimentalização sub-celular permite a organização de reações bioquímicas complexas no espaço e no tempo, subjacentes a processos vitais como homeostasia, divisão e desenvolvimento. No entanto, vários compartimentos não contêm uma barreira física. Estes organelos não membranares são normalmente constituídos por mRNA imobilizado e por proteínas que são sujeitas a separação de fase líquido-líquido (LLPS), sendo denominados de grânulos de ribonucleoproteína (RNP). Estes líquidos proteicos estão geralmente envolvidos na regulação da expressão genética e no processamento de ácidos nucleícos.

Proteínas que guiam o processo de LLPS contêm normalmente uma composição não estruturada, sendo referidas como proteínas intrinsecamente desordenadas (IDPs). *Fused in sarcoma* (FUS) é uma IDP ubiquamente expressa, composta por vários domínios desordenados, como o domínio de baixa complexidade (LC), três domínios arginina-glicina-glicina (RGG) e um sinal de localização nuclear de prolina-tirosina (PY-NLS). FUS contém ainda dois domínios globulares envolvidos em funções relacionadas com RNA, o domínio de reconhecimento de RNA (RRM) e o domínio *zinc finger* (ZnF). Em certas condições de stress, a FUS sofre LLPS no citoplasma levando à formação de grânulos de stress. A formação destes grânulos de RNP aumenta o risco de formação de fibrilas proteícas detetadas em doenças neurodegenerativas.

Embora se saiba que o ambiente celular desempenha um papel crucial na mediação da formação de grânulos de RNP, os mecanismos e determinantes moleculares que levam a LLPS ainda não são claros. Neste contexto, o objetivo principal deste trabalho é elucidar a influência do ambiente na formação de grânulos de FUS e compreender os mecanismos por detrás do processo de LLPS. Para tal, explorou-se a influência da temperatura, pH e metabolitos celulares abundantes, no processo de LLPS.

Usando ensaios de turbidez em microplacas, foi possível avaliar o grau de LLPS da FUS sob diferentes condições. A FUS apresentou uma temperatura de solução crítica superior (UCST), submetendo-se a separação reversível de fases a baixa temperatura. Observou-se que a separação de fases é significativamente intensificada quando a FUS apresenta uma carga global neutra (pH 9.40), e na presença de concentrações ótimas de metabolitos carregados, indicando que o processo de LLPS é mediado por interações eletrostáticas. Além disso, os metabolitos que induzem compactação de proteínas e que destabilizam interações hidrofóbicas, inibiram a LLPS da FUS, sugerindo que o processo possui também um caráter hidrofóbico e que a desordem estrutural da FUS é crucial para a formação de grânulos. Através de espetroscopia de RMN, verificou-se que os domínios globulares sofrem desnaturação reversível a frio, a uma temperatura em que o processo de LLPS é promovido. Juntamente com os ensaios de separação de fase, que demonstraram que o RNA e o Zn^{2+} promovem a LLPS, propõe-se que tanto o domínio RRM e o ZnF estão envolvidos no processo de separação de fases, mediando interações intermolecular eletrostáticas ao sofrerem desnaturação. Notavelmente, foi também demonstrado que a FUS mantém a sua estrutura geral após a separação de fases. Através de ensaios de microscopia, foi possível observar os grânulos de FUS e identificar características de líquidos, como capacidade de molhar e fusão. No geral, foi demonstrado que o processo de LLPS é extremamente sensível e controlado pelas condições circundantes.

Palavras-chave: FUS; separação de fase líquido-líquido; organelos não membranares; proteínas intrinsecamente desordenadas, interações intermoleculares

Abstract

Subcellular compartmentalization allows the organization of complex biochemical reactions in space and time, underlying vital cell processes such as homeostasis, division and development. Several compartments, however, lack a physical barrier. These membraneless organelles are usually an assembly of stalled mRNA and proteins that undergo liquid-liquid phase separation (LLPS), being termed as ribonucleoprotein (RNP) granules. These proteinaceous liquids are usually involved in regulation of gene expression and nucleic acid processing.

Proteins that drive LLPS process normally exhibit an overall unstructured composition, being referred as intrinsically disordered proteins (IDPs). Fused in sarcoma (FUS) is a ubiquitously expressed IDP, composed of several disordered domains such as the low complexity (LC) domain, three arginine-glycine-glycine (RGG) boxes and a proline-tyrosine nuclear localization signal (PY-NLS). In addition, FUS contains two globular domains involved in RNA-related functions, the RNA recognition motif (RRM) and the zinc finger (ZnF) domain. In certain stress conditions, FUS can undergo LLPS in the cytoplasm leading to formation of stress granules. Formation of these RNP granules increases the risk of self-templating protein fibrils that underpin fatal neurodegenerative diseases.

Although the cell environment is known to play a crucial role in mediating RNP granule formation, the mechanisms and molecular determinants that drive LLPS are still unclear. In this context, the main objective of this work is to elucidate the influence of the environment on the formation of FUS granules and to comprehend the mechanisms behind LLPS process. For that purpose, it was explored the influence of the temperature, pH and abundant cellular metabolites, on the LLPS process.

Using turbidity microplate assays it was possible to assess the degree of FUS LLPS under different conditions. FUS presented an upper critical temperature solution (UCST) phase separation, undergoing reversible phase separation at low temperature. It was observed that phase separation is significantly enhanced when FUS presents an overall neutral charge (pH 9.40) and in the presence of optimal concentration of charged metabolites, indicating that LLPS is mediated through electrostatic interactions. Moreover, stabilizing metabolites that induce protein compaction and the destabilization of hydrophobic interactions inhibited FUS LLPS process, suggesting that this process has also a hydrophobic character and that FUS structural disorder is crucial for FUS granule formation. Through NMR spectroscopy it was found that FUS globular domains undergo reversible cold denaturation at a temperature in which LLPS is enhanced. Together with the phase separation assays that demonstrated that RNA and Zn^{2+} enhance LLPS, it is proposed that both RRM and ZnF domain are involved in the phase separation process, undergoing electrostatic intermolecular interactions upon unfolding at low temperature. Remarkably, it was also showed that FUS maintains its overall structure upon phase separation. Using microscopic imaging, it was possible to observe FUS granules and to identify liquid-like characteristic such as wetting and fusion. Overall it was demonstrated that FUS LLPS process is extremely sensitive and controlled by the environmental conditions.

Keywords: FUS; Liquid-liquid phase separation; membraneless organelles; intrinsically disordered proteins, intermolecular interactions

Table of contents

List of figures

List of tables

List of abbreviation and symbols

^{1}H	Hydrogen proton
^{13}C	Carbon-13 isotope
^{15}N	Nitrogen-15 isotope
A_{280nm}	Absorbance at 280 nm
AD	Alzheimer's disease
ALS	Amyotrophic lateral sclerosis
Atm	Standard atmosphere unit
βME	β-mercaptoethanol
CAPS	N-cyclohexyl-3-aminopropanesulfonic acid
CTD	C-terminal domain
DLVO	Derjaguin-Landau-Verwey-Overbeek
DNA	Deoxyribonucleic acid
DSS	4,4-dimethyl-4-silapentane-1-sulfonic acid
E. coli	*Escherichia coli*
EDTA	Ethylenediaminetetraacetic acid
FET	FUS/EWS/TLS
FL	Full-length
FTLD	Frontotemporal lobal degeneration
FUS	Fused in sarcoma
G	Gibbs free energy
His_6	Polyhistidine tag
HSQC	Heteronuclear multiple quantum coherence
IDP	Intrinsically disordered protein
IEX	Ion exchange chromatography
IMAC	Immobilized metal affinity chromatography
Kapβ	Karyopherin β protein
kDa	Kilodalton
LB	Luria-Bertani
LC	Low complexity
LCST	Lower critical solution temperature
LLPS	Liquid-liquid phase separation
LysHCl	Lysine hydrochloride
mRNA	Messenger ribonucleic acid
MBP	Maltose binding protein
MW	Molecular weight
MWCO	Molecular weight cut-off
NaGlu	Sodium glutamate
NES	Nuclear export signal
Ni-NTA	Nickel-nitrilotriacetic acid
NLS	Nuclear localization signal

NMR	Nuclear Magnetic Resonance
OD_{595nm}	Optical density at 595 nm
OD_{600nm}	Optical density at 600 nm
PDB	Protein Data Bank
pI	Isoelectric point
pK_a	Logarithmic acid dissociation constant
Ppm	Parts per million
RGG	Arginine-glycine-glycine
RNA	Ribonucleic acid
RNP	Ribonucleoprotein
RRM	RNA recognition motif
SDS	Sodium dodecyl sulfate
SDS-PAGE	Sodium dodecyl sulfate polyacrylamide gel electrophoresis
TEV	Tobacco etch virus protease
Tris	Tris(hydroxymethyl)aminomethane
UCST	Upper critical solution temperature
UV-Vis	Ultraviolet-visible
WT	Wild-type
ZnF	Zinc finger
μ	Chemical potential

Amino acids abbreviations		
Alanine	Ala	A
Arginine	Arg	R
Asparagine	Asn	N
Aspartate	Asp	D
Cysteine	Cys	C
Glutamate	Glu	E
Glutamine	Gln	Q
Glycine	Gly	G
Histidine	His	H
Isoleucine	Ile	I
Leucine	Leu	L
Lysine	Lys	K
Methionine	Met	M
Phenylalanine	Phe	F
Proline	Pro	P
Serine	Ser	S
Threonine	Thr	T
Tryptophan	Trp	W
Tyrosine	Tyr	Y
Valine	Val	V

1. INTRODUCTION

“Life, this anti-entropy, ceaselessly energy, is a climbing force, toward order amidst chaos…”

A. Claude

1. Introduction

Inside the human body, millions of chemical reactions occur per second in each cell. In order to organize these reactions, eukaryotic cells contain a series of membrane-limited organelles which provide an independent and distinct chemical environment.[1] This compartmentalization allows the organization of complex biochemical reactions in space and time.[2,3] Subcellular organization of macromolecules is essential for vital cellular processes such as homeostasis, division and development.[4-6]

In the cell, a compartment must have a boundary that permits separation from the cytosolic environment. Moreover, the components must be able to diffuse freely across it, so that chemical reactions can take place.[2,7] Many organelles are delimited by a lipid bilayer membrane including the mitochondria, the lysosome and the nucleus.[8] Such membranes allow passive and active transport of large and small molecules.[9]

Surprisingly, several cellular compartments lack a physical barrier. These non-membrane-limited organelles, can compartmentalize and concentrate specific set of molecules without the presence of a physical boundary.[10]

Membraneless organelles behave as fluid droplets, having liquid-like properties, such as shear flow deformation, fusion, high viscosity and rapid exchange of components with the cytoplasm (**Figure 1**).[11,12] The first example of a liquid compartment was the P granules from *Caenorhabditis elegans* embryos.[13] P granules are assembly of RNA and RNA-binding proteins that play a role in germ-cell specification.[11] P granules can target mRNA for decapping and degradation under regular and stress conditions.[14]

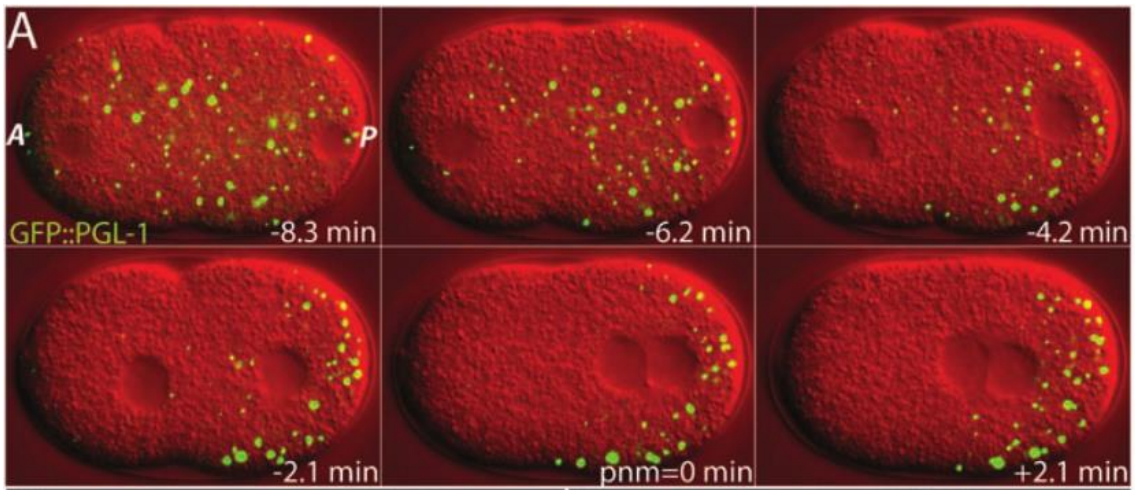

Figure 1 – Liquid-like properties of P granules – P granules (in green; GFP tagged) exhibit liquid-like properties such as diffusion and fusion overtime in *C. elegans* embryos. Time relative to pronuclear meeting (pnm). A – anterior, P- posterior. Modified from Brangwynne *et al*.[11]

A wide variety of membraneless organelles have been described ever since. These structures are typically comprised of RNA and proteins, being termed as ribonucleoprotein (RNP) bodies or granules. These include nuclear structures such as Cajal bodies (CBs)[15], cleavage bodies[16], nucleoli[17], paraspeckles[18], nuclear speckles[19],

chromatin[20], histone locus bodies (HBLs)[21], nuclear stress bodies (nSBs)[22], Oct1/PTF/transcription (OPT) domains[23], polycomb bodies (PcG bodies)[24], perinucleolar compartment (PNC)[25], promyelocytic leukaemia nuclear bodies (PML nuclear bodies)[26] and the Sam68 nuclear bodies (SNBs)[25]. In the cytoplasm, RNP granules are less numerous and diversified. These comprise centrosomes[27], neuronal RNA bodies[28], P-bodies[29] and stress granules[30]. Moreover, in the mitochondria is observed a unique subdomain structure, the mitochondrial RNA granule.[31] Hence, a variety of RNP bodies are present in the cytoplasm, mitochondria and nucleus of eukaryotic cells. Despite their diversity in structure, morphology, function and distribution, all of these membraneless subcellular structures are ubiquitous in cells, and contribute to numerous vital biological functions, including processing and storage of RNA and other biomolecules.[4,32]

1.1 Stress granules

Stress granules are RNP cytosolic bodies that assemble from pools of untranslated mRNA and RNPs.[30,33] In the cytoplasm, stress granules regulate RNA stability and protein translation in response to stress stimuli.[34]

Arising from mRNA stalled in translation initiation, stress granules contain several translation initiation factors, RNA-binding proteins (comprising ~ 50%) and non-RNA-binding proteins.[35] Non-RNA-binding proteins are vital for RNA processes, including post-translation modification enzymes, metabolic enzymes, and protein or RNA remodeling complexes.[35-37]

1.1.1 Morphology and function of stress granules

Stress granules are not uniform structures, normally containing two distinct layers: a core protein-rich structure and a dynamic shell.[33,37] The shell is thought to be a scaffold for dynamic exchange with the outside, while the core maintains the stress granule structure and provides further confinement for biomolecule sequestration (**Figure 2**).[38]

Stress granule formation is a dynamic and reversible process. Assembly of stress granules begins with the formation of the core followed by the shell. The reverse process is also a stepwise process that begins with the less-stable shell dissipation followed by core clearance.[38]

Multiphase coexistence is well described outside living systems and can be demonstrated with simple mixtures of organic solvents. A stress granule with lower surface tensions tends to envelop one of higher surface tension.[39]

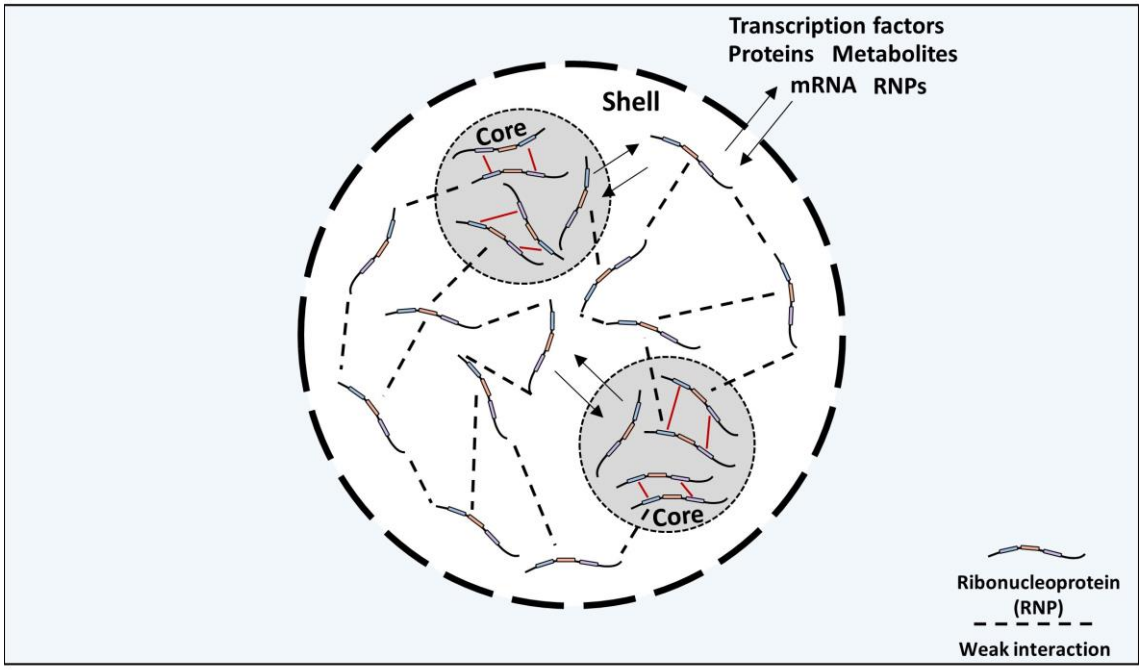

Figure 2 – Representative illustration of a stress granule composition – Stress granules exhibit a biphasic composition, structured by a protein-rich core surrounded by a dynamic shell.[38]

Stress granule assembly is known to be highly redundant since several and distinct post-translational modifications such as protein methylation, phosphorylation and glycosylation, influence differently the stress granule assembly.[40-42] In fact, several stress-granule-promoting proteins contain specific motifs for such modifications, such as RGG motifs, which are sites for arginine methylation.[43]

Stress granules have a broad effect on the physiology of the cells, not accounting for mRNA processing. Due to the high local concentration of components, stress granules can recruit numerous proteins in certain stress responses. For example, during viral infections, stress granules recruit several antiviral proteins such as RIG-1 and PKR, enhancing the immune response and viral resistance.[44] Moreover, stress granules can sequester numerous components, inhibiting several signaling pathways such as the apoptosis stress-responsive MAPKS pathway, or the TNR-α-mediated NG-$_K$B proinflammatory signaling pathway, as a protective mechanism against the apoptotic or inflammatory response under stress conditions.[45,46] In fact, having this into account, there were developed chemotherapeutic agents that promote controlled stress granule formation.[47,48]

1.1.2 Stress granules in disease

Mutations that lead to functional impairment of stress granules have been implicated with many neurodegenerative diseases such as amyotrophic lateral sclerosis (ALS), frontotemporal lobar degeneration (FTLD) and inclusion body myopathy (IBM).[49] In most cases, the mutations are directly on the RNA-binding proteins (e.g. FUS, TDP-43, TIA1), increasing the stress granules self-assembly.[49-51] Ultimately, this leads to the accumulation of stable and irreversible amyloid-like structures, which can result

in misregulation of RNA processing and signaling pathways, or defects in nuclear-cytoplasmic transport of RNPs.[52,53]

Stress granules present an evident mechanism of assembly through regulated protein aggregation. However this process can soon evolve into pathological protein aggregates.[54]

The classical model for pathological protein aggregation, proposed by Dobson and Lansbury, describes the conversion mechanism of soluble protein into insoluble protein deposits.[55,56] In this model, monomers of aggregation prone proteins can undergo random misfolding, under certain conditions.[10,11] The misfolded species oligomerize and aggregate to form fibrils, through nucleated growth mechanism, leading to non-functional deposits.[11]

The rate of aggregation is dictated by mass action and energy minimization.[54] Stress granules are comprised of proteins containing high number of charged and aromatic residues. These residues increase the propensity of oligomerization through electrostatic and aromatic interactions. Paired with increased cytoplasmatic concentration of these proteins, favored through mutation or persistent stress, the assembly of pathological aggregates is promoted.[54,57]

Hence, although stress granule formation is crucial for cell survival, their assembly pathway through regulated protein aggregation is vulnerable to disruption, which can lead to severe neurotoxicity.

1.2 Formation of membraneless organelles

As stated earlier a compartment must have a boundary and the components must diffuse freely across it. For that purpose, and in order to understand the compartmentalization through membraneless organelles, we need to understand the mechanisms behind their assembly and how molecules can diffuse in and out. Moreover, it is necessary to comprehend how such compartments can stay stable under aqueous cytosol and what are the properties that drive their assembly.

1.2.1 Liquid-liquid phase separation

The liquid nature of nuclear and cytosolic membraneless organelles seems counterintuitive. Thermodynamically, two miscible liquids mix in order to evolve towards the state of higher entropy, according to the second law of thermodynamics.[58] However, stress granules can coexist in the cytosol without fusing with the surroundings.[3]

Interestingly, liquids can undergo demixing process. In these cases, the phase separation is driven by interactions between the molecules that constitute each liquid. Thermodynamically, the system progresses towards lower energy if molecules of the same species interact. Here, the gain in energy reduction overcomes entropy increase tendency, driving the system towards demixing.[2]

The current accepted process that drives the cytosolic demixing and the consequent formation of stress granules is liquid-liquid phase separation (LLPS).[10,59,60] The LLPS process occurs when a mixture of molecules form a network of multivalent weak interactions, allowing components to become locally concentrated.[33]

LLPS is a process mediated both by thermodynamics and kinetics.[61,62] The composition of the two phases at equilibrium is dependent on temperature. For this purpose, the LLPS mechanism is normally explained by temperature-composition diagram. This phase diagram is characterized by a coexistence curve, in which the boundaries show the composition of the phases that are in equilibrium in various temperatures (at a constant pressure, normally 1 atm). The coexistence curve has a critical point defined by a critical temperature (T_c) and a critical concentration (C_c), temperature and concentration in which phase separation occurs.[60,61]

Proteins can exhibit two distinct types of phase separation behavior: **upper critical solution temperature (UCST)** type of behavior, or a **lower critical solution temperature (LCST)** type of behavior. The UCST is the highest temperature at which phase separation occurs. Above this temperature the system is homogenous, and hence, phase separation occurs at temperatures lower that the UCST. At LCST regime, which is less common, phase separation occurs when temperature is higher than LCST, and protein solubility is higher at lower temperatures.[60,61]

Phase diagrams often represent also the spinodal curve. This curve separates the metastable from the unstable region. Inside the unstable region occurs spontaneous phase separation (i.e. the mixture is unstable and the phase separation occurs spontaneously), whereas in the metastable region demixing only occurs if seeds are present. Depending on the type of phase separation behavior, the LCST or UCST point is where the coexistence and spinodal curves intersect (**Figure 3**).[63]

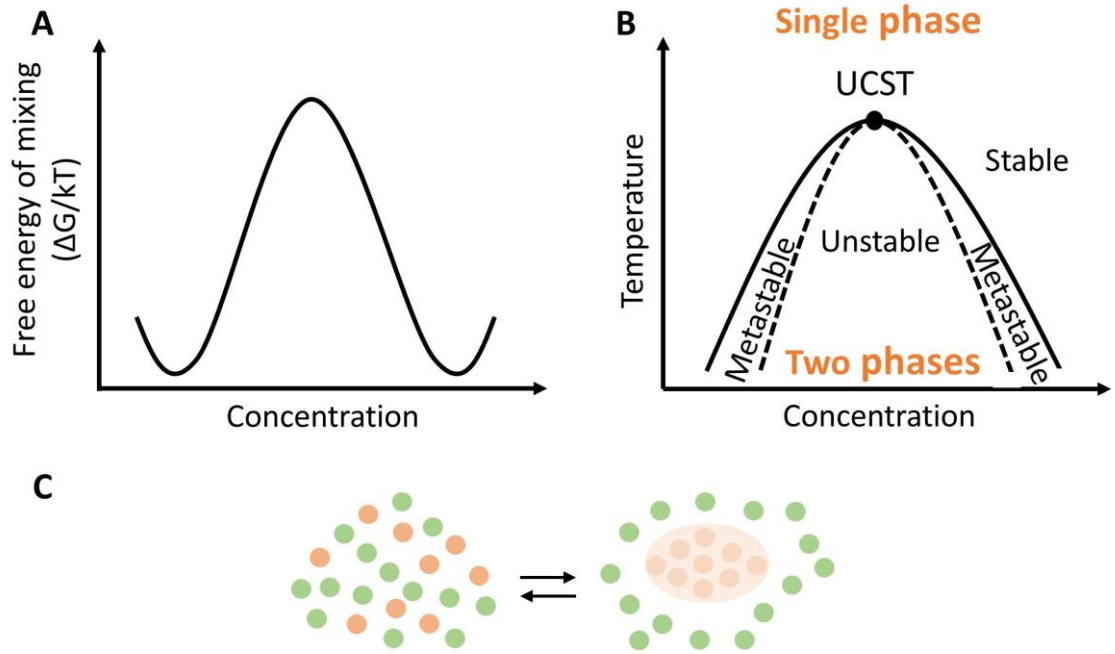

Figure 3 – Thermodynamics of liquid-liquid phase separation – Example of a UCST type of phase separation behavior **(A)** LLPS is a thermodynamic process in which a binary mixture can lower its free energy of mixing by decomposing in two distinct phases; **(B)** LLPS process is dictated through temperature and concentration. Temperature-composition diagram of a binary mixture contains a boundary that separates the single from the double phase (coexistence curve – black curve), and a curve that separates the metastable from the unstable region (spinodal curve – dashed curve). **(C)** In a binary mixture, when the equilibrium is reached (G=0) phase separation occurs and components demix from the surroundings.[10,61]

At T_c the two phases are in equilibrium and the Gibbs free energy of the system is minimized. Considering a simple mixture, the molar Gibbs energy (G_m) is equal to the chemical potential (μ). In brief, μ is the measure of the potential that a substance has for undergoing change in a system, in this case, phase separation. LLPS is achieved when the system is at equilibrium, i.e. the chemical potential of the substance is the same throughout the sample, regardless of how many phases are presented. Hence, even when protein concentration is differently distributed, with a protein-rich phase and a protein-power phase, μ at those different locations is equal.[61] As stated earlier, in a cellular compartment, components must diffuse freely through it. Considering a membraneless organelle formed by a protein in a cell, the chemical potential of this protein is $\mu 1$ inside the organelle, and $\mu 2$ in the cytoplasm. In order to keep the stability of this membraneless organelle, $\mu 1$ must be equal to $\mu 2$. Yet, since the protein can diffuse in and out the organelle, Gibbs energy of the system changes, and thus $\mu 1$ and $\mu 2$ should be different.[2,61]

For example, when an infinitesimal amount dp of the protein is transferred from the organelle to the cytoplasm, the Gibbs energy of the system changes by $-\mu 1 dp$, considering the removal of the protein from the organelle. On the other hand, the Gibbs free energy of the system also change by $+\mu 2 dp$ considering the protein that is added to the cytoplasm. Hence, the overall change in Gibbs energy of the whole system is $dG=(\mu 2- \mu 1)dp$. In these cases, the phase stability (when $G=0$) is maintained since molecules move stochastically from one phase to another. Although there is diffusion of protein in and out of the phase, Gibbs energy is zero since equal number of molecules are going in and out of the phase. So, when the chemical potential in one location is raised, the components diffuse into the other location, maintaining the chemical potentials equal across the cell.[2,61]

The tendency to maintain $G=0$, and thus, maintain the phase separation, is dictated by the competition of interactions between the protein and the solvent (i.e. the cytoplasm).[64]

The polypeptide backbone of protein is an array of dipoles. Since aqueous-based solvent are also dipolar, there are three possible dipolar interactions: polypeptide-solvent, polypeptide-polypeptide and solvent-solvent. The energetic balance between the three types of interactions is quantified by the Flory-Huggins interaction parameter, χ.[65,66] The poor solubility and preference of polypeptide backbones for globules is due to the poor solvent feature of water ($\chi > 0$). Hence, when $\chi > 0$, the net attraction between protein dipoles overcomes the protein-solvent interaction. Consequently, the energetic polypeptide-polypeptide term surpasses the mixing entropy, favoring the bulk phase separation at higher concentrations.[64]

Therefore, even when there is a protein concentration gradient across the cell, and when there is diffusion in and out of the phase, the net attraction between the protein dipoles drives the system towards equilibrium, reaching phase separation.[2]

As a result, it is easy to comprehend that not all proteins benefit from interacting with other proteins instead of the solvent, and hence do not undergo LLPS.

Protein associated with membraneless organelles normally exhibit an overall unstructured composition, being referred as intrinsically disordered proteins (IDPs).[67,68]

The hydrophobic deficient and polar enriched amino acid sequence of IDPs encode an intrinsic preference for conformational disorder, which inhibits the proper folding into a well-defined three-dimensional structure.[69] A particular subset of disordered

regions, termed low complexity (LC) domains , are remarkably overrepresented in proteins that drive LLPS.[12,40,70]

In the LC domains, the sequences are often repetitive and enriched in glycine (G). The side-chain of this amino acid does not participate in hydrogen bonding when glycine is in the context of a protein and thus it cannot be regard as a polar residue. However, it cannot also be estimated as hydrophobic, since the methane side-chain is perhaps too small to have hydrophobicity contribution. Hence, since there is not an unequivocal agreement on glycine polarity across several hydropathy scales, in this study glycine will be regarded as having neutral polarity.[71-74]

LC domains also contain additional polar side-chains such as glutamine (Q), serine (S) and asparagine (N), positively charged side-chains such as arginine (R) and lysine (K), negatively charged side-chains such as aspartic acid (D) and glutamic acid (E), or aromatic side-chains such as phenylalanine (F) and tyrosine (Y).[64]

The LC domain of the IDPs has been reported to play an imperative in the mediation of RNP granules formation.[57] In fact, specific sequences play an imperative role in driving the LLPS process, such as YG/S-, Q/N-, FG-, RG-, GY-, KSPEA- and SY- rich motifs, as well as sections of alternating charges. The repetitive patterns promote multivalent inter-molecular interactions such as charge-charge, π-charge and π-π stacking.[64,67]

1.3 Fused in Sarcoma protein

Fused in sarcoma (FUS), also known as Translocated in liposarcoma (TLS), is a nuclear nucleic acid binding protein involved in regulation of gene expression, DNA/RNA processing and maintenance of genomic integrity.[75-78] In certain stress conditions, FUS undergoes liquid-liquid phase separation leading to stress granule formation in the cytoplasm.[79,80]

FUS has been implicated with several neurodegenerative diseases. Remarkably, FUS is a major component of pathological inclusion in over 5% of all types of ALS and 9% of FTLD cases.[53,81]

1.3.1 FUS structural architecture and function

Initially identified in 1993 as a fusion oncogene in human myxoid liposarcomas, FUS is a ubiquitously expressed 526 amino acid (53.42 kDa) nuclear RNP.[82,83]

This multidomain protein contains a low complexity (LC) domain that is enriched with glutamine, glycine, serine and tyrosine (QGSY) residues, a nuclear export signal (NES) inserted in a RNA recognition motif (RRM), a cysteine$_2$-cysteine$_2$ zinc finger (ZnF) domain and a proline-tyrosine nuclear localization signal (PY-NLS).[84,85] FUS has also present three arginine-glycine-glycine (RGG) boxes in its structure, known to be involved in mediation of protein-nucleic acid interaction (**Figure 4**). FUS has the ability to bind to nucleic acids such as single- and double-stranded DNA, as well as RNA.[85,86]

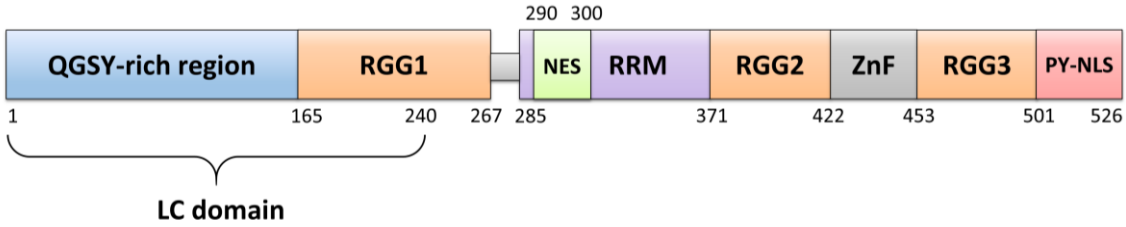

Figure 4 – **Schematic representation of human FUS structure –** Representation of the organization of FUS several domains. QGSY = glutamine, glycine, serine and tyrosine; RGG: = arginine-glycine-glycine box; NES = nuclear export signal; RRM = RNA recognition motif; ZnF = zinc finger; PY-NLS = proline-tyrosine nuclear localization signal.

FUS is a member of the FUS/Ewing's sarcoma (EWS)/TATA-binding protein-associated factor 15 (TAF15) FET family, a group of abundant and ubiquitously expressed RNPs.[77,87] FET proteins are found in multicellular organisms including vertebrates, plants, nematodes and insects, and all share an homologous domain architecture (**Figure 5**).[77]

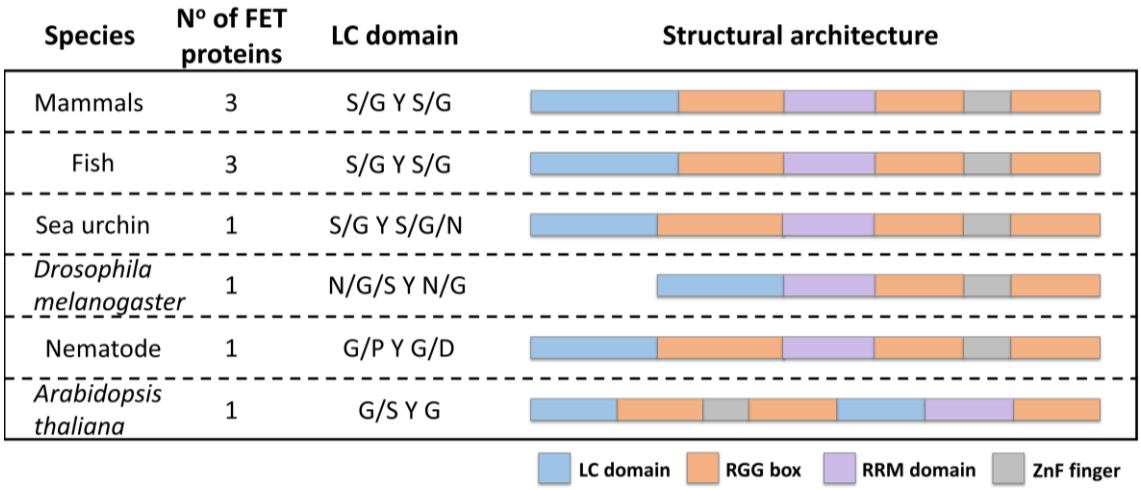

Figure 5 – Structural architecture of FET proteins across different species – The structure of FET proteins is conserved among several multicellular organisms. Domain organization, excluding *Arabidopsis thaliana*, is consistent. The number of LC domains repeats can vary, which is accountable for different lengths of this domain within species. The number and length of RGG domains can also diverge among organisms.[77]

The RRM domain of FET proteins are distinguished from other RNP RRMs due to the extended "KK-loop" between the α1 and β2 of the β1α1β2β3α2β4 fold, and also the lack of aromatic amino acids on β3 (**Figure 6**).[88,89]

Lysine residues in the KK-loop of FUS are known to be crucial for RNA/DNA binding, by providing an interacting positively-charged surface. Remarkably, substitution of these residues impairs nucleic acid binding and, interestingly, FUS subcellular localization.[17]

In FUS RRM, the conventional binding pocket formed by β1 and β3 is highly distorted. Furthermore, the absence of key aromatic residues on β3, central for

nucleic acid binding in most RRM domains, suggests binding that diverges from the canonical RNA/DNA-RRM interaction.[88,90,91]

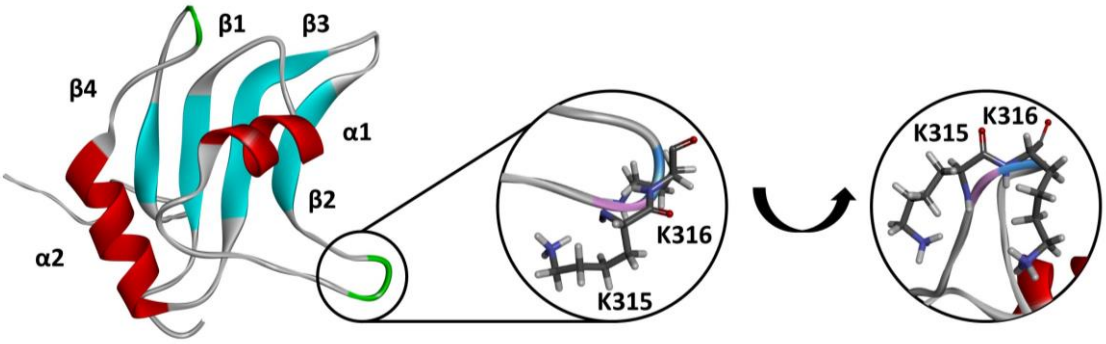

Figure 6 – RRM domain of human FUS – The RRM domain of FUS displays a β1α1β2β3α2β4 type of secondary structure, with a unique KK-loop between α1 and β2. Consecutive lysine residues in this loop (K315 and K316) are key for nucleic acid binding (PDB ID: 2LCW).[88]

The RGG motif and the ZnF domain also play a crucial role in FUS nucleic acid binding.[86,92]

RGG are a very abundant and evolutionary conserved intrinsically disordered regions (IDRs), being present in more than 1000 human proteins.[43] The RGG motifs are the second most common RNA-binding domain in the human genome, mediating interaction with distinct types of RNA, such as single- and double-stranded RNA and G-quartets.[93,94] The high flexibility of the RGG domain provides a larger interacting surface that can target a variety of RNAs.[95] RGG motif-containing proteins are often associated with a vast range of nucleic acid processing, such as regulation of apoptosis, translational repression, regulation of transcription, DNA damage signaling, and precursor mRNA splicing.[43]

The ZnF is among the most abundant domains in eukaryotic proteins.[96] This domain mediates a variety of processes such as DNA recognition and RNA packing, and regulates apoptosis, RNA transcription and protein folding.[96,97] All FET members share a C4-type ZnF characterized by four cysteine residues coordinating a zinc ion.[77,92] In FUS, the ZnF binds to GGUG-containing RNA and, interestingly, plays a more dominant role in RNA recognition that the RRM domain.[92]

A characteristic domain found in FUS, and all FET members, is the N-terminal LC domain. This unstructured region usually contains repeats of consensus motifs (**Figure 4**).[77] In FUS, the LC domain (1-239 residues) is enriched with glycine residues (28%), and contains several polar amino acids, such as serine (22.6%), glutamine (18%) and tyrosine (12.1%).[98] The FUS LC usually contains 20 repeats of (S/G)Y(S/G) motif, spread across two tandem repeats (RAC1 and RAC2) and 16 single motifs.[99]

The LC domain of FET proteins have an important role on protein self-association through LLPS.[100,101] Also, the LC can function as a transcriptional activation domain since this motif directly binds to the C-terminal domain (CTD) of RNA polymerase II, recruiting this protein into FET fibrils.[70]

Recently, Burke *et.* al demonstrated that RNA polymerase II CTD interacts not only with fibrillar forms of FUS LC but also with the phase-separated state. Moreover, RNA polymerase II nucleates the self-assembly of FUS LC.[102]

The FUS LC domain has also a role in oncogenesis. Aberrant chromosomal translocations can lead to fusion of the FUS LC domain to DNA-binding domains of transcriptional regulators such as CHOP. In this case, the LC domain also functions as a transcriptional activator, leading to abnormal tumor development, such as in human myxoid liposarcoma.[82,83,103]

Finally, the LC domains have an important role on protein self-association through LLPS. By promoting stress granule formation, these domains have large impact in the modulation of the biological and pathological function of FET proteins.[77]

The multidomain character of FUS provides an exceptional array of broad functions that mediate vital cellular processes, that go from transcriptional regulation to stress response (**Figure 7**). Therefore, it is intuitive to comprehend that missense mutations upon *FUS* gene can disrupt cellular homeostasis, triggering severe pathogenesis.[104]

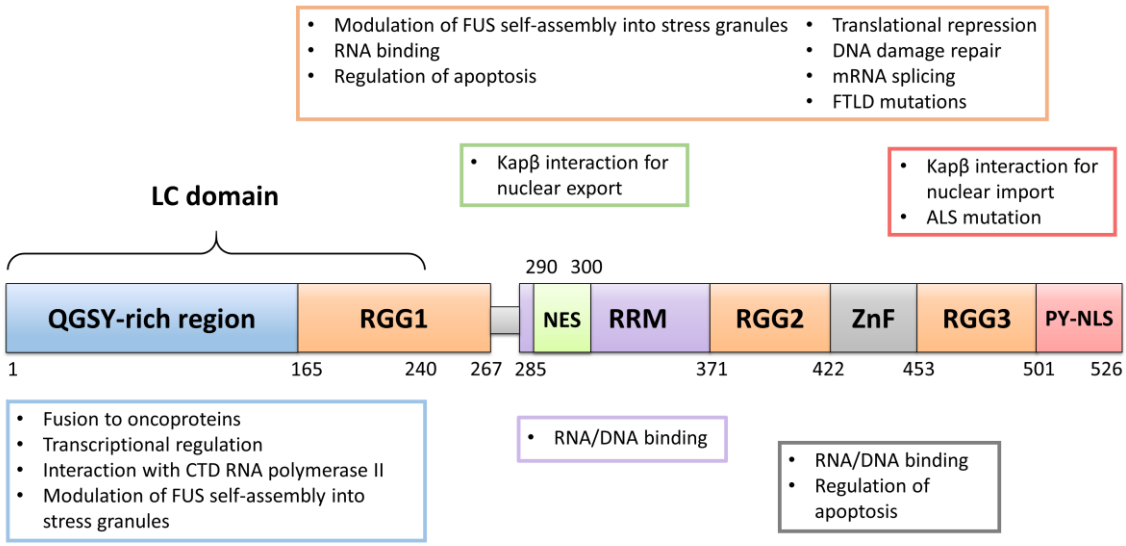

Figure 7 – Overview of FUS biological functions – FUS contains several functional domains involved in an array of cellular processes. Functions of each color-coded domain are depicted in boxes with the same representative color.

1.3.2 FUS localization and nuclear-cytoplasmatic shuttling

FUS is primarily localized in the nucleus where it regulates several nuclear functions such as transcription, pre-mRNA splicing and DNA repair.[103] Still, FUS can shuttle between the nucleus and the cytoplasm, participating in the biogenesis, transport and processing of cytoplasmatic mRNA.[103,105]

The nuclear-cytoplasmatic shuttling of FUS across the nuclear membrane is mediated by nuclear transport proteins of the Karyopherin β family. This family is responsible for most nuclear-cytoplasmatic translocation of proteins through the nuclear pore complex.[106] Karyopherin βs interaction with FUS are made upon the PY-NLS domain for nuclear import and the NES domain for nuclear export.[107] Nuclear

import of FUS is achieved through interaction of its non-classical C-terminal PY-NLS (500-526 residues) with the nuclear transporter Karyopherin β2 (Kapβ2), also known as Transportin 1 (**Figure 8**).[108,109]

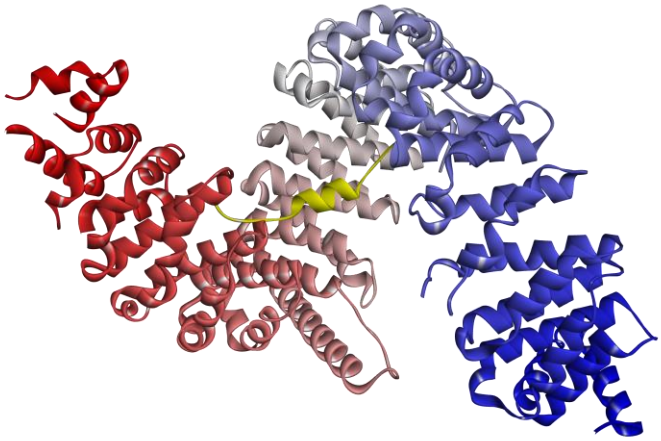

Figure 8 – Structure of Kapβ2 in a complex with FUS PY-NLS – FUS PY-NLS (yellow) occupies the C-terminal arch of Kapβ2 (red-grey-blue), interacting through the PY-NLS N-terminal PGKM hydrophobic motif, a central arginie-rich α-helix and the C-terminal PY-motif (PDB ID: 5VYG).[110]

Unlike the classical Importin α/β system which recognizes the compact and conserved NLS, Kapβ2 interacts with PY-NLS, a more complex domain that lacks a consensus sequence.[107] Therefore, PY-NLS domains are normally described as a collection of weak consensus motifs composed of a structural disordered hydrophobic or basic N-terminal and a C-terminal $RX_{2-5}PY$ motif.[111] Kapβ2 can recognize and bind diverse basic and hydrophobic N-terminal motifs, due to its acidic/hydrophobic surface.[109]

Impairment of FUS nuclear import due to mutations that affect the PY-NLS, can lead to accumulation of abnormal protein inclusions in the cytosol, which is found in ALS and FTDL patients.[112] Moreover, in 2012 Dormann D. *et al*. demonstrated that Kapβ2 can also recognize the RGG motif that precedes the PY-NLS, and that this recognition is dependent on post-transcriptional arginine methylation of the RGG motif. If the RGG motif is methylated, Kapβ2 is unable to recognize FUS, which halts its nuclear import, leading to its accumulation in the cytoplasm.[113]

1.3.3 FUS stress granules

In order to reestablish homeostasis in stress conditions, cells activate several pathways that normally involve gene expression regulation or, ultimately, apoptosis.[104,114] As stated earlier (see section ***1.1 Stress granules***) stress granules are transient membraneless cytosolic structures that mediate the fate of gene expression, degradation, or suppression, in response to cellular stress.[10]

Mediating several stages of gene expression, is not surprising that FUS plays an imperative role in cellular stress response.[104] Cells exposed to environmental stress, such as oxidative stress, hypoxia, viral infection or osmotic stress, actively recruit cytoplasmatic FUS into stress granules.[115-117] However, the stress environment does not induce translocation of FUS from the nucleus to the cytoplasm.[118] Rather, FUS

must be in the cytoplasm and already poised to enter stress granules during the stress condition. Therefore, mutations that affect the PY-NLS domain of FUS, and consequently, the reimport of FUS into the nucleus, contribute to FUS stress granule accumulation.[110,117]

FUS undergoes LLPS *in vivo* and *in vitro*, self-assembling into liquid-like stress structures, at incredibly low concentration (1 μM).[119,120] Cytoplasmatic demixing of FUS allows rapid and local concentration of FUS and, presumably, a myriad of additional factors required for stress response.[121] However, high local concentration of FUS might trigger liquid-to-solid transition, from droplets granules into aggregated inclusions. Hence, stress granules are presumably precursors to pathological inclusions found in neurodegenerative diseases.[120]

The LC domain of FUS is crucial for self-assembly of FUS.[102] The aromatic residues of FUS LC mediate short range interactions that promote the LLPS. On the other hand, the abundant hydrophilic character of this domain dictates the solubility of FUS, consequently opposing LLPS once the aromatic interactions are degenerated. Furthermore, phosphorylation of tyrosine and serine residues in FUS LC disassembles liquid droplets.[100,102] Thus, the LC domain of FUS seems to modulate the protein phase separation.

The RGG domains are also crucial for FUS LLPS.[101,122] In fact deletion of the RGG domains, specially RRG1, reduces significantly FUS phase separation.[123]

FUS stress granules are highly dynamic, displaying constant exchange of components with the cytoplasm and rapid internal rearrangement. Therefore, if the cell uses a dynamic liquid compartment to perform physiological relevant functions, it will have to constantly contradict thermodynamic driven aggregation. Hence, FUS-related diseases are often associated with late onset pathology, when the quality control machinery starts to degenerate.[10,124]

1.3.4 FUS in neurodegenerative disease

FUS cytoplasmatic inclusions is a common hallmark of both amyotrophic lateral sclerosis (ALS) and frontotemporal lobar degeneration (FTLD).[103,104]

ALS is the most frequent neurodegenerative disease in the human motor system.[125] Common manifestations encountered in ALS patients include muscle weakness and atrophy, and fasciculation in the motor neurons and brain stem.[125,126] Progressive weakening of the respiratory muscles leads to dyspnea and consequently respiratory failure, leading to low survival rate.[125] About 50% of ALS patients die within 30 months of symptom onset and about 20% of patients survive between 5-10 years after the symptoms appear.[127]

FTLD is the second most common cause of dementia in presenile age group (<65%), behind Alzheimer's disease (AD). This neurodegenerative disease is characterized by progressive degeneration of the frontal and anterior temporal lobes. This leads to progressive alterations and disturbances in personality, and/or language problems.[128] Although the memory preservation in the initial phase of FTLD is higher than in AD, the overall survival is shorter and the cognitive functions decline more rapidly in FTLD.[103,128]

ALS and FTDL form a clinical disease continuum, since up to 15% of ALS patients meet the clinical criteria of FTLD and 15% of FTLD patients meet the clinical criteria of ALS.[129]

ALS can be divided in two major groups: sporadic ALS and familial ALS. Sporadic ALS accounts for about 90% of all ALS diseases, but its aetology is unknown. The rest 10% of ALS cases are familial, which is a form of hereditary ALS.[130]

In the familial ALS, several defects on genes have been identified in patients. These include mutation in *SOD1* that encodes for copper/zinc superoxide dismutase (20% of familial ALS) and *TARDBP* that encodes for TDP-43 (5-10% of familial ALS).[125,131] In 2009, the *FUS* gene was identified as the primary disease-associated gene for familial ALS6, which accounts for 5% of familial ALS.[132] *FUS*-linked ALS and FTLD is designated as ALS-FUS and FTLD-FUS, respectively.

Cytoplasmatic depositions of FUS stress granules containing is a common hallmark for both FTLD-FUS and ALS-FUS subset.[103,133] However, there are several distinctions between the two diseases (**Figure 9**). In contrast to ALS-FUS, FTLD-FUS is rarely associated with *FUS* gene mutations.[134]

In FTLD-FUS there is a neuronal cytoplasmatic co-deposition of FUS and all other FET family members (EWS and TAF15), along with Kapβ2 Moreover, this neurodegenerative disease also displays low nuclear concentration of all three FET proteins.[135-137] Interestingly, protein inclusions in FTLD-FUS patients contain unmethylated FUS (see section ***1.3.2 FUS localization and nuclear-cytoplasmatic shuttling***).[113] In this case, unmethylated RGG3 domain can cause overly tight binding of the FET proteins to Kapβ2, inhibiting the FET-Kapβ2 dissociation in the nucleus. Hence, FET proteins are continuously re-exported to the cytoplasm which leads to cytoplasmatic FET deposits.[103]

Opposed to FTLD-FUS, ALS-FUS show an exclusive deposition of FUS, excluding EWS, TAF15 and Kapβ2.[136] In this case, point mutations in the *FUS gene* that truncate or modify the FUS PY-NLS domain, can lead to impairment of nuclear import. Consequently, FUS accumulates in the cytoplasm and clusters into cytoplasmatic aggregates.[112,116]

In both ALS-FUS and FTLD-FUS, cellular stress can further dysregulate the balance of FUS nuclear import/export and mediate the assembly of cytoplasmatic FUS inclusions in neuronal cells.[103]

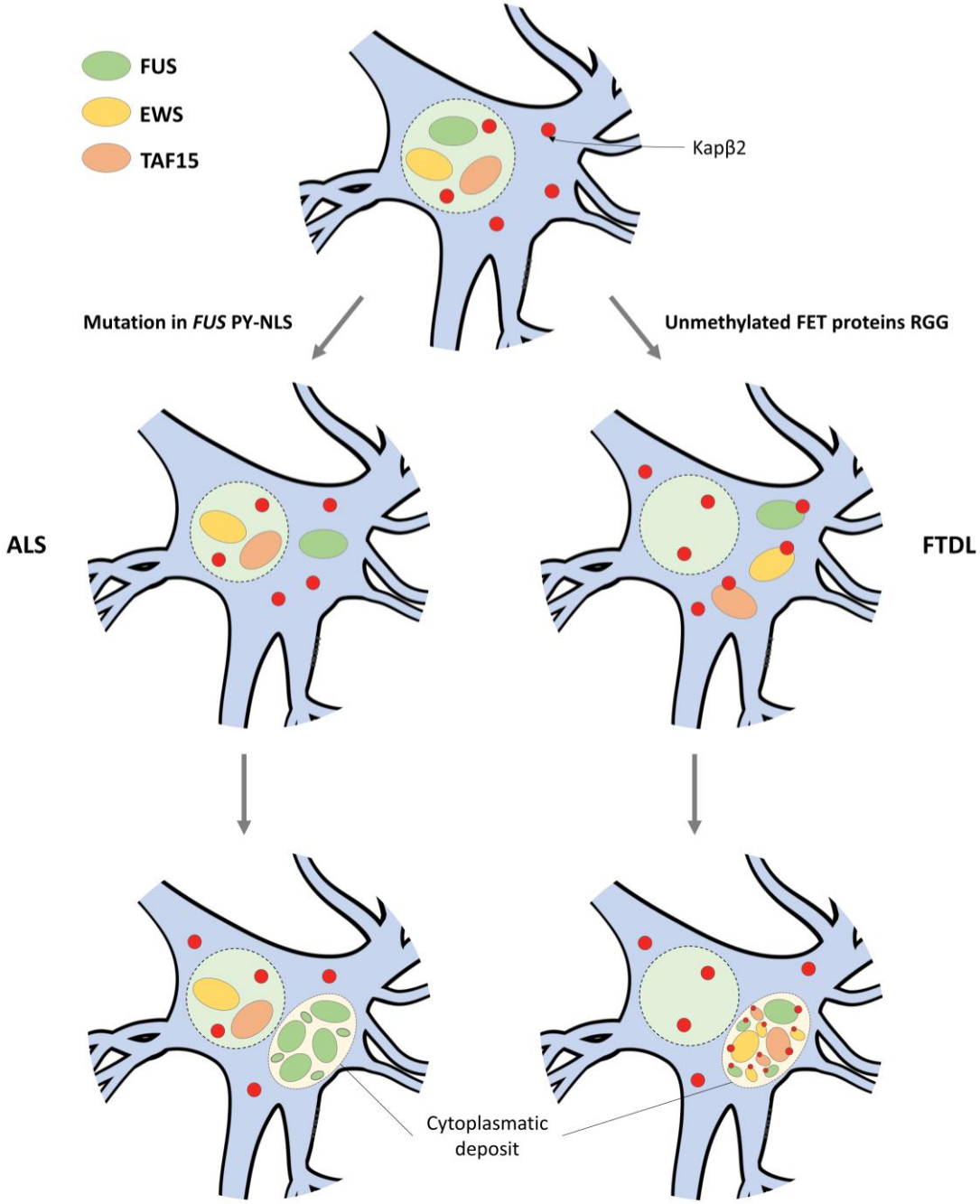

Figure 9 – Pathological mechanisms of ALS-FUS and FTLD-FUS – In homeostatic conditions, FET proteins (FUS, EWS and TAF15) are properly imported into the nucleus by Kapβ2. In ALS-FUS, missense mutations in the *FUS gene* that affect the FUS PY-NLS domain, cause impairment of the FUS-Kapβ2 interaction. This hinders the re-import of FUS into the nucleus, which ultimately leads to cytoplasmatic deposits of aggregated FUS; In FTLD-FUS, unmethylated RGG domain of FET proteins leads to irreversible binding to Kapβ2 which inhibits the release of FET proteins in the nucleus, leading to cytoplasmatic deposits of aggregated FET proteins.[103]

The toxicity of FUS fibrillar assemblies in motor neuron cells is supported by three hypotheses that are not mutually exclusive: stress granule gain-of-function, stress granule loss-of-function, and nuclear loss-of-function.[49]

The first model proposes that dysregulated assembly of FUS leads to fibrillar aggregates that perturb the physiological stress responses. Thus, there is a gain of toxic properties of FUS protein aggregates.[123,138]

The loss-of-function model focus of the loss of FUS physiological role. As this protein is recruited in stress granules, there is an impairment in the FUS cytoplasmatic function.[139,140]

Lastly, nuclear loss-of-function is consistent with the fact that FUS has a crucial physiological role in the nucleus. In both ALS-FUS and FTLD-FUS there is a depletion of nuclear FUS, which impairs several nuclear processes such as transcriptional regulation.[53,75]

Despite the cause of neurotoxicity, the inclusion of stable fibrillar FUS assemblies is a requisite in motor neuron cells in ALS-FUS and FTLD-FUS diseases.[79] Several efforts are being carried in order to understand the biochemical mechanisms and pathways that leads to FUS cytoplasmatic inclusions, with the hope of develop solutions to mitigate these neurodegenerative diseases.[123,141-143]

1.4 Outline and aim of the study

Given the importance of FUS stress granules in both physiological and pathological conditions, the aim of this study is to elucidate the mechanisms and determinants that drive their assembly.

The concept is based on the fact that cells have a complex milieu that impact and tune several processes. The conviction is that different environments, and consequently different interactions, can uniquely influence the FUS LLPS mechanism.

Therefore, the main objective is to assess the influence of diverse environmental conditions in the formation of FUS stress granules and attempt to unravel the role of the different FUS domains in their assembly. For this purpose, it is explored the transition between dispersed and phase-separated WT-FUS using different biochemical techniques such as NMR, microplate and microscopic assays.

Insights on the environment role can prove valuable in understanding the physiological and pathological conditions that can trigger WT-FUS stress granule assembly. This comprehension can help us link different cellular conditions to the appearance of cytoplasmatic FUS stress granules, that are crucial templates for pathological inclusions found in neurodegenerative diseases.

For that purpose, the main tasks set for this work are:

- Expression and purification of non-labeled and ^{15}N-labeled WT-FUS
- Study of the environment influence on FUS self-assembly, including pH, temperature and abundant cellular metabolites, through microplate turbidity assays
- Elucidation of the mechanisms involved in FUS LLPS
- Observation of FUS stress granules through microscopic imaging
- Comprehension of the impact of temperature on FUS overall structure by NMR spectroscopy
- Elucidation of the structural transition between dispersed and phase-separated FUS by NMR spectroscopy

2. EXPERIMENTAL PROCEDURES

”Information is not knowledge. The only source of knowledge is experience”

A. Einstein

2. Experimental procedures

2.1 General methodologies and materials

In this section the general methodologies and commonly used materials will be described and any alteration to the general procedures will be referred in the appropriate section.

Buffers were prepared using distilled water or Milli-Q water, both obtained from laboratory facility instruments. The pH measurements were made with Docu-pH Meter (*Sartorius*).

Centrifugation steps were executed in different centrifuges according to the sample volume. Microcentrifuge tube centrifugations (≤ 2 mL) were carried out by a MIKRO 120 centrifuge (*Hettich*). Centrifuge canonical tubes (≤ 30 mL) were centrifuged in a centrifuge 5804R (*Eppendorf*) with a F-34-6-38 fixed-angle rotor (*Eppendorf*). For higher volumes (≤ 500 mL), centrifugations were performed in an Avanti J-26 XPI centrifuge (*Beckman Coulter*) with JA fixed-angle rotors (*Beckman Coulter*). Besides from small volume samples (≤ 2 mL), centrifugations were carried out in Nalgene PPCO canonical tubes (*Thermo Fisher Scientific*).

Small volume incubations were carried out in an Orbital Shaker-incubator ES-20 (*Grant-Bio*). For bacterial growth, incubations were executed in an Orbital Shaker-incubator (*Optic-Ivymen System*). Optical density was measured in a UltroSpec 2100 Pro UV-Vis spectrophotometer (*GE Healthcare*) in polystyrene cuvettes (*Sigma-Aldrich*).

Sodium dodecyl sulfate polyacrylamide gel electrophoresis (SDS-PAGE) was prepared in a discontinuous manner, employing a Tris-tricine buffer system.[144] In brief, 10% separating gel and 4% stacking gel are independently prepared and respectively casted at the bottom and at the top of the electrophoretic glass apparatus. The separating gel allows effective separation of proteins with molecular weights ranging from 1 to 100 kDa. Detailed composition of the Tris-SDS-PAGE gel and Tris-tricine buffer system are described in the appendix (**Appendix - Table A. I and Table A. II**). For the Tris-SDS-PAGE procedure, samples were prepared by mixing 15 µL of protein sample and 5 µL of SDS-PAGE sample buffer (**Appendix - Table A. III**). The samples were subsequently heated at 100°C for 5 min and centrifuged at 14000 rpm for 1 minute. From the prepared sample, 18 µL were applied to the gel along with 2 µL of protein marker (*NZYTech Colour Protein Marker II, NZYTech*) with reference bands covering a range of molecular weights from 11 to 245 kDa. The Tris-SDS-PAGE electrophoresis were executed in an electrophoresis apparatus (*Bio-Rad*). The power supply settings employed were 200 mA, 200 V and 50 W. Each electrophoretic run proceeded for about 40 min. The gels were stained and destained by Coomassie Blue Staining Method for 1 and 2 hours, respectively, at 37°C and 50 rpm (**Appendix - Table A. IV**).

Protein purifications were carried out in ÄKTA start chromatographic system (*GE Healthcare*) following A_{280nm} using UNICORN Start software (*GE Healthcare*). Both buffers and samples were filtered prior to each purification step using 0.22-µm membrane filters (*GE Healthcare*).

All dialysis steps were achieved using 7K MWCO SnakeSkin Dialysis Tubing (*Thermo Fisher Scientific*). Concentration and diafiltration of samples were performed using Vivapsin Turbo 15 10 MWCO (*Sartorius*) for sample volumes up to 15 mL, and Vivapsin Turbo 4 10 MWCO (*Sartorius*) for sample volumes between 2 and 4 mL.

Protein concentrations were obtained from A_{280nm} measured on a NanoDrop ND-1000 UV-Vis spectrophotometer (*Thermo Fisher Scientific*), using the molar extinction coefficients estimated by ProtParam ExPASy software (**Appendix - Table A. V)**.[145]

2.2 Protein expression and purification

Recombinant MBP-FUS-FL-WT construct was kindly gifted by Nicolas Fawzi (Addgene plasmid #98651). The plasmid was constructed using a PETM-41 vector, to express the human WT-FUS full-length protein which included a His_6-MBP moiety and a TEV cleavage site (MBP-FUS) (**Appendix - Figure A. 1**).

2.2.1 General expression

Escherichia coli strain BL21 (DE3) competent cells were transformed with the MBP-FUS plasmid through the heat shock method. For the transformation 1 µL (50 ng/µL) of plasmid DNA encoding WT-MBP-FUS was mixed with 50 µL pf *E. coli* BL21(DE3) competent cells and kept on ice for 30 min. Then, cells were incubated at 42ºC (*AccuBlock Digital Dry Bath, Labnet International*) for 40 s and transferred to ice for 5 min. Finally, 950 µL of Luria-Bertani medium (LB) (**Appendix - Table A. VI**) was added to the samples, and subsequently incubated at 37ºC for 60 min.

The transformed *E. coli* cells were plated overnight at 37ºC in agar LB (**Appendix - Table A. VII**) supplemented with 50 µg/mL kanamycin (*NZYTech*). A single isolated colony from the plated *E. coli* cells was chosen and incubated overnight at 37ºC and 200 rpm, in 150 mL LB supplemented with 50 µg/mL kanamycin.

2.2.1.1 Non-labeled FUS expression

Non-labeled recombinant FUS was expressed in 1 L LB (x6) until mid-exponential growth (OD_{600nm}~0.8), and subsequently induced with 0.5 mM isopropyl-β-d-1-thiogalactoside (IPTG) (*NZYTech*) for 16 h at 18ºC and 180 rpm. Cells were recovered by centrifugation at 6700 rpm (JA-10 rotor) for 15 min, at 4ºC. The cell pellet for each liter of culture was resuspended in 30 mL of lysis buffer containing 20 mM sodium phosphate buffer (Na_2HPO_4 – *Honeywell*, NaH_2PO_4 – *Sigma-Aldrich*), 300 mM NaCl (*Acros*), 40 mM imidazole (*Affymetrix*), 10% glycerol (*Scharlau*), 5 mM β-mercaptoethanol (βME) (*Sigma-Aldrich*), 2 mM benzamidine (*Sigma-Aldrich*) and 1 protease inhibitor tablet (*cOmplete Mini EDTA-free Protease Inhibitor Cocktail, Roche*), at pH 7.50.

The cell lysis was performed through sonication, using an Ultrasonic Processor UP100H 100-W dismembrator equipped with 1/8-inch tip (*Hielscher*), for 10 min using a 2s on/2s off pulse program with 80% amplitude. The lysate was cleared by

centrifugation at 20000 rpm (JA-25.50 rotor) for 60 min, at 4ºC. The supernatant was recovered for the subjacent purification steps.

2.2.1.2 Uniformly ^{15}N-labeled FUS expression

Uniformly ^{15}N-labeled recombinant FUS was expressed in M9 minimal medium (**Appendix - Table A. VIII and Table A. IX**), using $^{15}NH_4Cl$ as the only nitrogen source. The expression followed the previously described process (see section ***2.2.1.1 Non-labeled FUS expression***), being retrieved the supernatant for purification.

To maximize the yield of labelled protein, FUS was also recovered from inclusion bodies. To accomplish this, after the sonication step a mild solubilization of the inclusion bodies was performed, following the procedure reported by Singh *et al*.[146] In summary, the resulting pellet from 1 L of culture was resuspended in 1 mL H_2O Milli-Q and solubilized in 9 mL of solubilization buffer containing 100 mM CAPS (*Alfa Aesar*), 2 M urea (*Sigma-Aldrich*), 100 mM NaCl, 20% glycerol, 5 mM βME and 0.1% (w/v) SDS (*Panreac*), at pH 12.00. The solubilized proteins were incubated at room temperature for 30 min and later centrifuged at 11000 rpm (F-34-6-38 rotor) for 30 min, at 4ºC. Then, for the refolding step, 10 mL of solubilized protein was added to 90 mL of refolding buffer containing 50 mM Tris-HCl (*Fluka*), 2 M urea, 100 mM NaCl, 10% glycerol, 5 mM βME and 1 protease inhibitor tablet, at pH 8.00. The refolding was carried out at 4ºC in a pulsatile manner, adding the solubilized protein at 1 mL/min to the refolding buffer, with constant stirring. The refolded protein was cleared by centrifugation at 11000 rpm (F-34-6-38 rotor) for 45 min, at 4ºC. Cleared samples were diafiltrated against 20 mM sodium phosphate buffer, 40 mM imidazole, 300 mM NaCl, 10% glycerol, 5 mM βME, 2 mM benzamidine and 1 protease inhibitor tablet at pH 7.50. The refolded protein was then added to the labeled protein retrieved from the supernatant, for subsequent joint purification.

2.2.2 Purification of non-labeled and uniformly ^{15}N-labeled FUS

The purification of non-labeled and uniformly ^{15}N-labeled FUS followed the same protocol. Recombinant MBP-FUS was primarily purified by ion metal affinity chromatography (IMAC) using two 5 mL HisTrap FF crude Ni-NTA columns (*GE Healthcare*), connected in series. The protein was applied to the equilibrated columns and washed with the binding buffer containing 20 mM sodium phosphate buffer, 40 mM imidazole, 300 mM NaCl, 10% glycerol, 5 mM βME, 2 mM benzamidine and 2 protease inhibitor tablets, at pH 7.50. Protein elution was achieved with an imidazole gradient (0-500 mM) settled by elution buffer containing 20 mM sodium phosphate buffer, 500 mM imidazole, 300 mM NaCl, 10% glycerol, 5 mM βME, 2 mM benzamidine and 1 protease inhibitor tablet, at pH 7.50. Fractions containing MBP-FUS protein were pooled and further concentrated.

Protein desalting was performed to remove the excess imidazole and the protease inhibitors, that interfered with the subsequent step. The protein was applied to a HiTrap Desalting column (*GE Healthcare*) and eluted with a buffer containing 20 mM sodium phosphate buffer, 300 mM NaCl, 10% glycerol and 5 mM βME at pH 7.50.

The removal of the MBP moiety was accomplished by TEV cleavage. The TEV protease was added to the protein in a ratio of 1 A_{280nm} of TEV protease per 100 A_{280nm} of MBP-FUS. The digestion was carried out overnight at 4ºC. The cleaved product was

then centrifuged at 11000 rpm (F-34-6-38 rotor) for 20 min, at 4ºC, to remove the precipitated TEV protease and some resulting precipitated protein. The cleared product was applied to a second HisTrap Ni-NTA column (5 mLx2) following the same procedure as referred in the first IMAC purification step. Such step removes the His_6-MBP moiety since this affinity tag binds to the column while FUS is eluted in the flow-through.

A second protein desalting step was performed in order to remove NaCl and imidazole, that are incompatible with the downstream purification step. The protein was applied to the desalting column and eluted with a buffer containing 20 mM Tris-HCl, 10% glycerol and 5 mM βME, at pH 8.00. Fractions including FUS were pooled and concentrated.

As the last purification step, FUS was purified by ion exchange chromatography (IEX). The protein was applied to a cation exchange HiScreen SP FF column (*GE Healthcare*) and washed with the binding buffer (20 mM Tris-HCl, 10% glycerol, 5 mM βME, at pH 8.00). The protein was eluted in a NaCl gradient (0-500 M) with 1 M NaCl-containing buffer.

The resulting purified FUS was dialyzed against H_2O Milli-Q, lyophilized and stored at -20ºC.

2.3 FUS phase separation assays

To assess the degree of FUS self-assembly through LLPS, turbidity assays were performed by absorbance microplate reading. The influence of the temperature and different cellular metabolites on FUS LLPS mechanism was evaluated as described below.

All the assays were carried out with 5 μM of FUS in three different buffers with different pH values (20 mM Tris-HCl pH 7.00, 20 mM CAPS pH 9.40 and 20 mM CAPS pH 11.00), to take into account the effect of the overall protein charge on the LLPS process. Exceptions were made when the pH influenced the solubility or the stability of the metabolites, as referred ahead.

Presence of co-purified DNA and RNA, that could interfere with the turbidity measurements, was verified. The $A_{260nm}/_{280nm}$ ratio of FUS was between 0.58-0.60 indicating a nucleic acid-free protein.

Buffer and the metabolites were mixed in reaction volumes of 100 μL in 96-well clear microplates (*Corning*), and subsequently incubated for 60 min at the chosen temperature. Lyophilized FUS was then added, incubated for additional 10 min and briefly mixed, prior to the turbidity assays. The OD_{595nm} was monitored using a Benchmark Microplate Reader (*Bio-Rad*). All measurements were made in triplicate.

2.3.1 Temperature influence on FUS liquid-liquid phase separation

To evaluate the effect of the temperature on the LLPS process, and to assess the FUS phase separation behavior (see section ***1.2.1 Liquid-liquid phase separation***), turbidity assays were performed at three different temperatures: 4ºC, 25ºC and 37ºC.

The temperature control was distinct in two cases. At 25ºC and 37ºC, the temperature was maintained constant by the temperature control system of the microplate reader. At 4ºC, the temperature was extrinsic to the apparatus, meaning

that the temperature was maintained by the temperature in the room and not by the microplate reader itself. The measurements were performed in a refrigerated room with a constant temperature of 4ºC. The microplate reader was incubated in the refrigerated room for 3 h to ensure that the apparatus was cooled down before the measurements. The room temperature was constantly verified by a thermometer. Samples of FUS protein were prepared in buffer and incubated as described above. Sample-containing microplates were mixed and the OD_{595nm} was retrieved.

2.3.2 Metabolite influence on FUS liquid-liquid phase separation

Abundant metabolites found in the cell, particularly in the cytoplasm, were selected to determine their impact on the phase separation of FUS. The chosen metabolites included salts (NaCl), sugars (glucose), charged amino acids (lysine and glutamate), metallic ions (Ca^{2+} and Zn^{2+}) and ribonucleic acids (RNA).

Freshly prepared samples of FUS in different pH values (pH 7.00, pH 9.40 and pH 11.00) and increasing metabolite concentrations, were mixed and the OD_{595nm} was recorded. Final concentration range of metabolites in the microplates are summarized in **Table I**.

Table I – Metabolite concentration range applied in FUS microplate turbidity assays

Metabolite	Concentration range (mM)
NaCl (*Acros*)	0, 50, 150, 300
Glucose (*Sigma-Aldrich*)	0, 1, 2, 3
Lysine-HCl (*Sigma-Aldrich*)	0, 1, 2, 5
Na-Glutamate (*Panreac*)	0, 1, 2, 5
$ZnCl_2$ (*Merck*)	0, 0.3, 0.5, 1
$CaCl_2$ (*Panreac*)	0, 0.3, 0.5, 1

The mass ratio between RNA:FUS went from 0:1 (0 µg:26.65 µg), 0.2:1 (5.33 µg: 26.65 µg), 0.4:1 (10.66 µg: 26.65 µg), 1:1 (26.65 µg: 26.65 µg), 2:1 (53.30 µg: 26.65 µg), and 4:1 (106.60 µg: 26.65 µg).

Turbidity of FUS in the presence of $ZnCl_2$ was only measured at pH 7.00, since this metabolite presented insoluble at pH 9.40 and 11.00.

2.4 Imaging of FUS stress granules

For the protein droplets imaging, lyophilized FUS was resuspended in 20 mM CAPS and 150 mM NaCl, at pH 9.40, to a final concentration of 200 µM and 1 mM. 10 µL of FUS were loaded onto the glass slides and covered with glass coverslips. Samples were analyzed using a LSM 710 META confocal laser scanning microscope (*Zeiss*) at room temperature. All images obtained were processed using Fiji software.[147]

2.5 NMR experiments

All NMR experiments were acquired in a Bruker Avance III NMR spectrometer (*Bruker BioSpin*) operating at 600 MHz ^{1}H frequency, equipped with a 5 mm triple-resonance cryogenic probe (CP TCI). In all samples, the ^{1}H chemical shifts were calibrated through indirect referencing using 50 µM DSS *(Eurisotop*). All data was processed using Bruker TopSpin 3.5™ software (*Bruker BioSpin*).

2.5.1 Preparation of NMR samples

For NMR studies, lyophilized ^{15}N-labeled FUS samples were resuspended in 90% H_2O/10% $^{2}H_2O$ (*Eurisotop*) and transferred into 3 mm NMR tubes. Protein samples were prepared to a final concentration of 200 µM.

2.5.1.1 Dispersed FUS

Dispersed FUS sample was prepared by resuspending 2.13 mg of ^{15}N-labeled lyophilized FUS in 200 µL of buffer containing 20 mM sodium phosphate buffer, 2 mM DTT (*NZYTech*), 10% glycerol, 0.05% sodium azide (NaN_3) (*Panreac*), 1 protease inhibitor tablet and 10% $^{2}H_2O$, at pH 7.10.

2.5.1.2 Phase-separated FUS

In order to achieve phase separation, the dispersed FUS sample was diafiltrated using a buffer containing 20 mM sodium phosphate buffer, 150 mM NaCl, 0.05% NaN_3, 1 protease inhibitor tablet and 10% $^{2}H_2O$, at pH 7.10. In brief, 200 µL of dispersed FUS were diluted in 3 mL of buffer and concentrated to the initial volume (200 µL) at 5000 rpm (F-34-6-38 rotor) for 10 min, at 6ºC. This step was repeated 4 times to ensure the removal of the glycerol and DTT, and the complete addition of the NaCl.

In order to minimize the loss of phase-separated FUS, the resulting 200 µL of diafiltrated product were transferred to the NMR tube and the following procedures were applied directly to the tube.

The FUS sample was initially heated to 42ºC for 5 min to clear initial cloudiness, and then cooled to the room temperature. Subsequently, the sample was quenched on ice for 10 min to further drive the LLPS. Finally, the NMR tube containing the FUS sample was manually centrifugated to settle at the bottom the phase-separated FUS. The supernatant was removed and A_{280nm} was retrieved to ensure that FUS was in phase-separated state and not in the supernatant. The supernatant was then applied to the protein-dense phase and the solution was homogenized.

2.5.2 NMR experiments on dispersed FUS

To assess temperature influence on the structure of dispersed FUS, 2D-NMR ^{1}H-^{15}N HSQC spectra were obtained at 5ºC, 15ºC and 25ºC. The ^{1}H-^{15}N HSQC spectra (hsqcetfpf3gpsi2 pulse sequence from Bruker library) were acquired with 512 scans

on a matrix with 2048 x 128 complex points, and a sweep width of 9615.385 Hz (centered at the water resonance frequency) x 2311.077 Hz (centered at 118 ppm), in the ^{1}H and ^{15}N dimension, respectively.

On the same sample, consecutive spectra were recorded increasing the temperature (5ºC → 15ºC → 25ºC), followed by a mirrored experiment decreasing the temperature (25ºC → 15ºC → 5ºC).

2.5.3 NMR experiments on phase-separated FUS

To explore FUS overall conformational changes upon phase separation, 2D-NMR ^{1}H-^{15}N HSQC of phase-separated FUS was obtained. The spectrum was acquired with the same acquisition parameters as referred previously for ^{1}H-^{15}N HSQC spectra of dispersed FUS (see section ***2.5.2 NMR experiments on dispersed FUS***). To maximize phase-separation the experiment was conducted at 5ºC.

3. RESULTS AND DISCUSSION

"I am just a child who has never grown up. I still keep asking these "how" and "why" questions. Occasionally, I find an answer"

S. Hawking

3. Results and discussion

3.1 Expression and purification of non-labeled and uniformly ^{15}N labeled FUS

Following the expression of non-labeled and uniformly ^{15}N-labeled FUS, both proteins were purified by two consecutive steps of affinity chromatography, followed by a cation exchange chromatography. Since the elution of both non-labeled and ^{15}N-labeled FUS followed similar profiles, it is presented the results for the ^{15}N-labeled FUS purification process. All remaining data are present in the **Appendix** (**Appendix - Figure A. 2, Figure A. 3 and Figure A. 4**).

After the isolation of solubilized recombinant protein, an IMAC step was performed as the first purification step. The proteins of interest contained a N-terminal polyhistidine tag that displayed high affinity to the Ni-NTA HisTrap column matrix. The histidine imidazole ring has the ability to form coordination bonds with the Ni^{2+} metal ion immobilized on the column matrix. The proteins are then eluted adding high concentrations of free imidazole to the column buffer, that competes with the histidine imidazole group and releases the protein from the matrix.[148]

To elute the proteins bound to the column an imidazole gradient (0-500 mM) was applied. The protein of interest was eluted at 150 mM imidazole (**Figure 10**).

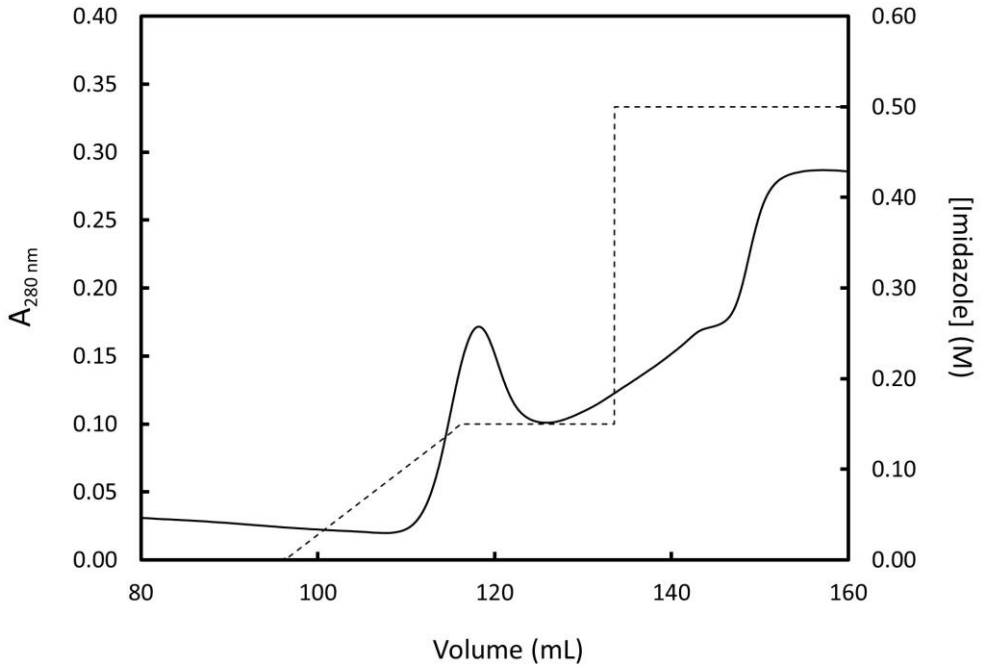

Figure 10 – First purification step of ^{15}N-labeled FUS by Ni-NTA affinity chromatography – Elution profile for the first IMAC purification step of ^{15}N-labeled FUS. HisTrap column (5 mLx2) equilibrated with 20 mM sodium phosphate buffer, 40 mM imidazole, 300 mM NaCl, 10% glycerol, 5 mM βME, 2 mM benzamidine and 2 protease inhibitor tablets, at pH 7.50. Primary and secondary y-axis correspond the to the variation in absorbance at 280 nm (solid line) and the imidazole gradient (dashed line), respectively. Protein eluted at 150 mM imidazole and fraction collected between 110 mL and 124 mL.

Following the first purification step that removed most of the contaminants, the His_6-MBP moiety was cleaved from FUS by TEV digestion. A second IMAC purification step was then applied to remove the affinity tag. Like the polyhistidine tag, the MBP moiety is also an affinity tag on its own, being able to bind to amylose matrices. However, MBP tags have a dual purpose, being able to assist not only on purification but also on expression, improving target protein solubility. MBP is a naturally occurring 42 kDa *E. coli* protein known to significantly enhance the solubility of poorly soluble proteins by a still unclear mechanism.[149] In the case of FUS, the MBP improves the stability of the protein in solution. Hence, after its cleavage protein tends to precipitate. Due to the lack of His_6-MBP moiety, the protein of interest was eluted in the flow-through and the His_6-MBP moiety was eluted at about 330 mM imidazole (**Figure 11**).

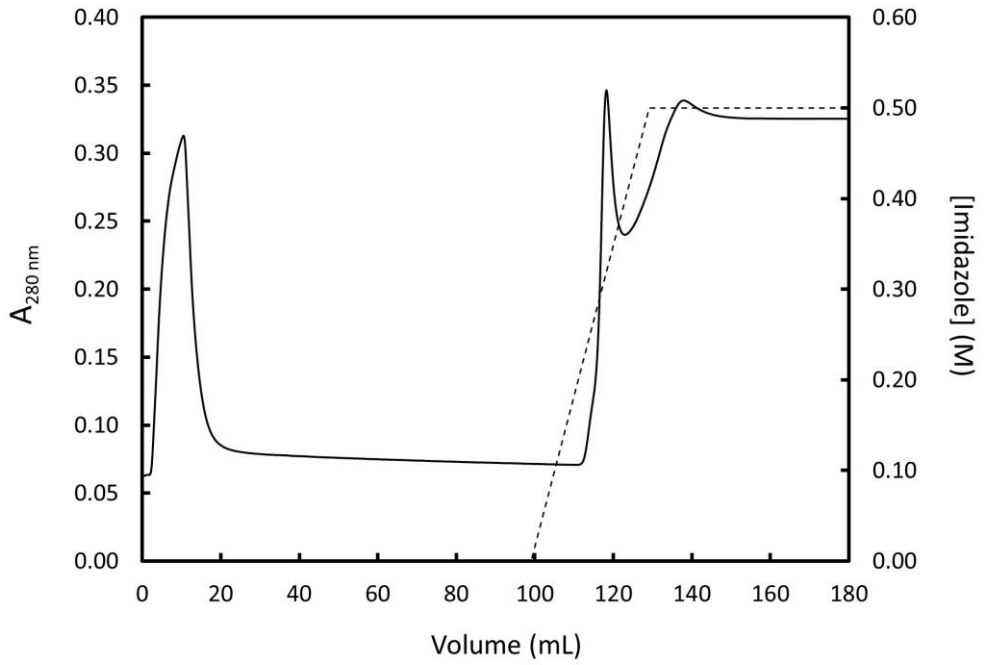

Figure 11 – Second purification step of ^{15}N-labeled FUS by Ni-NTA affinity chromatography – Elution profile for the second IMAC purification step of ^{15}N-labeled FUS. HisTrap column (5 mL x2) equilibrated with 20 mM sodium phosphate buffer, 40 mM imidazole, 300 mM NaCl, 10% glycerol, 5 mM βME, 2 mM benzamidine and 2 protease inhibitor tablets, at pH 7.50. Primary and secondary y-axis correspond to the variation in absorbance at 280 nm (solid line) and the imidazole gradient (dashed line), respectively. Protein eluted in the flow-through corresponding to the first peak in absorbance. Protein fraction collected between 2 mL and 21 mL. His_6-MBP moiety eluted at 330 mM imidazole

As a final polishing step, a cation exchange chromatography was performed. FUS is a very basic protein with an isoelectric point of 9.40, determined by ProtParam ExPASy software.[145] Thus, under the conditions applied (at pH 8.00) FUS strongly binds to the cation HiScreen SP column through electrostatic interactions. The bound protein was then eluted with NaCl that competes for ionic binding to the column and releases the protein from the matrix. FUS was eluted at 250 mM NaCl (**Figure 12A**).[150]

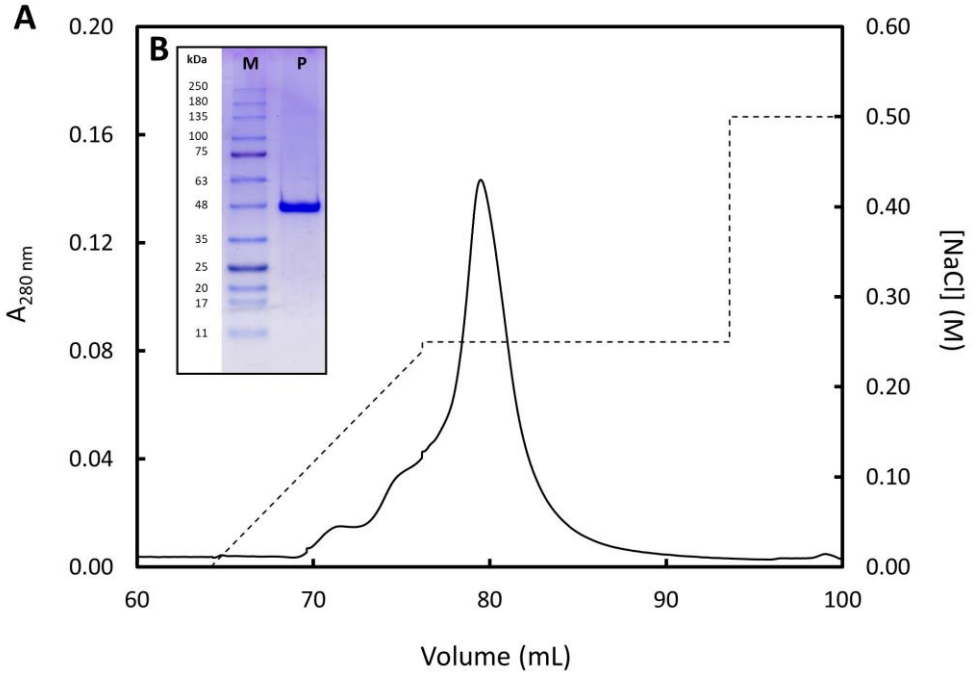

Figure 12 – Final purification step of ^{15}N-labeled FUS by ion exchange chromatography – (A) Elution profile for the third and final IEX purification step of ^{15}N-labeled FUS. HiScreen SP column equilibrated with 20 mM Tris-HCl, 10% glycerol and 5 mM βME, at pH 8.00. Primary and secondary y-axis correspond to the variation in absorbance at 280 nm (solid line) and the NaCl gradient (dashed line), respectively. Protein eluted at 250 mM NaCl and fraction collected between 77 mL and 87 mL. **(B)** Inset of the protein purity analysis by SDS-PAGE. Lane: M – Prestained protein marker, P – ^{15}N FUS after ion exchange chromatography. Corresponding MW of the protein marker on the left.

After the purification steps, the purity of the protein was confirmed by SDS-PAGE with a corresponding band in MW region of approximately 50 kDa, which goes in agreement with the expected 54.15 kDa of ^{15}N FUS (**Figure 12B**).

The overall yields of purified FUS protein for the non-labeled and uniformly ^{15}N-labeled FUS, were 3.7 mg and 2.5 mg per liter of culture, respectively.

3.2 Temperature dependence of FUS liquid-liquid phase separation

Proteins and polymers that undergo self-assembly are highly influenced by the temperature. Phase separation can exhibit two distinct types of behavior: either the LLPS occurs above a critical solution temperature (LCST) or under the critical solution temperature (UCST) (see section ***1.2.1 Liquid-liquid phase separation***). For example, microtubule-associated protein Tau is known to have a LCST phase separation behavior, while ALS-related protein hnRNPA1 exhibits a UCST behavior.[59,151]

To investigate the dependence of FUS LLPS on temperature, turbidity of a 5 μM FUS solution was measured at three distinct temperatures: 4ºC, 25ºC and 37ºC. The obtained results are presented in **Figure 13**.

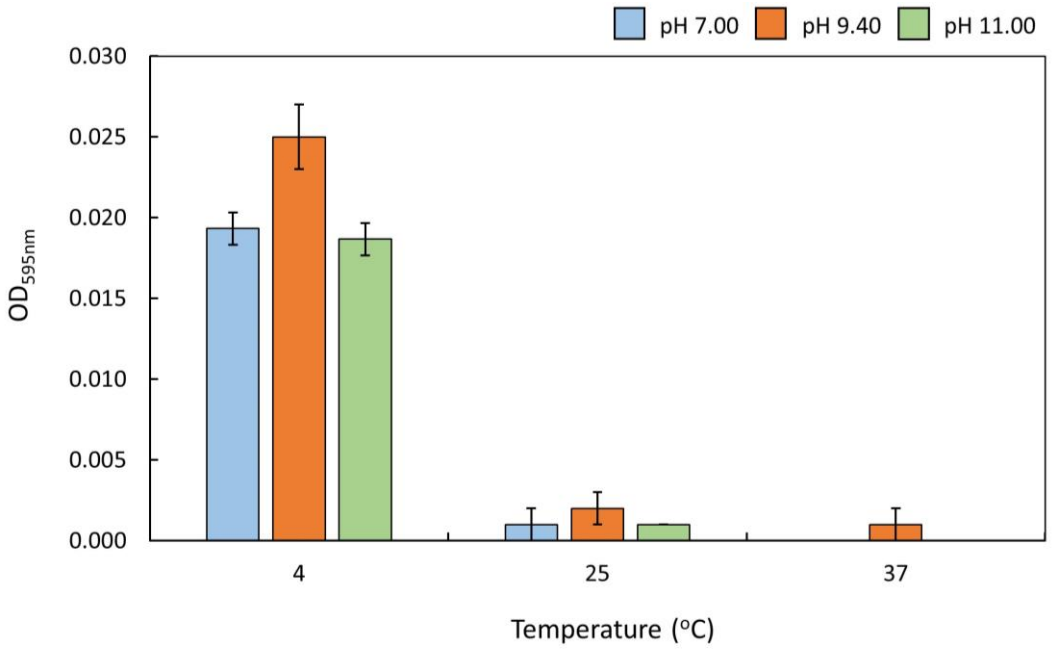

Figure 13 – Influence of temperature on FUS phase separation – Monitorization of 5 μM FUS phase separation at three distinct temperatures. Data collection at each temperature started 10 min after addition of lyophilized FUS to the solution. Data represented as the mean of three independent measurements, with standard deviation error bars.

At 25ºC and 37ºC little solution turbidity was detected suggesting that FUS is present as a dispersed monomeric protein at these temperatures. At 4ºC, turbidity increased by almost 20-fold indicating FUS granule formation. These results are in agreement with previous reports.[99,152] Along with the temperature dependence, it was also observed that turbidity depended on the solution pH, reaching a maximum when pH matched the protein's pI (pH 9.40). At physiological temperature, turbidity is only detected at pH 9.40, which might suggest that at this temperature stress granule formation is promoted by other factors. The dependence of pH solution on FUS LLPS is extensively discussed in the next section.

Data shows that FUS phase separation is promoted at lower temperature and is rapidly reversible with increasing temperature. These results indicated that FUS has a UCST-type of LLPS behavior.

Polymer phase behavior is significantly influenced by subtle chemical and structural variations.[153] In proteins, this behavior is determined by the amino acid composition. High content on lysine residues is known to favor LCST-type of phase separation, while high content on arginine residues is associated with UCST. This goes in agreement with FUS amino acid content, since it contains a high percentage of arginine residues but a low lysine content (**Figure 14**). Moreover, zwitterionic phase separation is known to exhibit UCST behavior which agrees with the observed increased turbidity at pH 9.40.[154]

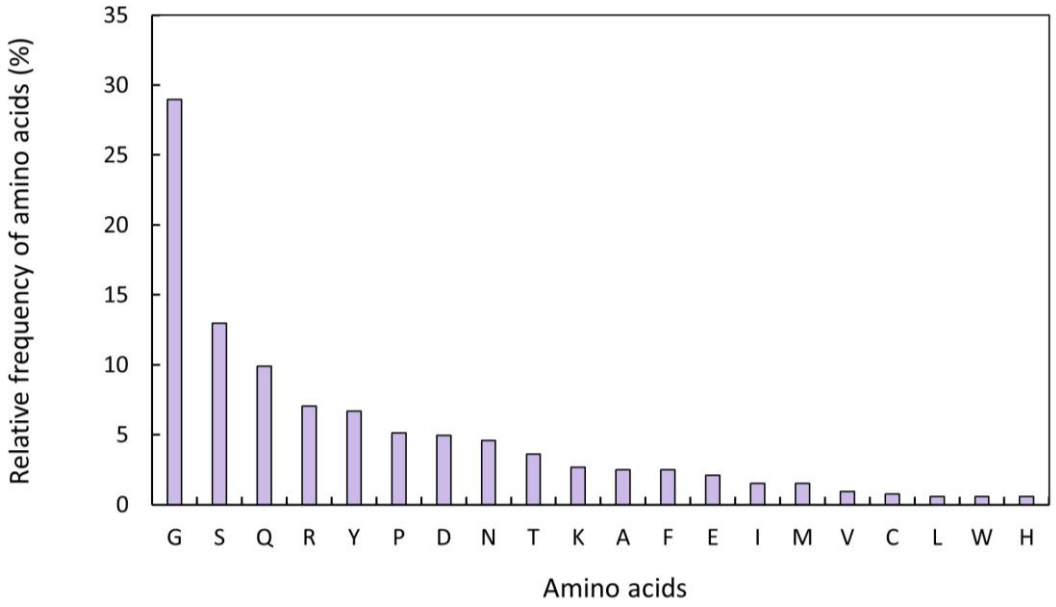

Figure 14 – Relative content of amino acids in FUS protein – Relative amino acid frequencies calculated from a total of 526 amino acids of full-length WT FUS.

Intriguing, FUS phase separation seems to occur under relevant physiological conditions, since at 37ºC turbidity is almost non-detectable, only a small fraction is present at pH 9.40. This might reveal that at the physiological context, stress granule formation must be enhanced by additional factors.

3.3 Metabolite influence on FUS liquid-liquid phase separation

As stated in detail in the introduction, FUS is a nuclear protein able to shuttle to the cytoplasm where its poised to form membraneless organelles through LLPS. Such organelles are visible as an opalescent turbidity in solution, which can be quantified by measuring the optical density at 595 nm.

The cytoplasm is a complex environment capable of modulating cellular functions including protein folding, enzyme catalysis, intracellular signaling and transport, and molecular localization.[155] The cytosol is the liquid phase of the cytoplasm of a membrane-enclosed intact cell, excluding the organelles.[156] The cytosol is mainly composed by water, which makes up for about 70% of the content volume. However, the cytosol is also highly crowded, being comprised of ions, metabolites and macromolecules (proteins, nucleic acids, polysaccharides, *etc*.). In a prokaryotic *E. coli* cell, the total protein concentration is in the range of 200-300 g/L while nucleic acids range from 75 to 150 g/L.[157] In mammalian cells, protein concentration ranging from 50 to 250 g/L and nucleic acid concentration of 50 g/L have been determined, varying according to the cell type.[158] In each case, macromolecules occupy about 10-40% of the total cell volume.[159]

Such crowded environment has a great impact on the physiological reactions inside living cells. Since two molecules cannot occupy the same space at the same time, reactions that depend on available volume can be affected by the crowded environment. This phenomenon is called volume exclusion effect which is the major

mechanism by which macromolecular crowding affects proteins. Minimization of volume exclusion and consequent maximization of entropy can be achieved through changes in hydrodynamic volumes or in association rates. Hence, macromolecular crowding can modulate protein stability, folding and compaction, or influence protein-protein interactions, protein-nucleic acid interactions, protein oligomerization, pathological aggregation and phase separation.[160]

Not accounting for the macromolecular crowding effects, in the cytoplasm FUS is surrounded by cytoplasmatic metabolites. Small molecules such as metabolites have negligible crowding effect (according to the their *in-vivo* concentration) but are able to interact and influence biochemical reactions.[160] As a result, natural occurring metabolites should influence the phase separation phenomena.

Taking all into account, the intended goal was to gain insight on the impact of different natural abundant metabolites on the degree of FUS LLPS. In this study, the influence of macromolecular crowding was not explored.

As reported in the previous section (see section ***3.2 Temperature dependence of FUS liquid-liquid phase separation***), FUS displays a UCST-type of phase separation, undergoing LLPS at low temperature. Hence, the turbidity assays were performed at 4ºC, in order to maximize phase separation.

Although is difficult to provide an exact range of intracellular metabolite concentration, due to tissue and specie specificity, the values in this section refer to estimated intracellular concentrations found in the literature for mammalian cells and were assumed as typical.

NaCl

The first abundant metabolite tested was NaCl. Inorganic ions such as sodium (Na^+) and chloride (Cl^-) have an extracellular concentration of ~144 mM and ~110 mM, respectively. Intracellularly, Na^+ has a concentration of about 12 mM and Cl^- 10 mM. However, the intracellular concentration of Cl^- varies immensely depending on the cell type, ranging from 5 mM in skeletal muscle to 80 mM in red blood cells.[161] The influence of NaCl in FUS phase separation is presented in **Figure 15**.

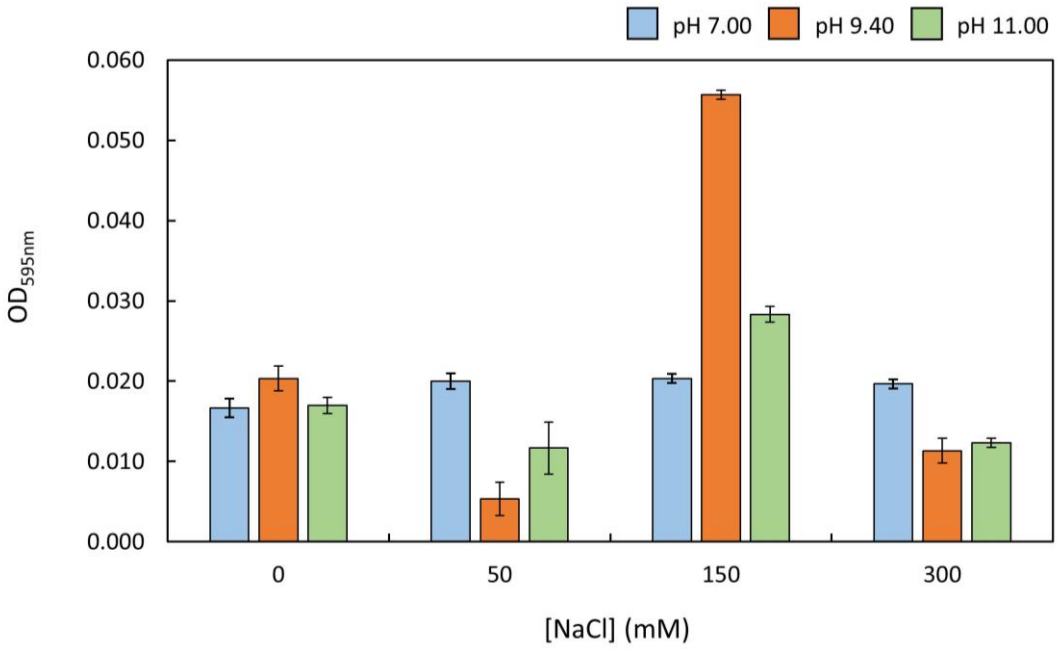

Figure 15 – Influence of NaCl on FUS phase separation – Monitorization of 5 μM FUS phase separation in the presence of increasing NaCl concentration. Turbidity assays were performed at 4ºC. Data collected 10 min after addition of lyophilized FUS to the solutions. Data represented as the mean of three independent measurements, with standard deviation error bars.

The results obtained show that FUS phase separation is highly sensitive to the presence of NaCl in a pH dependent manner.

When FUS has a global neutral charge, at pH 9.40, phase separation shows the highest sensitivity to variation in ionic strength. At 150 mM NaCl, phase separation increases significantly, dropping quickly when the concentration of NaCl is doubled (300 mM).

At pH 7.00 and pH 11.00, when FUS is positively charged and negatively charged, respectively, phase separation is less responsive to variation in NaCl concentration. Changes in ionic strength are known to have pronounced effects on the conformational properties of disordered proteins. IDPs are highly enriched in charged amino acids, being referred as polyelectrolytes.[162] Charge screening by dissolved salts controls the interactions between polyelectrolytes, hence phase behavior is strongly dependent on the solution ionic strength.[163]

The high degree of FUS phase separation at pH 9.40 suggest that FUS-FUS interactions are attractive at the given pH. Protein-protein interactions in salt solutions are poorly understood due to the sheer complexity of both proteins and salt ions. The traditional way to approach these systems is to adapt colloid theories, such as Derjaguin-Landau-Verwey-Overbeek (DLVO) theory. The DLVO theory describes the stability of colloidal solutions, modeling the interactions of charged colloidal particles in a continuum solvent by the balance of repulsive long-ranged electrostatic interactions and attractive short-ranged van der Waals interactions.[164,165] By this approach, proteins are treated as colloidal spheres that interact isotropically with salt ions through symmetric van der Walls and electrostatic interactions.

A simplified scheme of the DLVO interaction potential energy is represented in **Figure 16**.

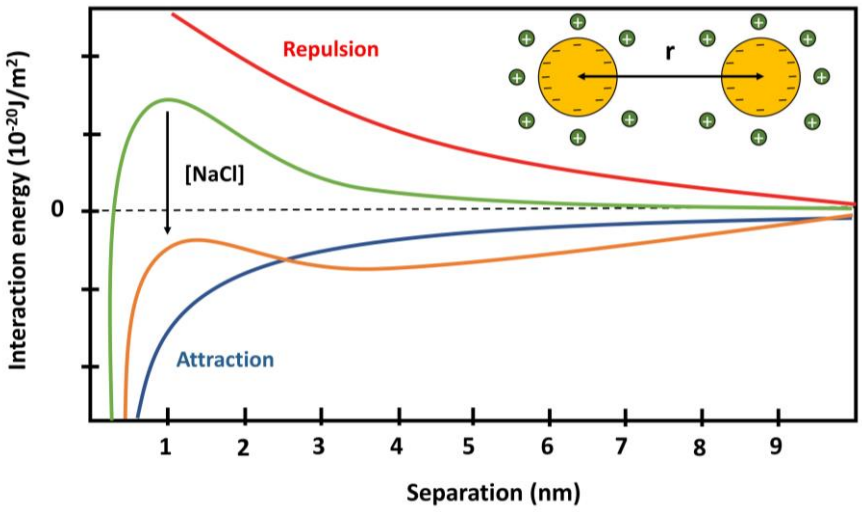

Figure 16 – Schematic representation of DLVO interaction potential energy – The DLVO interaction energy (green and orange line) results from the sum of the repulsive electrostatic energy (red) and the attractive van der Walls potential (blue). Increased electrolyte concentration and/or reduced particle charge density can lead to a minimum in the potential energy. As a result, particles might undergo reversible aggregation due to the decrease in the energy barrier.[166]

Interacting particles such as proteins exhibit an overall net charged surface based on the pH of the solution and depending on the pI of the protein. Salt ions dissolved in the solution are able to form counterion cloud around the protein surface, screening the surface charge. By decreasing the DLVO interaction potential, salt ions effectively decrease the repulsive interactions, promoting self-aggregation.[166,167]

Based on the DLVO theory, at pH 9.40, the electric double-layer repulsion between the FUS proteins should be small (due to FUS neutral charge) and the net DLVO interaction should mainly arise from the attractive van der Waals force. Due to reduced surface charge density complemented with increasing salt ions concentration (150 mM NaCl), the energy barrier falls below zero and the protein self-assembles rapidly.

It would be expected that above a certain ionic strength value, the self-assembly would be proportional to the NaCl concentration until it reached a plateau. Such value is commonly termed as critical coagulation concentration (CCC), and it is defined as the minimal required concentration of counterions to induce aggregation of colloidal particles.[168] As suggested by Mason *et al*., the fact that the LLPS process is sensitive to the presence of electrolytes suggests that the intermolecular attractive interactions have also an electrostatic character.[17] In other words, the results obtained indicate that certain NaCl concentrations might partially screen crucial intermolecular electrostatic interactions, decreasing droplet formation as observed at 300 mM NaCl. Hence, at 300 mM NaCl, ionic strength hinders intermolecular attractive interactions, and aggregation promoting charge screening cannot be accountable.

In the case when FUS is not neutrally charged, a low variation in the degree of LLPS in the presence of NaCl, is observed. Approaching once again through the DLVO theory, these results suggest that charge screening by salt ions is ineffective, perhaps due to the high protein charge density at pH 7.00 and 11.00. Hence, repulsive forces cannot be canceled, and phase separation is not enhanced with increasing ionic

strength. However, comparing the variation in turbidity with respect to changes in ionic strength at pH 7.00 and 11.00, it is observed a higher variation in phase separation behavior at pH 11.00. Moreover, at pH 7.00, phase separation remains very insensitive to changes in ionic strength. To try to understand this difference, the protein net charge with respect to the pH was calculated through **Equation 1**:

$$Net\ charge = \sum_{i=1}^{n} q_i f_i \quad (1)$$

Where *qi* and *fi* are the charge and the fraction of the *i*th ionizable group in the charged state, respectively.[169] The fraction of ionized negatively and positively charged groups, derived from the Henderson-Hasselbalch equation, is expressed as **Equation 2**:

$$f(-) = \frac{10^{(pH-pK_a)}}{10^{(pH-pK_a)}+1} \quad (2)$$

$$f(+) = \frac{10^{(pK_a-pH)}}{10^{(pK_a-pH)}+1}$$

To calculate protein net charge as a function of pH, it was assumed the set of pK_a values of ionizable groups used by ExPASy software, from Bjellqvist *et al*.[170] The results are presented in **Figure 17**.

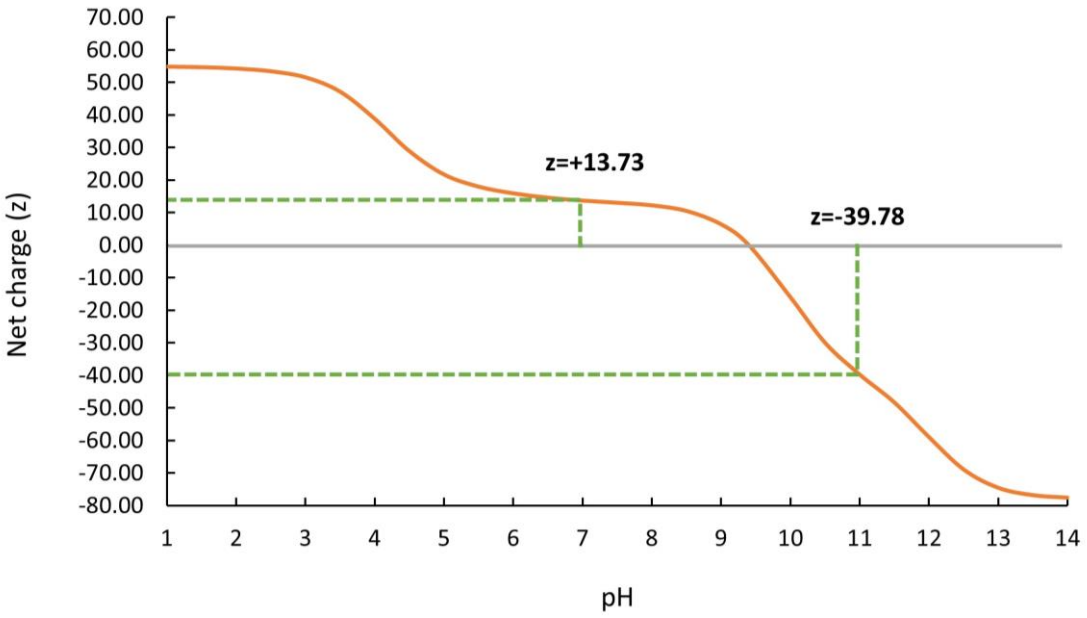

Figure 17 – Plot of FUS net charge as a function of pH – FUS is a basic protein with a pI of 9.40. At pH 7.00 FUS has an overall positive charge of z=+13.73, at pH 9.40 FUS is neutrally charged with z=0 and at pH 11.00 FUS bears an overall negative charge of z=-39.78. Protein net charged calculated according to the set of pK_a values from Bjellqvist *et al*.[170]

From the relationship between FUS net charge and pH, one might expect that since charge density is higher in magnitude at pH 11.00, charge screening would prove more difficult than at pH 7.00. Yet, the turbidity results suggest otherwise.

Explanation to these results might be based in the specific nature of each ion. The Hofmeister series classify ions according to their ability to salt in or salt out proteins (**Figure 18**).[171]

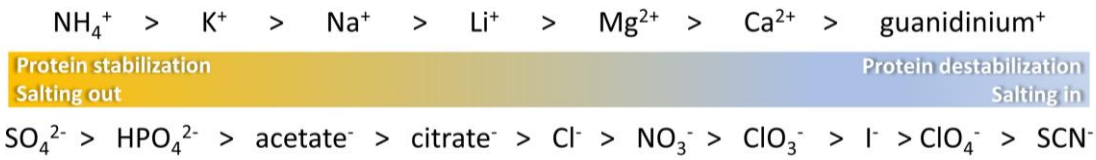

Figure 18 – Cationic and anionic Hofmeister series – Ions are ordered by the ability to stabilize or destabilize proteins, by salting out or salting in, respectively.[172]

Na^+ and Cl^- are strongly hydrated cation and anion, respectively. Cations usually follow the Hofmeister order, with strongly hydrated cations being less efficient in salting out proteins than weakly hydrated ones. However, for anions is not straightforward, having different effects when interacting with the protein backbone or with charged side-chains. At the backbone, anions follow the Hofmeister order, with strongly hydrates anions salting out more efficiently than weakly hydrated ones. Still, when interacting with positively charged side-chains, anions follow a reversed Hofmeister series with the effectiveness in salting out ordered as ClO_4^->SCN^->I^- >ClO_3^->NO_3^->Cl^-.[173]

Although the FUS charge density magnitude at pH 11.00 is higher than at pH 7.00, at the later pH FUS is highly positive, and following the reverse Hofmeister series, Cl^- is less effective in screening the positive charged residues. This might explain the low variation of phase separation with increasing ionic strength at pH 7.00 when compared to at pH 11.00.

Finally, Burke *et al*. showed that at pH 7.40, there was an invariance in turbidity until 150 mM NaCl and a significant decline in turbidity at 300 mM NaCl.[174] This decline was not visible in presented study, at pH 7.00. This difference might be explained by the fact that FUS has a higher overall positive charge at pH 7.00 than at pH 7.40, hence intermolecular attractive electrostatic interactions could not be canceled even at 300 mM NaCl. Still, one question remains, the nonlinear dependence of FUS phase separation with ionic strength until 150 mM NaCl, at pH 9.40 and pH 11.00.

Undoubtedly, the study of the effect of ions in proteins is very complex in nature as a consequence of the complexity of both proteins and ions, and the wide range of interplaying interactions and variables. Since Hofmeister, several efforts have been made to rationalize the protein solution behavior in the presence of ions, and it is still not completely understood.[173,175-179] Adding the complexity of phase separation into such equation, makes the observations much more difficult to justify. Further studies would have to be carried out to gain insight on the exact influence of NaCl in the phase separation mechanism of FUS.

Glucose

The second abundant metabolite tested was glucose. This sugar is one of the most abundant organic metabolites found in the human serum, with a concentration of ~5 mM.[180] The intracellular glucose concentration is estimated to be between 0 and 1 mM, since glucose is rapidly phosphorylated into glucose-6-phosphate inside the cells.[181] The results of the turbidity assays of FUS in the presence of glucose are represented in **Figure 19.**

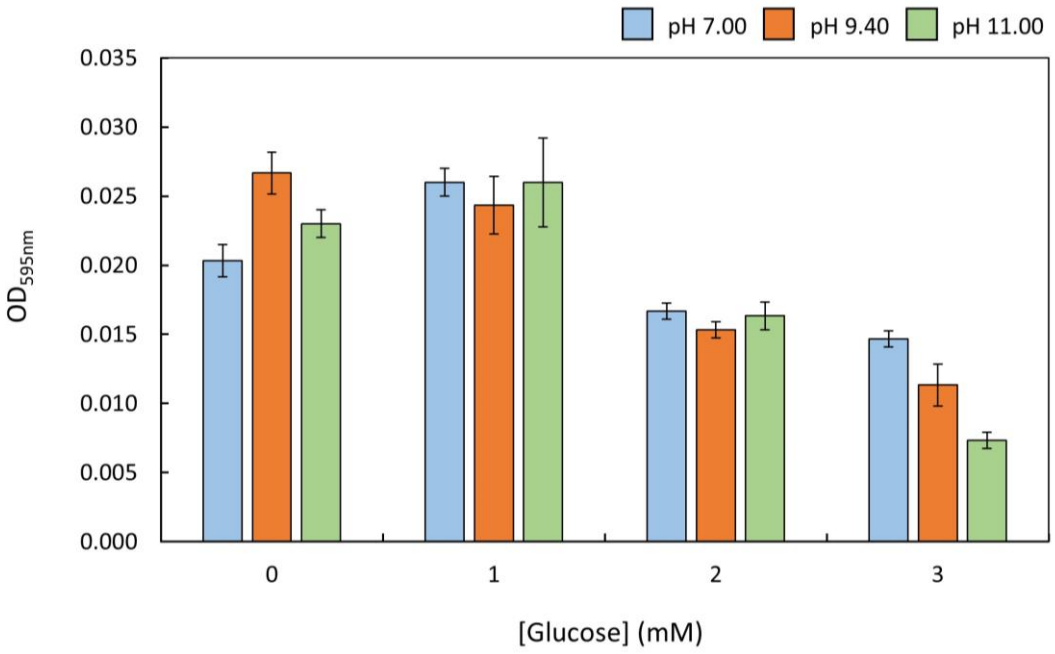

Figure 19 - Influence of glucose on FUS phase separation – Monitorization of 5 μM FUS phase separation in the presence of increasing glucose concentration. Turbidity assays were performed at 4ºC. Data collected 10 min after addition of lyophilized FUS to the solutions. Data represented as the mean of three independent measurements, with standard deviation error bars.

In the presence of glucose, FUS phase separation in all tested pH values seems to follow the same overall pattern, with droplet formation decreasing with increasing glucose concentration. Only exception is at pH 7.00, when turbidity slightly increases at 1 mM glucose.

Glucose is a well-known metabolite able to stabilize proteins through induced preferential hydration. Addition of sugars to a protein solution results in a positive free energy change, and its value is proportional to the protein surface area.[182]

In an IDP the surface area is higher when compared to a globular protein, hence the contact of sugar with an IDP is thermodynamically more unfavorable than with a globular protein (*i.e.* sugar molecules are largely excluded from the protein surface). As a result, an IDP as a greater preferential hydration than a globular protein in the presence of a sugar.[183] In other words, in aqueous solution all points on the protein surface must be in contact with water. In order to interact, solutes must displace water molecules from the protein surface. Simplistically, preferential interactions are balanced by the competition equilibrium between water and ligands at the surface of

the protein.[184] Therefore, the free energy of binding at a protein site (ΔG^b) is defined by **Equation 3**:

$$\Delta G^b = \Delta G^L - \Delta G^W \quad (3)$$

Where ΔG^L and ΔG^W are the free energies of interaction of the protein with the ligand and with water, respectively. If the free energy has a negative sign, there is a preferential binding to the ligand. On the order hand, if the free energy has a positive sign, there is a preferential binding to the water, and hence preferential hydration. The positive change in chemical potential induced by sugars should favor the self-assembly state of FUS, as the total surface area of the protein decreases upon FUS-FUS association, which would result in reduction of the chemical potential.[184] Such effect is not clear through the turbidity assays. A simple explanation might be in the base that glucose can lead to compaction through intramolecular interactions rather than intermolecular. This would suggest that the intrinsic disorder of FUS is important for its phase separation, has the compaction can lead to inaccessibility of FUS domains that participate in LLPS.

Moreover, over three decades ago, Na *et al*. observed that glycerol solution inhibited the self-assembly of collagen fibrils. Glycerol, such as glucose, is known to stabilize proteins through preferential hydration and has such, should also promote self-assembly of structured proteins and not inhibit it.[185] They found that, the effect of glycerol in the inhibition directly correlated with the critical association concentration of collagen. Hence, with increasing concentrations of glycerol, higher concentration of protein would be needed to promote self-assembly.[185] Although glycerol is a stabilizer co-solute, that promote protein compaction by preferential hydration, is widely known that glycerol prevents protein aggregation, being routinely used in protein refolding. Vincent *et al*. showed the mechanisms underlying the contradicting effects of glycerol. Besides the known effect of the induced preferential hydration that leads towards assembly and compaction, the researchers proposed that glycerol prevents protein self-assembly by stabilizing aggregation-prone domains of the protein through preferential interactions with hydrophobic residues that favor the interface orientation of glycerol.[186] This effect might justify the results obtained. The inhibition of FUS phase separation by glucose might indicate that the FUS LLPS is also mediated by hydrophobic interactions. In fact, it was observed visually that 10% glycerol prevented FUS phase separation, even at low temperature.

A full thermodynamic analysis would have to be performed to confirm these results, including the thermodynamic contribution of the cosolvent interactions and the decomposition of measured preferential binding into the protein surface by cosolvent and water. Nevertheless, the results obtained clearly indicate that glucose inhibits FUS phase separation whether by the screening of crucial hydrophobic residues or by FUS structural compaction.

Metal ions (Zn^{2+} and Ca^{2+})

The next step was to study the influence of calcium (II) and zinc (II) ions on FUS phase separation. The intracellular concentration of free metallic ions such as Zn^{2+} and Ca^{2+} is very low, ranging from ~0.5 nM for Zn^{2+} and ~85 nM for Ca^{2+}, since they

are mostly bound to proteins or stored within organelles.[187,188] These ions are known to play crucial structural and functional roles in proteins.[96,189-197]

Zinc (II) is an essential trace element in eukaryotes. Despite its low intracellular concentration, zinc is the second most abundant trace metal in higher animals, falling only behind iron. On average, the adult human body bears about 2.3 g of zinc, taking into account the free and bound form.[192] Intracellularly, the total concentration of Zn^{2+} is in the range of 180-250 μM.[190]

FUS contains a non-classical ZnF known to play a dominant role in RNA recognition (see section ***1.3.1 FUS structural architecture and function***). Contrarily to the previous studied metabolites, Zn^{2+} can directly bind to FUS through the ZnF domain. The influence of $ZnCl_2$ salt ion in FUS phase separation was investigated and the results are present in **Figure 20**.

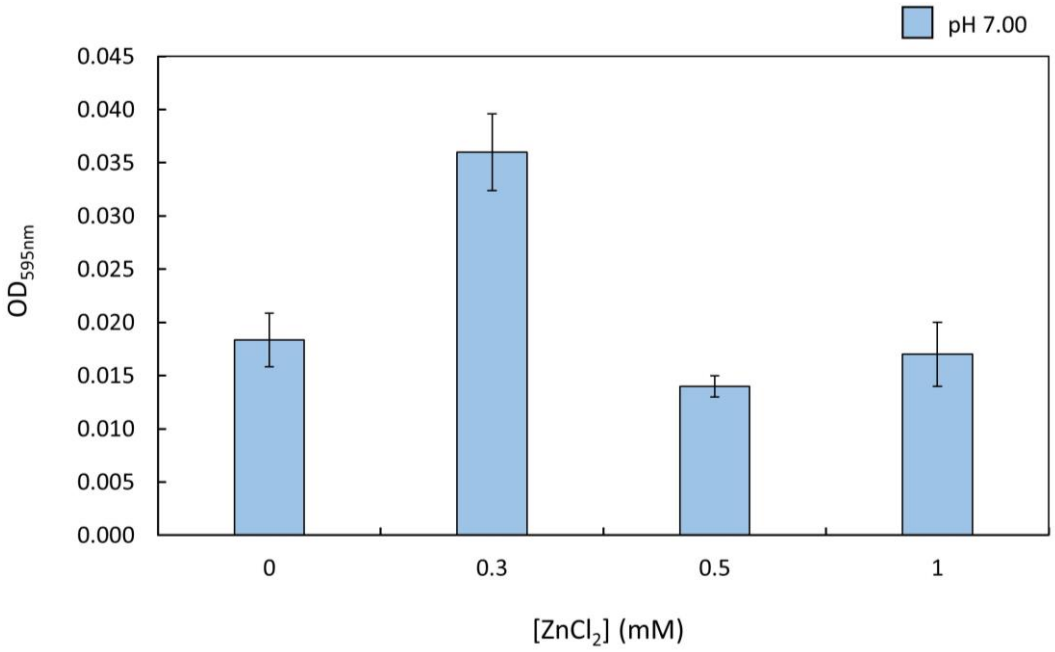

Figure 20 – Influence of $ZnCl_2$ on FUS phase separation – Monitorization of 5 μM FUS phase separation in the presence of increasing $ZnCl_2$ concentration. Turbidity assays were performed at 4ºC only at pH 7.00 due to decrease in Zn^{2+} solubility at higher pH values. Data collected 10 min after addition of lyophilized FUS to the solutions. Data represented as the mean of three independent measurements, with standard deviation error bars.

As mentioned before, the solubility of Zn^{2+} decreases rapidly with increasing pH, with formation of white precipitates at pH 9.40 and pH 11.00.[198] As a result, the turbidity assays were only performed at pH 7.00.

Up to this point, phase separation of FUS at pH 7.00 has not been significantly enhanced by metabolites. However, in the presence of 0.3 mM $ZnCl_2$ the turbidity increases almost by 2-fold compared in the absence of $ZnCl_2$.

In FUS, Zn^{2+} can be coordinated by four cysteines at the structured ZnF domain. The coordination of the Zn^{2+} by cysteines is mediated through the cysteine side-chains thiol groups. [191] Hence, the ionization state of the thiol group of cysteine residues modulates the ability of FUS to bind to Zn^{2+}. Compared to all ionizable residues, the pK_a of cysteine thiol group is the closest to the physiological pH (about

7.00).[199] As a result, small variation within the physiological pH range perturbs the ability of cysteine groups to act as nucleophiles and confers significant electrostatic changes.[200]

In the reducing cytoplasmatic environment, disulfide bonds are very unstable compare to thiolate- Zn^{2+}-thiolate bridges. Such interactions allows Zn^{2+} to be tightly bound to the motif and yet available, since oxidant species can oxidize the sulfur groups releasing Zn^{2+} ions. This binding and releasing of zinc ions make ZnF domains efficient redox switches.[189,201]

This suggests that under cellular stress such as photooxidative stress, the intracellular free Zn^{2+} increases. Kroncke *et al*. proposed that free Zn^{2+} activates the phosphoinosite 3'-kinase (PI3K)/Akt signaling cascade which is consider a stress-response cascade that mediates antiapoptotic and cytoprotective effects, gene expression and insulin signaling.[189]

Taking this into account, upon certain stress conditions Zn^{2+} ions released from zinc-binding proteins, activate the PI3K/Akt signaling cascade and at the same time interact with FUS inducing its phase separation, as observed in the turbidity results. This goes accordingly with the fact that FUS droplet formation is known to be induced under stress conditions, including oxidative stress.[202]

Interestingly, in ALS, the PI3K/Atk cascade is normally inhibited which leads to motor neuron apoptosis.[203] In ALS, the inactivation of the PI3K/Atk might render an unanswered response to stress stimuli. The resultant persistent stress might lead to further increase in free Zn^{2+} concentration. As a result, increasing cytoplasmatic Zn^{2+} ions are available to interact with FUS which might enhance FUS self-assembly and ultimately FUS co-depositions, as observed in ALS-FUS.

Despite the role of Zn^{2+} as direct ligand to the ZnF moiety of FUS, Zn^{2+} is a divalent metal ion that can also perform charge screening. Divalent metal ions are capable to interact with the negatively charge side chains. At pH 7.00, both the aspartate and glutamate side-chains are deprotonated, bearing a negative charge. In 2012, it was shown that Zn^{2+} ions screen more efficiently the negative charges, when compared to several other divalent ions. This screening might be implicated in the influence of Zn^{2+} in the enhancement of FUS phase separation.[204] The influence of Zn^{2+} in the LLPS mechanisms is more complicated to justify due to the fact that this metabolite can effectively bind to FUS. Nevertheless, it is clear that FUS phase separation is also sensitive to $ZnCl_2$.

The second metal ion studied was calcium (II). Just like Zn^{2+}, free Ca^{2+} has a low intracellular concentration. However, the total concentration of this metal ion is quite high, going from 20 μM in the erythrocytes to 4 mM in the heart cells. Axons contain between 200-400 μM Ca^{2+}. Intracellular free Ca^{2+} performs a fundamental task in signaling of a large number of physiological activities in numerous subcellular compartments. As a result, this metal ion undergoes large cytosolic concentration fluctuations in response to stimuli.[205]

Since Ca^{2+} is such an important ion in cellular functions and since free Ca^{2+} can reach high concentration in the cytosol, the influence of $CaCl_2$ in FUS LLPS was also explored. The results are present in **Figure 21**.

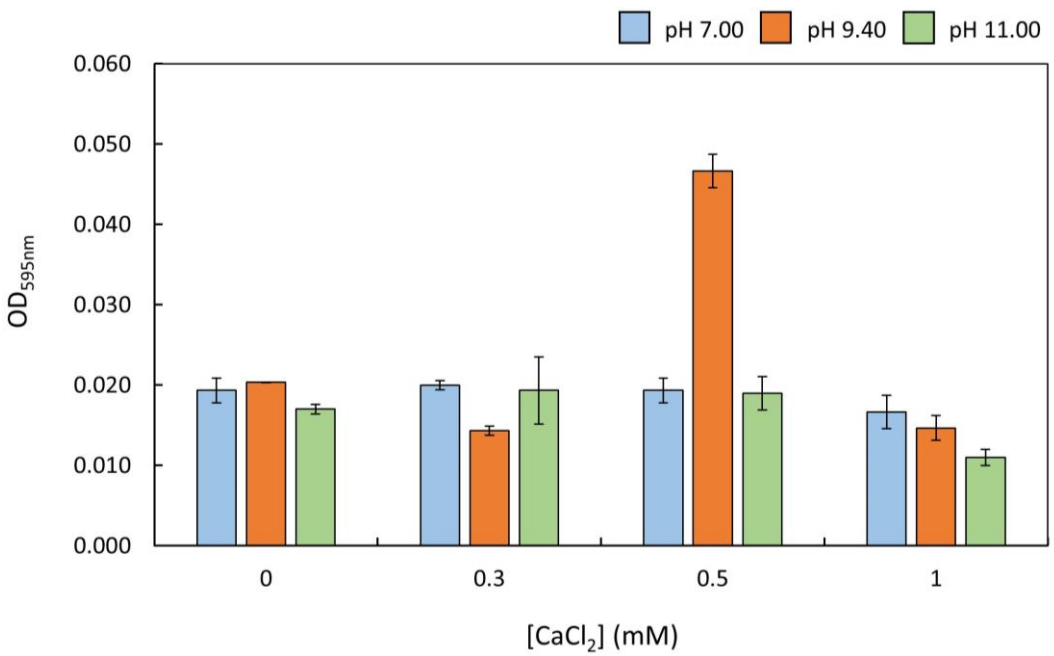

Figure 21 – Influence of $CaCl_2$ on FUS phase separation – Monitorization of 5 μM FUS phase separation in the presence of increasing $CaCl_2$ concentration. Turbidity assays were performed at 4ºC. Data collected 10 min after addition of lyophilized FUS to the solutions. Data represented as the mean of three independent measurements, with standard deviation error bars.

The influence of $CaCl_2$ on FUS phase separation seems to follow the same mechanism as NaCl. It is observable that phase separation is enhanced at pH 9.40, when FUS is neutrally charged. Ca^{2+}, such as Na^+, is a strongly hydrated cation, as a result is less efficient in salting out proteins. However, strongly hydrated cations have strong affinities for negative charged side-chain residues.[173]

The behavior of divalent transition metals and divalent alkali earth cations such as Zn^{2+} and Ca^{2+} is different from that of monovalent cations such as Na^+. Such metal ions can form coordination complexes which leads to charge transfer between metal center and binding ligand. As a result, these interactions lead to stronger binding than those of Hofmeister-type ion pairing. As such, the ion-specificity of divalent first-row metal ions to amines and thiols follows the Irving-Williams series (**Figure 22**).[206]

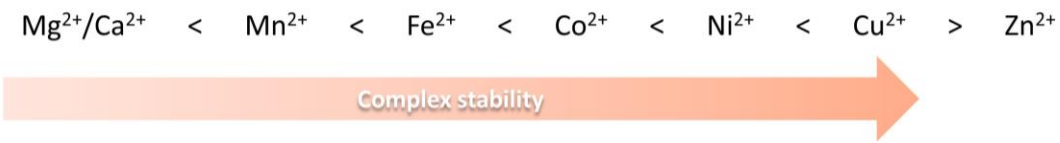

Figure 22– Divalent Irving-Williams series – Divalent ions are ordered by increasing the complex stability formed by the ions and target ligand accompanied by decreasing ionic radius. The only exception is Zn^{2+} that has lower ionic radius but leads to less complex stability.[206]

In this series, as the ionic radius decreases there is an increase in complex stability, the only exception being Zn^{2+}. The driving force in the Irving-Williams order is the charge transfer between the metal and its ligand, which reaches a maximum for Cu^{2+}

and its weaker for the ions on the left of the series. Since Zn^{2+} contains filled d orbitals, the charge transfer is very weak. Nevertheless, these ions can also follow the Hofmeister series, assuming that charge transfer processes with amines and thiols are not involved.[173]

The complex stability between protein-Ca^{2+} is lower than protein-Zn^{2+}. However, Zn^{2+} can directly bind to FUS. Such facts might explain the different influence of both metal ions on FUS phase separation. Nevertheless, the stronger binding between metal ions and the protein comparing to Na^+ and Cl^- ions, might justify the fact that metal ions needs about 300-fold less concentration when compared to NaCl, to reach approximately the same degree of LLPS.

At pH 9.40, FUS is neutrally charged, and as discussed, the electric double-layer repulsion is minimal and phase separation is enhanced. At this pH, both aspartate and glutamate residues have a charge of -2, which may lead to proper charge screening by both metallic ions. At pH 11.00, both these residues also bear a -2 charge, however the charge screening might be ineffective due to the large protein net charge. Again, as discussed in the NaCl case, the low variation in phase separation at pH 7.00 might be justified by the fact that Cl^- is poorly efficient in screening positively charged side-chains. Just as discussed in the NaCl case, the decrease in turbidity above a certain concentration might be due to the screen of important electrostatic interactions.

Increase in intracellular Ca^{2+} concentrations in postsynaptic neuron is known to activate signaling cascade that modulates gene expression, neuronal survival and synaptic plasticity.[207] Interestingly, perturbation in calcium homeostasis has been observed in neurodegenerative diseases such as ALS. This deregulation ultimately leads to Ca^{2+} overload in the cytoplasm which causes severe damage to the cells, mainly by the formation of reactive oxygen species.[208] Once again, FUS phase separation in the cytoplasm might be enhanced by Ca^{2+} overload, in these stress conditions. In fact, high concentrations of cytosolic Ca^{2+} promotes SOD1 protein inclusions, which is a protein also linked to ALS.[209]

Charged amino acids (glutamate and lysine)

The influence of charged amino acids in FUS LLPS was exploit. The cells contain free amino acids pools which provide monomers for protein synthesis and act as energy-providing metabolic intermediates.[210] Glutamate is the most abundant amino acid in the cells with a concentration of ~4.5 mM in the skeletal muscle cells and about 60 mM in synaptic vesicles.[211,212] More than participating in protein synthesis and as a metabolic intermediate, glutamate is the major excitatory neurotransmitter in the nervous system.[213] In average, a mammalian brain contains about 12.25 mM of glutamate.[213] Such high intracellular glutamate concentration must be experienced by cytoplasmatic FUS. The influence of this neurotransmitter in FUS phase separation is presented on **Figure 23**.

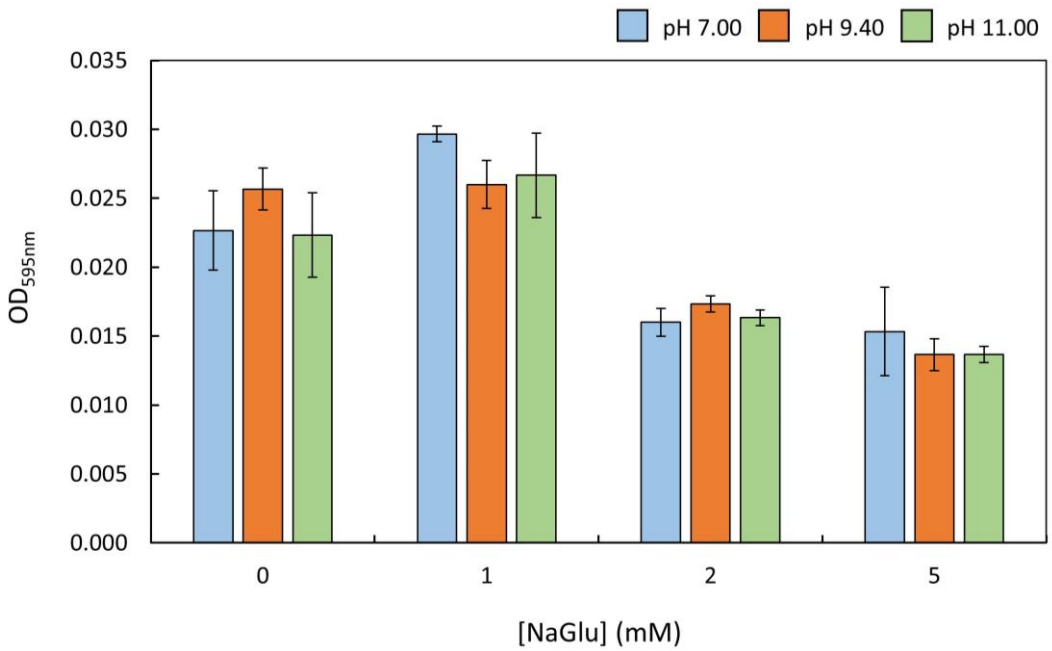

Figure 23– Influence of NaGlu on FUS phase separation – Monitorization of 5 μM FUS phase separation in the presence of increasing NaGlu concentration. Turbidity assays were performed at 4ºC. Data collected 10 min after addition of lyophilized FUS to the solutions. Data represented as the mean of three independent measurements, with standard deviation error bars.

As a free amino acid, glutamate contains three ionizable groups: the backbone amino (-NH_2) and carboxyl groups (-COOH), and the side-chain -COOH group. Depending on the pH of the solution, these groups can be protonated or deprotonated, according to their pK_a values, which confers the overall charge of glutamate. The glutamate charge according to the pH is represented on **Figure 24**.

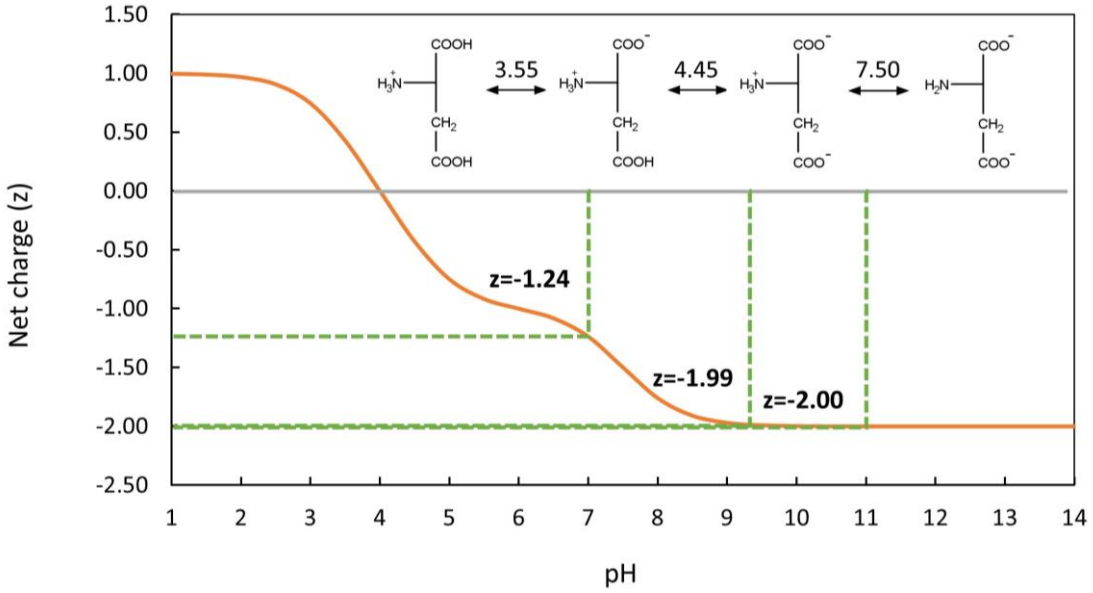

Figure 24 – Plot of free glutamate net charge as a function of pH – Free glutamate contains three ionizable groups which confers a positive charge at pH below 3.55 and negative charge above that pH. At pH 7.00, 9.40 and 11.00, this metabolite has an overall negative charge. Amino acid net charged calculated according to the set of pK_a values from Bjellqvist *et al*.[170]

As represented by **Figure 24**, the overall charge of glutamate is negative at every pH employed in the turbidity assays.

In the presence of NaGlu, a low disparity in phase separation between each pH is observed, as seen previously with glucose. A small increase in phase separation is detected with 1 mM glutamate, followed by an accentuated decline with the increase of the metabolite concentration.

In 1984, Tsutomu *et al*. studied the mechanism of action of NaGlu in protein stabilization.[214] The authors demonstrated that for all studied proteins there was a large preferential hydration in the presence of NaGlu. As discussed previously, preferential hydration can lead to protein compaction or protein self-assembly, in order to reduce the interacting surface. Moreover, over 4 decades ago, it was observed that the mechanism of NaGlu action is largely dependent on its concentration. NaGlu is able to stabilize tubulin at low concentrations and enhance self-association at 1 M.[215]

The turbidity data seem to indicate that in the current case, and similar to the glucose condition, NaGlu might be stabilizing FUS by compaction, inhibiting the LLPS. As proposed earlier, intrinsic disorder might be crucial for FUS phase separation, as compaction can lead to inaccessibility of FUS domains that participate in intermolecular interactions.

On another hand, as observed at the time by Tsutomu *et al*., the stabilization by NaGlu is largely influence by the chemical nature of the protein surface.[214] This might be due to the ability of glutamate to directly interact with residues of the protein. Negatively charged glutamate can form salt bridges with positively charged residues on the protein surface.[216]

As a result, not only accounting for the probable compaction of FUS that leads to intermolecular interactions inaccessibility, glutamate might also be hindering positively charged amino acids that are crucial for FUS phase separation.

The small increase in turbidity with 1 mM of glutamate, might be due to partial screening of the positive charges by the negatively charged glutamate. This enhancement is observed specially at pH 7.00 due to the positive net charge of FUS. Nonetheless, it was detected that as NaGlu concentration raises there is a progressive inhibition of FUS phase separation, which might be a result of the increase in preferential hydration and salt bridge formation.

In ALS, neurons can release high amounts of intracellular glutamate which leads to over-activation of glutamate receptor. Subsequently, there is an excessive synaptic transmission that leads to a high influx of Ca^{2+} ions into the neurons, and as referred before, causes a widespread damage to cellular structures.[217] As a result, low intracellular glutamate in ALS damaged neurons leads to high concentration of Ca^{2+}, which, as observed previously, leads to FUS phase separation. High glutamate concentration in healthy neurons, buffers phase separation, inhibiting FUS droplet formation.

In the human body, lysine participates mainly in protein synthesis, playing an important role in protein structure due to its ability to form salt bridges with negatively charged residues. The intracellular concentration of free lysine is quite high, since it needs to be available to be incorporated in newly synthetized proteins. The average concentration of free lysine in a cell is ~1.15 mM.[212] The influence of this positively charged amino acid in FUS droplet formation was studied and the results are presented in **Figure 25**.

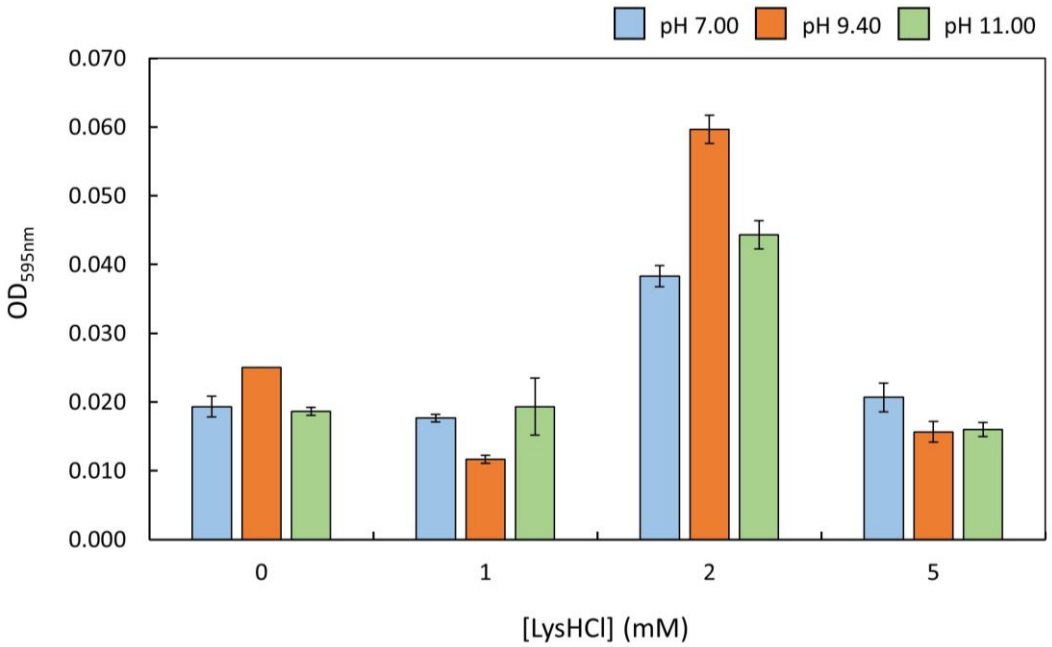

Figure 25 – Influence of LysHCl on FUS phase separation – Monitorization of 5 μM FUS phase separation in the presence of increasing LysHCl concentration. Turbidity assays were performed at 4ºC. Data collected 10 min after addition of lyophilized FUS to the solutions. Data represented as the mean of three independent measurements, with standard deviation error bars.

Lysine is also a polar amino acid which bears a positive charge at physiological pH. Such as glutamate, lysine as a free amino acid also has three ionizable groups: the backbone -NH_2 and -COOH groups, and the side-chain -NH_2 group. The charge of lysine according to the pH is represented on **Figure 26**.

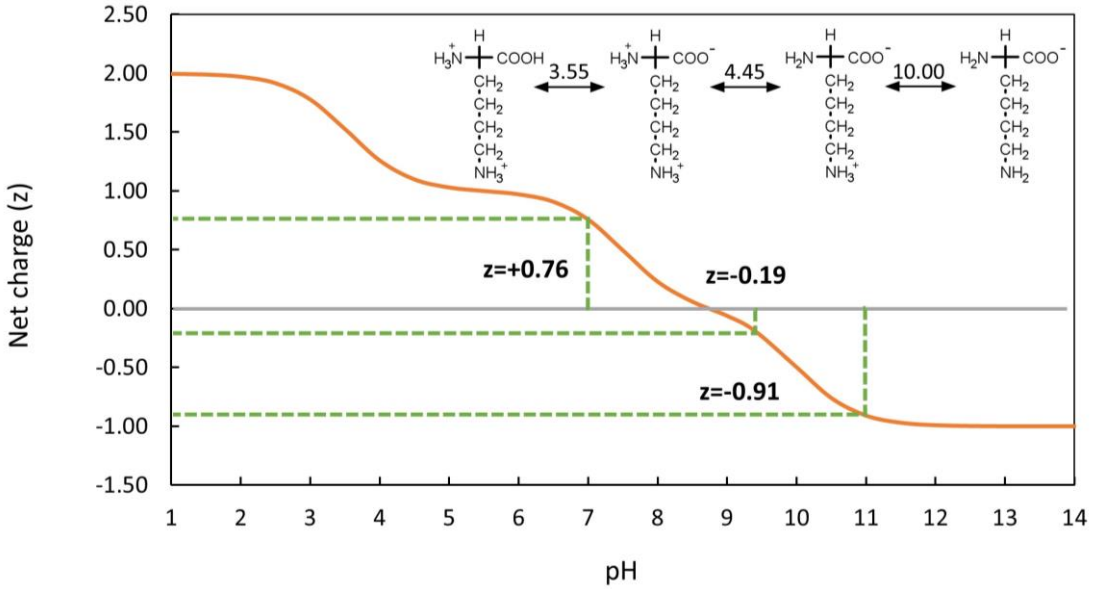

Figure 26 – Plot of free lysine net charge as a function of pH – Free lysine contains three ionizable groups which confers a positive charge at pH below 8.75 and negative charge above that pH. At pH 7.00, this metabolite has an overall positive charge. At pH 9.40 and 11, free lysine has a negative charge. Amino acid net charged calculated according to the set of pK_a values from Bjellqvist *et al*.[170]

Contrarily to glutamate and as observed in the **Figure 26** , lysine has different charges at the different pH values employed in the turbidity assays.

In the presence of LysHCl, it is observed a phase separation pattern similar to NaCl and $CaCl_2$, in which there is an enhancement in LLPS at pH 9.40, at the approximate physiological metabolite concentration.

Again, in the 1984 paper by Tsutomu *et al*, the authors also explored the influence of LysHCl in the stabilization of tubulin. Compared with NaGlu, LysHCl is a weaker protein stabilizer reflected by the lower induced preferential hydration.[214] As a result, FUS compaction might not be as effective and consequently, LysHCl does not disturb the intrinsic disorder of FUS that might be crucial for the phase separation process.

Lysine can interact directly with the protein, forming salt bridges with negatively charged residues. This interaction would be expected only at pH 7.00, when lysine is positively charged. Just as in the case of glutamate, one would expect that salt bridge formation would inhibit phase separation due to blocking of important residues for the LLPS process. However, by the data presented, it is observed that lysine does not inhibit phase separation at pH 7.00. This might be due to the fact that at this pH free lysine has a low positive net charge (z=+0.76) resulting in a weaker interaction between lysine and protein residues. At pH 9.40 and 11.00, free lysine has an overall negative charge and salt bridge formation with the protein is not expected. As mentioned before, FUS phase separation in the presence of LysHCl highly resembles the influence of NaCl and $CaCl_2$. At pH 9.40, although free lysine is negative, it has

an overall net charge close to zero (z=-0.19). The zwitterionic character of lysine at this pH, with a negative -COO^- group and a positive -NH_3^+, might result screening of the protein surface. Along with the neutral charge of FUS at this pH, phase separation is enhanced. Such behavior of lysine would justify the resemblance of turbidity data between LysHCl, NaCl and $CaCl_2$.

RNA

Finally, the influence of RNA on FUS LLPS was explored. As mentioned in the introduction, membraneless cytosolic bodies are composed of RNA and RNPs that assemble from pools of stalled mRNA. FUS is an RNP that is able to bind to RNA through the RRM, RGG and ZnF motifs. Therefore, it was tested wheter RNA can drive FUS phase separation and the results are presented on **Figure 27**.

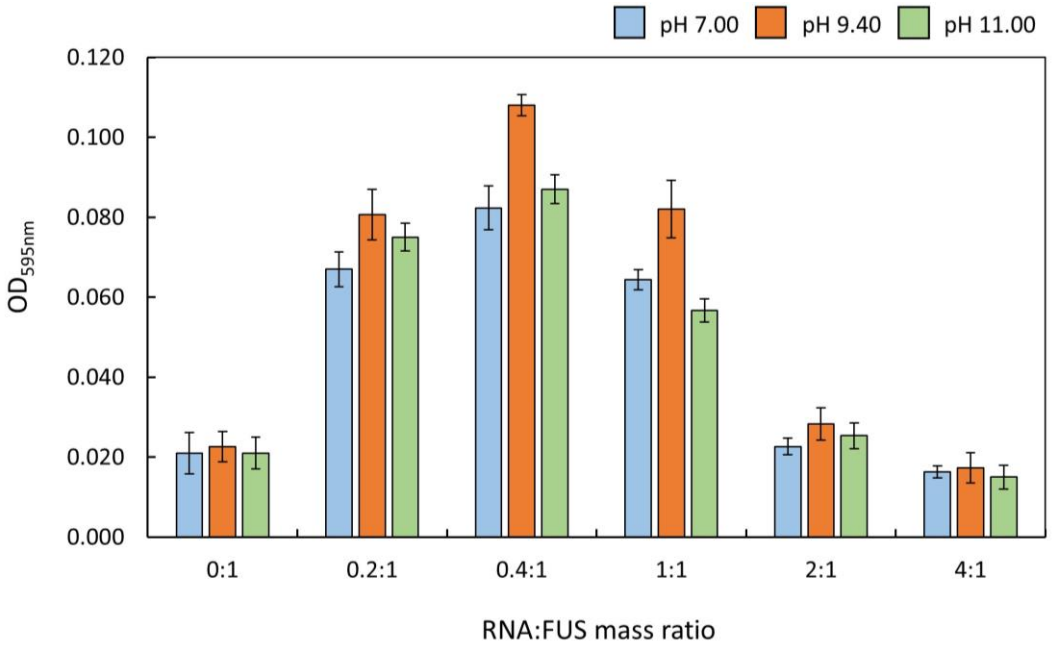

Figure 27 – Influence of total RNA on FUS phase separation – Monitorization of 5 μM FUS phase separation in the presence of increasing RNA:FUS mass ratio. Turbidity assays were performed at 4ºC. Data collected 10 min after addition of lyophilized FUS to the solutions. Data represented as the mean of three independent measurements, with standard deviation error bars.

In agreement with previous work, it was observed that RNA promotes significantly phase separation at very low RNA/protein ratios.[12,218] Remarkably, increasing RNA/protein ratios led to inhibition of FUS assembly. Such behavior has been observed by Maharana *et al*., and it was suggested that RNA as the ability to buffer FUS self-assembly.[219] In the nucleus, the RNA concentration is higher than in the cytoplasm. As such, in the nucleus FUS is kept soluble and in a non-toxic state. Upon stress conditions, cytoplasmatic FUS undergoes phase separation and forms stress granules. After the removal of stress, FUS can shuttle back to the nucleus where the stress granules are dissolved, and the protein can return to its regular nuclear functions.[219]

Interestingly, in 2011, it was showed that ALS-causing FUS mutations increased the interaction of FUS with cytoplasmatic RNA.[89] As previously referred, ALS-FUS is characterized by cytoplasmatic deposition of FUS due to improper reimportation of FUS into the nucleus.[110,116] Increased FUS cytoplasmatic concentration together with increased interaction with target cytoplasmatic RNA, supported by the ability of RNA to drive FUS self-assembly, could reinforce the formation of FUS aggregates present in ALS-FUS.

The mechanism by which RNA can enhance FUS phase separation and inhibition is not completely understood. The first complication arises from the complexity of RNA. RNA is a nucleic acid composed of an array of nucleotides. All nucleotides are characterized by a phosphate group which is linked to a ribose that is in turn linked to an organic base. In RNA, the organic bases are adenine (A), guanine (G), cytosine (C) and uracil (U). Unlike DNA, RNA can assume an array of secondary structures such as stem-loops, hairpins, pseudoknots, etc.[220] The second complication arises from the fact that RNA can bind to multiple FUS domains: The RRM, the ZnF and RGG domains. The third complication comes from the array of different interactions that are involved in protein-RNA complexes.[221]

FUS contains a βαββαβ-type of RRM, which forms a four-stranded β-sheet packed against two α-helices (see section ***1.3.1 FUS structural architecture and function***, **Figure 6**). The RRM-RNA interaction in this type of RRM topology is usually at the β-sheet interface, through π-stacking, hydrogen bonding and electrostatic interactions.[222] However, since in FUS several aromatic acids are absent in the RRM motif, π -stacking is not the primary interaction mechanism between FUS-RNA. As a result, in the RRM motif affinity and specificity towards DNA is very low.[88] As referred in the introduction, in the RRM domain the "KK" loop is known to be crucial for nucleic acid binding through electrostatic interactions. In the RGG motifs, RNA binding is through arginine residues that interact with nucleotide bases via hydrogen bonding and π-stacking.[223] In the ZnF domains, RNA recognition is usually modulated through hydrogen bonding and π staking with the nucleotide bases.[224]

Despite this intricate network in RNA-FUS interaction, it is clear that RNA interaction, either through RRM, RGG or ZnF motif, enhances phase separation. This suggests that these motifs contribute to FUS LLPS process. In fact, Burke *et al*. demonstrated that RNA does not enhance FUS LC domain phase separation.[174] Moreover, at high RNA:FUS ratios, all RNA must be bound to FUS which suggests that inhibition is either mediated by the free RNA in solution, or by the continuous interaction with FUS that hinders possible FUS-FUS interactions.

Taken together, it was shown that FUS droplet formation is readily reversible and very responsive to changes in the environmental conditions. It was observed that LLPS is highly sensitive to the nature and concentration of different metabolites in a pH dependent manner. In detail, FUS phase separation is greatly induced when the protein has an overall neutral charge. In such conditions, the electric-double layer repulsion is reduced and FUS self-assembly is promoted through attractive interactions. Charged electrolytes dissolved in solution, such as NaCl, $ZnCl_2$ and $CaCl_2$, promoted FUS phase separation by effectively charge screening the protein's surface, resulting in a complemented reduction of the repulsive interactions between FUS proteins. Divalent ions promoted FUS phase separation at a greater extent when compared to monovalent ions, since they are able to form coordination complexes

that lead to a more efficient charge screening at lower concentrations. The zwitterionic character of lysine at pH 9.40 might also result in charge screening of the protein surface, leading to an enhancement of LLPS. Moreover, stabilizing metabolites that induce preferential hydration, such as glucose and glutamate, inhibited phase separation by either protein compaction or destabilization of important intermolecular interactions. Glucose is able to destabilize hydrophobic interactions, while glutamate destabilizes electrostatic interactions. This might suggest that LLPS is mediated by both hydrophobic and electrostatic interactions. Inhibition by protein compaction suggest that intrinsic disorder of FUS is crucial for the self-assembly mechanisms. Metabolites that can directly bind to FUS, such as Zn^{2+} and RNA, greatly induced FUS LLPS. This finding suggests that both domains that bind to these metabolites, the RRM and ZnF motif, might mediate FUS self-assembly.

Interestingly, more than being sensitive to the nature of the metabolites, it was demonstrated that FUS LLPS is also highly dependent on their concentration. Although phase separation inhibition by either glucose or glutamate followed a linear dependence, with higher concentration of metabolite leading to a higher inhibition, enhancement by promoting metabolites seemed finely tuned by the metabolite concentration. Above a certain critical concentration that led to a maximum in FUS self-assembly, there is a sudden inhibition of the LLPS process. Such finding demonstrates that LLPS is very sensitive to an optimal concentration of promoting metabolites. Above that concentration, charge screening might hinder crucial electrostatic interactions and lead to inhibition of self-assembly, once again reinforcing the idea that FUS LLPS has an electrostatic character.

3.4 Imaging of FUS granules

Direct observation of *in vitro* phase-separated FUS was performed using a confocal laser scanning microscope at two FUS concentrations: 200 μM and 1 M.

Since measurements were performed at room temperature, phase separation was induced in a 20 mM CAPS buffer at pH 9.40 containing 150 mM NaCl. Lyophilized FUS was added as the last component to the sample to induce uniform phase separation. The microscopic observations are presented in **Figure 28.**

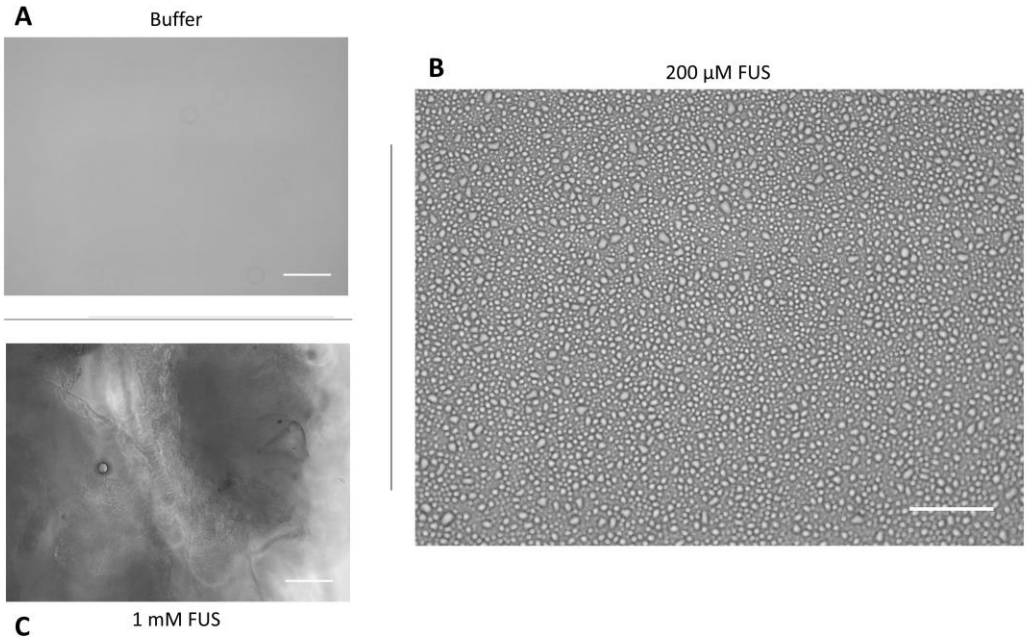

Figure 28 – Observation of *in vitro* FUS phase separation by confocal microscopy – (A) Control sample containing phase separation buffer (20 mM CAPS and 150 mM NaCl, at pH 9.40) without protein. **(B)** Liquid-liquid phase separation of 200 µM FUS in solution. **(C)** Liquid-solid phase separation of 1 mM FUS in solution. 10 µL of each solution was mounted on a glass slide and covered with a glass coverslip. Images obtained were processed by Fiji software.[147] Scale bars represent 50 µm.

As a control, phase separation buffer was imaged and presented no visible droplets (**Figure 28A**). At 200 µM FUS, it was observed the appearance of several droplets throughout the entire sample indicative of FUS phase separation (**Figure 28B**). However, phase-separated droplets normally exhibit a spherical fluid morphology in solution due to the tendency of liquids to adopt a spherical shape to minimize their surface area[34]. In the images obtained, droplets seem to vary in morphology with several displaying irregular shapes. In the glass apparatus used, adhesion forces between the droplets and the glass overcome the cohesion forces between the components in the droplet.[225] As a result, droplets exhibit wetting on the glass apparatus resulting in irregular shapes. Usually, phase-separated droplets are imaged in suspension by the use of an inverted microscope along with suitable vessels that contain surfaces with non-binding properties.[124,151,219] As a result, droplets are not enclosed between a glass slide and a cover slip, being possible to image them in suspension. Even if they settle in the bottom, the non-binding surfaces keeps the droplets spherical. Nevertheless, imaging droplets in the classical glass apparatus can provide useful information.

Processing the obtained image in the Fiji software to detect edges, enables a better visualization of the protein droplets (**Figure 29**).

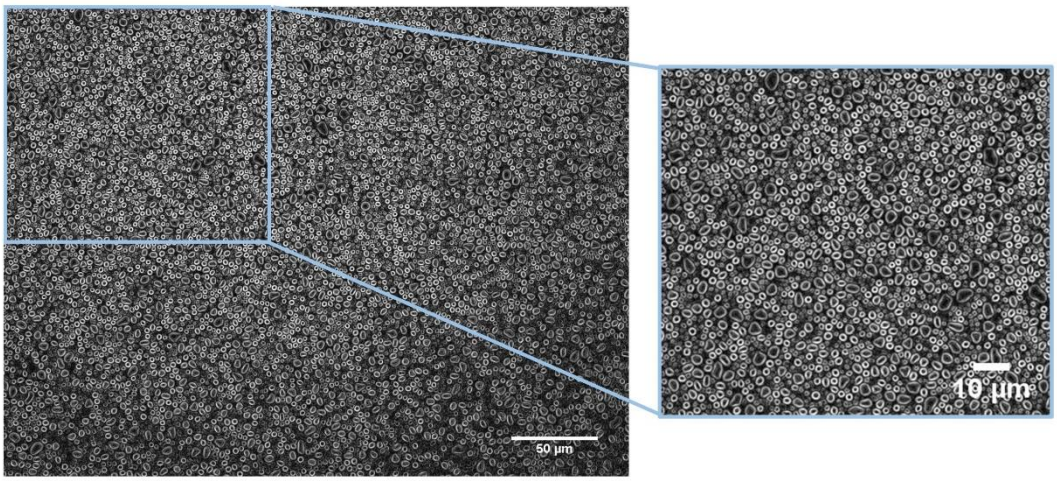

Figure 29 – Edge detection of the 200 µM FUS microscope image – Confocal microscope image processed by Fiji software.[147]

By edge detection it is easier to perceive the amount of protein droplets in the phase-separated solution. The different sizes observed suggests fusion events between droplets that result in the formation of larger droplets. Wetting and fusion behavior is indicative of the liquid nature of FUS droplets.[11]

At 1 mM FUS (**Figure 28C**), protein aggregation is observed throughout the sample indicating a liquid-solid phase separation. The transition from liquid-liquid to liquid-solid phase separation has been observed to be dependent on several factors, including time and protein concentration. In fact, Avinhash *et al*. demonstrated that FUS forms a fibrous hydrogel at 500 µM, which goes in agreement with the aggregation observed at 1 mM FUS.[120] Protein aggregation observed was irreversible, and its solubilization could not be achieved.

By *in vitro* microscopic observation it was possible to visualize FUS phase separation. At 200 µM FUS, it was observed protein droplets spread across the entire sample. The observed wetting and fusion behavior is indicative of the liquid nature of FUS droplets. Moreover, as expected, FUS irreversible aggregation is dependent on the protein's concentration.

3.5 NMR experiments

FUS is an overall intrinsically disordered protein. From the total 526 amino acids, only 117 are contained within a structured region, meaning that almost ~78% of the protein is structurally disordered.

The NMR technique plays a crucial role in the characterization of IDPs as it is the only spectroscopic technique that provides atomic-level structural and dynamic information of disordered and highly dynamic proteins.[226] The use of two-dimensional ^{1}H-^{15}N HSQC, which correlates the nitrogen and the amide the proton present in the backbone and side-chains of some amino acids, provides a signature of the protein. Each perturbation upon the protein can be accompanied by the chemical shift deviation of the affected amino acids. Such experiment is useful as it can easily identify IDPs since the high flexibility and disorder of IDPs has several consequences in the ^{1}H-^{15}N HSQC spectra. The first consequence is the low chemical shift dispersion

in ^{1}H-^{15}N HSQC spectra. This consequence arises from the conformational averaging due to the high dynamic and flexibility of the disordered chains, which collapses the chemical shifts in the random coil region (near ^{1}H 8.50 ppm) and causes resonance overlap. Chemical shifts are sensitive to local chemical environment of the given nuclei. In an IDP, the constant interconverting conformations lead to an average chemical environment, so chemical shifts resonate at nearly identical frequencies. Low chemical shift dispersion is more pronounced in ^{1}H than in other nuclei such as ^{13}C and ^{15}N, since there is no hydrogen bond network that would result in dispersive proton chemical shifts.[227] The second consequence is the broadening of the ^{1}H-^{15}N HSQC signals due to the exposure of the IDP's backbone to the solvent. Such exposure leads to extensive exchange processes between the amide protons and the water protons, resulting in loss of ^{1}H-^{15}N HSQC correlation signals.[228] In the studied case, although FUS is an overall IDP, it contains two globular domains that are expected to give rise to dispersed chemical shifts. Moreover, although the unstructured domains of FUS provide poor signals, if the temperature affects significantly the unstructured domains of FUS, it can be possible to identify the chemical shifts deviations.

3.5.1 Temperature influence on FUS structure

As previously observed, FUS phase separation is highly temperature dependent, displaying a UCST LLPS behavior (see section ***2.3.1 Temperature influence on FUS liquid-liquid phase separation***). As a result, it was interrogated if the temperature could have an effect on the overall FUS structure. For that purpose, the structure of dispersed FUS was examined by ^{1}H-^{15}N HSQC experiments, upon variations in temperature. To remove spectral analysis complications that would arise from the droplet formation at low temperature, FUS was maintained dispersed throughout the experiments by the use of 10% glycerol and 1 mM DTT. Since it was observed that FUS droplet formation is not only dependent but also reversible with temperature, two consecutive experiments were performed: the first one with decreasing temperature following the order of 25ºC → 15ºC → 5ºC, and the second one following the reverse order 5ºC →15ºC → 5ºC. The results of the first temperature experiment on dispersed FUS are presented in **Figure 30**.

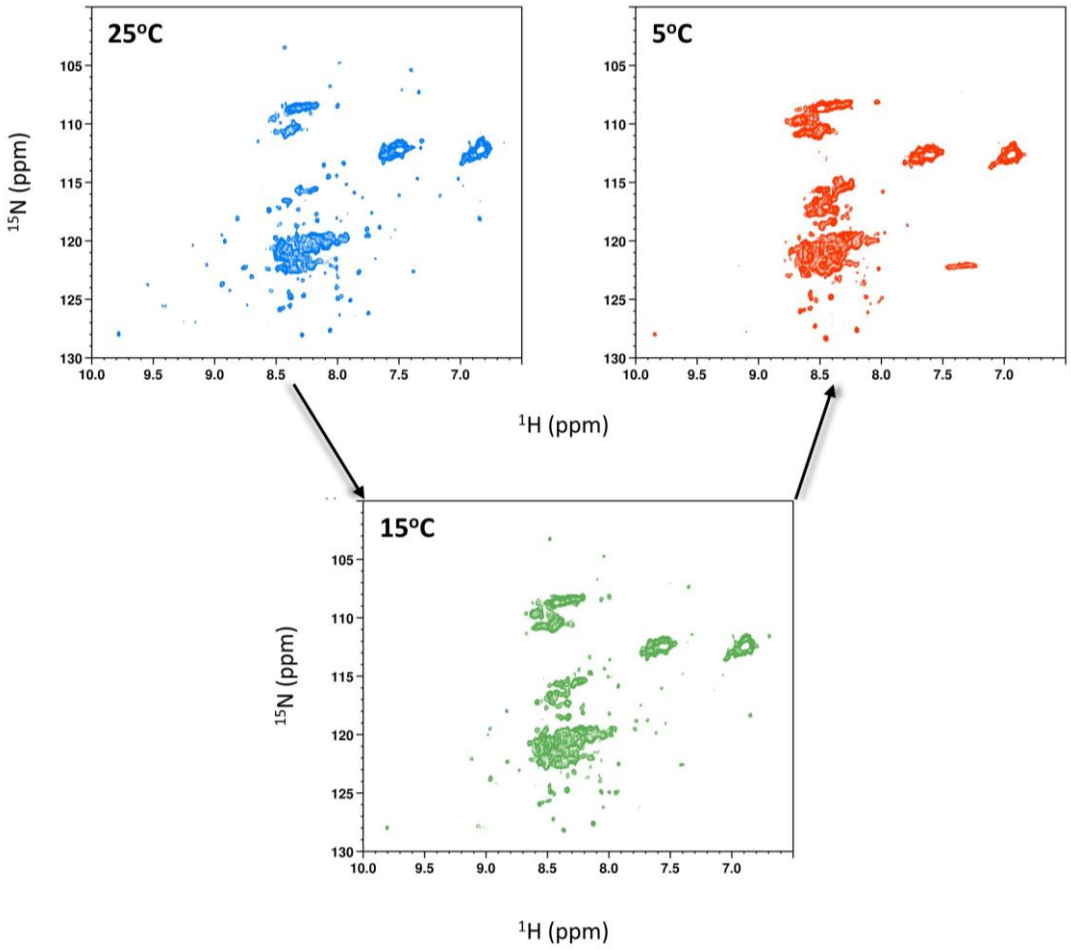

Figure 30 – ^{1}H-^{15}N HSQC spectra of dispersed FUS in the presence of decreasing temperature (25ºC → 15ºC → 5ºC) - ^{1}H-^{15}N HSQC spectra of 200 µM ^{15}N-labeled FUS recorded at different temperatures following the order of 25ºC, 15ºC and 5ºC, corresponding to the blue, green and red spectrum, respectively. Sample of dispersed FUS prepared in 20 mM sodium phosphate buffer, 2 mM DTT, 10% glycerol, 0.05% NaN_3, 1 protease inhibitor tablet and 10% $^{2}H_2O$, at pH 7.10. ^{1}H chemical shifts referenced through 50 µM DSS.

In the obtained ^{1}H-^{15}N HSQC spectrum at 25ºC it is possible to observe the collapsing of the chemical shifts near ^{1}H 8.50 ppm, indicative of the intrinsic disorder of FUS. The dispersed chemical shifts should arise from the FUS structured domains, the RRM and ZnF motif.

First, dispersed FUS was incubated at 25ºC for 10 min and the ^{1}H-^{15}N HSQC was obtained. Upon lowering the temperature to 15ºC, it was possible to see dispersed peaks disappearing and collapsing in the ^{1}H 8.50 ppm region. Lowering the temperature to 5ºC, temperature in which it is expected phase-separation, almost all cross-peaks collapsed in the random-coil region. ^{1}H and ^{15}N chemical shifts change linearly with temperature as long as there are no major conformational changes. The obtained results indicate that there are indeed conformational charges with the variation of temperature. As expected, chemical shift goes upfield at higher temperatures due to the thermal expansion of the hydrogen bond between the amide and the carbonyl group, resulting in a shielding of the protons by the solvent (**Figure 31**).[229,230]

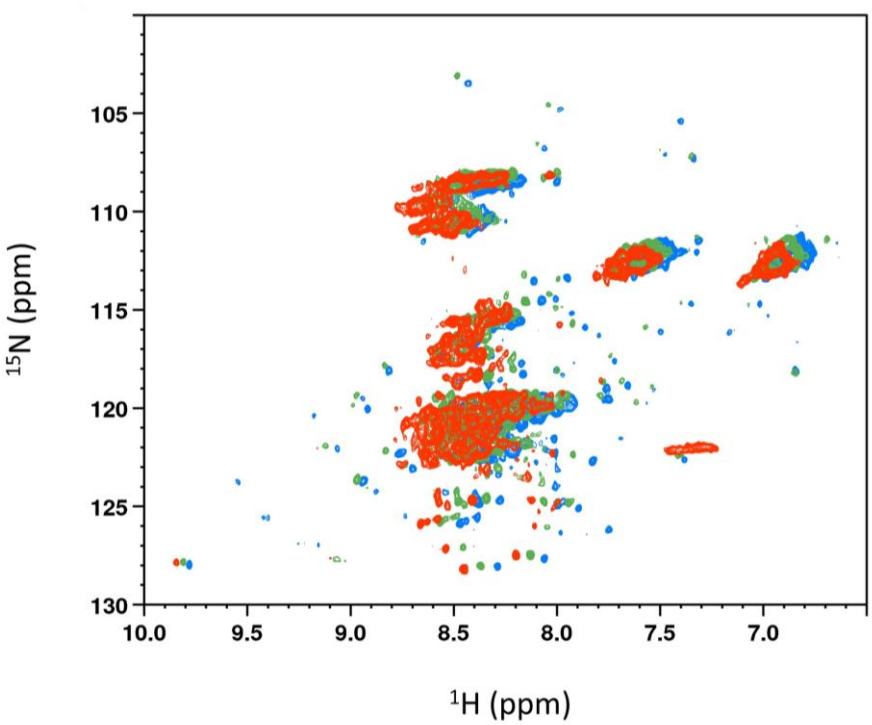

Figure 31 – Superposition of the ^{1}H-^{15}N HSQC spectra of dispersed FUS in the presence of decreasing temperature (25ºC → 15ºC → 5ºC) – Overlay of ^{1}H-^{15}N HSQC spectra of 200 µM ^{15}N-labeled FUS recorded at different temperatures following the order of 25ºC, 15ºC and 5ºC, corresponding to the blue, green and red spectrum, respectively. Sample of dispersed FUS prepared in 20 mM sodium phosphate buffer, 2 mM DTT, 10% glycerol, 0.05% NaN_3, 1 protease inhibitor tablet and 10% $^{2}H_2O$, at pH 7.10. ^{1}H chemical shifts referenced through 50 µM DSS.

At lower temperature, it would be expected that the dynamic disorder would be reduced due to the favored low energy conformation, which would result in a dispersion of the ^{1}H-^{15}N chemical shift.[227,231] Interestingly, structured domains of FUS seem to become more dynamic at low temperature as the dispersed chemical shifts collapse into the random-coil region. Such phenomena seem to indicate that FUS undergoes cold denaturation.

Denaturation of proteins at lower temperatures seems paradoxical. According to Le Chatelier's principle, a system that is under increasing temperature absorbs heat to return to equilibrium, which results in the breaking of enthalpically favorable interactions, and consequent increase in entropy. As a result, a protein that is subjected to high temperatures should become disordered by the disruption of the native protein structure. By the same argument, a decrease in temperature should induce processes that lead to an increase in order, thus to the stability of the ordered domains.[232]

The current accepted explanation for cold denaturation relies on changes in the interactions between water and the protein's hydrophobic groups. As the temperature decreases, the free energy cost of the entropically unfavorable interactions between water and hydrophobic residues becomes smaller, which leads to an increase in solvation of nonpolar groups. Moreover, in cold denaturation, lower temperatures lead to solvent-induced packing defects at the protein surface, allowing water to enter

through the interstitial spaces, which favors water-protein core hydration. Such hydration results in a destabilization of crucial hydrophobic interactions and consequently the loss of the structure stability.[232]

The primary thermodynamic driving force for the formation of a globular structure is the sequestration of nonpolar groups, by minimization of the hydrophobic surface that is exposed to water.[233] The hydrophobic effect is due to the ability of water molecules to form hydrogen bond networks with themselves, avoiding structural rearrangements where such network is perturbed. As such, non-polar amino acids tend to displace themselves from contact with water by forming structured hydrophobic cores.[234] As a result, weakening of the hydrophobic interactions renders a destabilized structure.[235] As expected, Both RRM and ZnF have high content in hydrophobic residues, with ~37% and ~31% relative content, respectively. In comparison, the unstructured LC domain contains only ~7%.

By the premise that FUS ability to phase separate is temperature dependent, and assuming that the structural changes of dispersed FUS can be correlated to those in phase-separated state, it was hypothesized that FUS cold denaturation should also be reversible. This would further confirm that cold denaturation process is directly linked the LLPS process. For that purpose, starting with dispersed FUS at 5ºC, the temperature was raised in the inverse order until 25ºC (**Figure 32**).

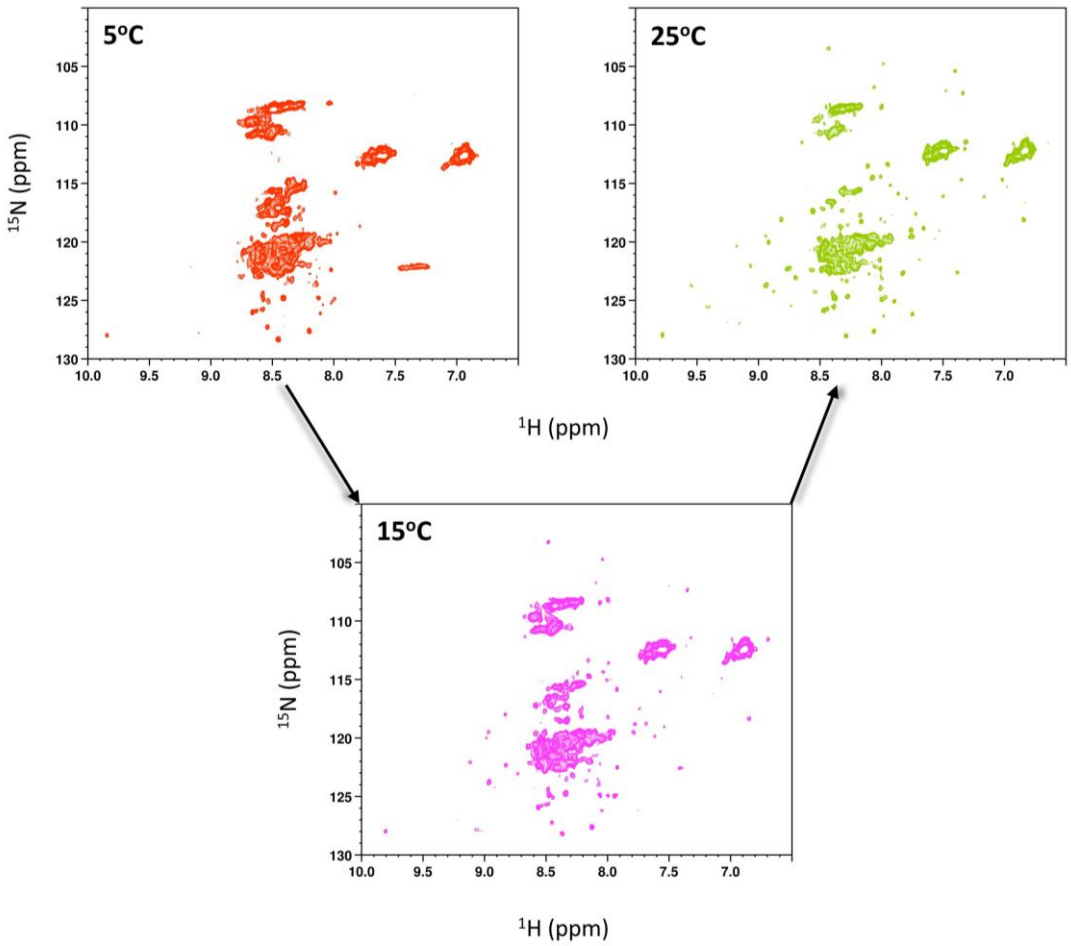

Figure 32 - ^{1}H-^{15}N HSQC spectra of dispersed FUS in the presence of increasing temperature (5ºC → 15ºC → 25ºC) - ^{1}H-^{15}N HSQC spectra of 200 µM ^{15}N-labeled FUS recorded at different temperatures following the order of 5ºC, 15ºC and 25ºC, corresponding to the blue, green and red spectrum, respectively. Sample of dispersed FUS prepared in 20 mM sodium phosphate buffer, 2 mM DTT, 10% glycerol, 0.05% NaN_3, 1 protease inhibitor tablet and 10% $^{2}H_2O$, at pH 7.10. ^{1}H chemical shifts referenced through 50 µM DSS.

In fact, upon increasing the temperature to the initial state at 25ºC, it was observed that cold denaturation was reversible, as the collapsed ^{1}H and ^{15}N chemical shifts became dispersed. Overlaying the spectra from the first experiment (with decreasing temperature) with the spectra from the second experiment (with increasing temperature), it was possible to observe that ^{1}H and ^{15}N chemical shifts returned to the same frequencies (**Figure 33**).

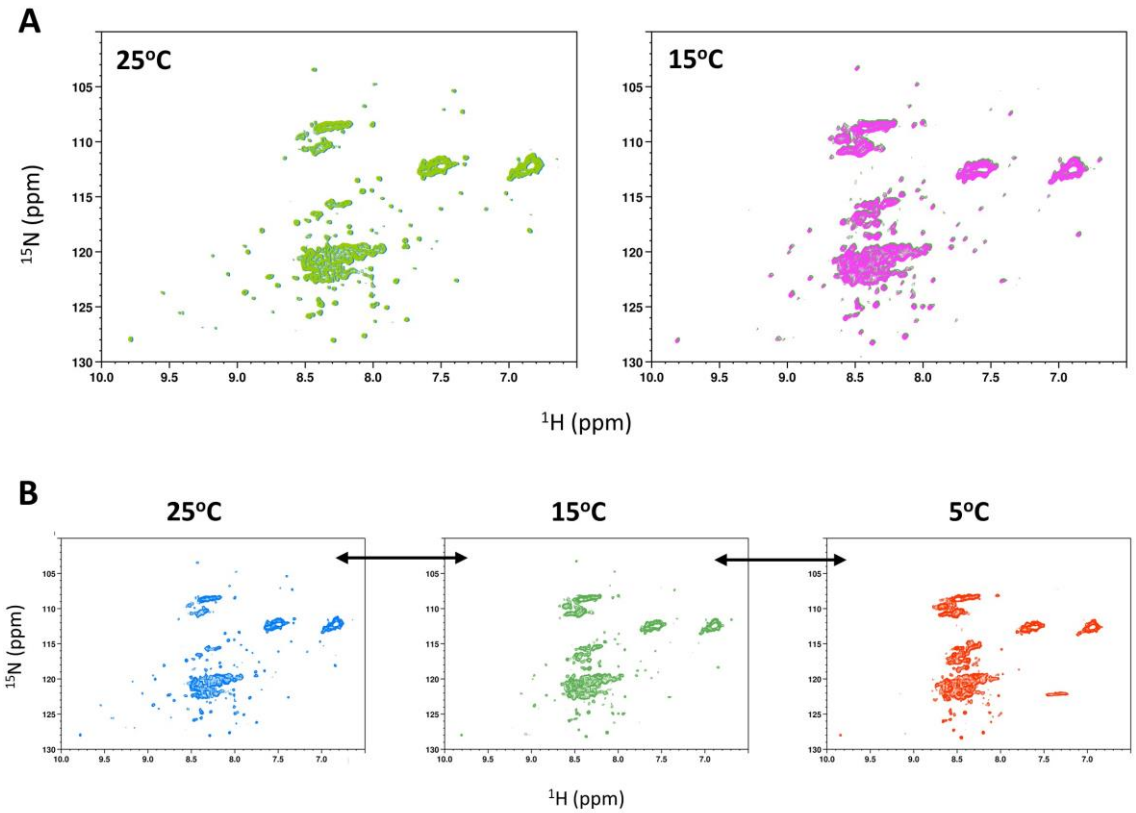

Figure 33 – Reversible cold denaturation of dispersed FUS – (A) Overlay of ^{1}H-^{15}N HSQC spectra of 200 µM ^{15}N-labeled FUS of the first experiment and second experiment, at 25ºC and 15ºC. Overlay of ^{1}H-^{15}N HSQC spectra at 25ºC, from experiment decreasing the temperature (blue spectrum) and increasing temperature (light green). Overlay of ^{1}H-^{15}N HSQC spectra at 15ºC, from experiment decreasing the temperature (green) and increasing temperature (purple). The spectra from the first experiment are not visible due to the perfect overlap with the second experiment. **(B)** Schematic figure of the reversible cold denaturation of dispersed FUS indicating that the ^{1}H-^{15}N chemical shifts return to the original frequencies at each temperature.

3.5.2 Phase separation impact on FUS structure

To further draw conclusions of the temperature influence on the FUS phase separation, correlation of temperature structural changes of dispersed FUS with phase-separated FUS had to be confirm. For that purpose, dispersed FUS was converted in phase-separated FUS by methods mentioned in the experimental section, and ^{1}H-^{15}N HSQC spectrum was obtained at 5ºC (**Figure 34**). The supernatant displayed a A_{280nm}=0.02, indicating that about 2.81 µM of the total 200 µM of FUS, was present in the supernatant.

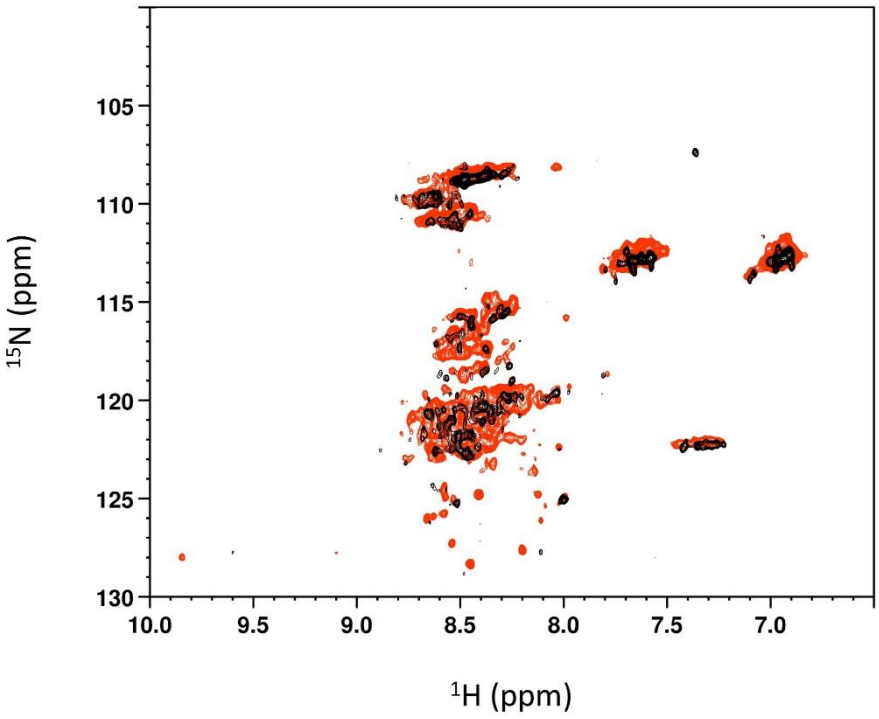

Figure 34 – Superposition of the ^{1}H-^{15}N HSQC spectra of dispersed FUS and phase-separated FUS – Overlay of ^{1}H-^{15}N HSQC spectra of 200 μM ^{15}N-labeled FUS in the dispersed and phase-separated state at 5°C, corresponding to the red and black spectrum, respectively. Sample of dispersed FUS prepared in 20 mM sodium phosphate buffer, 2 mM DTT, 10% glycerol, 0.05% NaN_3, 1 protease inhibitor tablet and 10% $^{2}H_2O$, at pH 7.10 Sample of phase-separated FUS prepared in the same buffer minus the glycerol and DTT, plus 150 mM NaCl, pH 7.10. ^{1}H chemical shifts referenced through 50 μM DSS.

Indeed, overlays of the spectra of dispersed FUS with phase-separated FUS shows high similarity, demonstrating that the overall structure of FUS is retained upon phase separation. This indicates that phase separation is not a spontaneous process, but indeed relies on the surrounding conditions. As such, if the temperature lowers, FUS undergoes cold denaturation, and upon phase separation, the structural rearrangement promoted by the environment is retained. As expected, upon the formation of liquid droplets there is an increase viscosity, which leads to a slower tumbling decreasing the intensity and broadening the signals.[236]

By these results, FUS seem to undergo cold denaturation at a temperature in which undergoes LLPS. Upon increase in the temperature, and as observed (see section ***2.3.1 Temperature influence on FUS liquid-liquid phase separation***) protein droplets dissolve and structured elements of FUS regain their native structure. Reversible cold denaturation suggest that this phenomenon is directly linked to the FUS phase separation. As observed, metabolites such as glucose can inhibit LLPS by protein compaction and/or interactions with hydrophobic residues. Interestingly, as mentioned, cold denaturation destabilizes protein's structures by hydration of the hydrophobic cores. As a result, it is expected that at low temperatures the hydrophobic residues of both RRM and ZnF domains are stabilized, and thus cannot participate in hydrophobic interactions. In this case, the destabilization of the overall structure of these domains might enhance other intermolecular interactions rather than hydrophobic ones. In fact, the RRM and ZnF domains have an extremely high

content in charged residues, accounting for 18% and 27% of all residues in each motif, respectively. Hence, cold denaturation might enhance LLPS by enabling intermolecular electrostatic interactions by these domains. Nonetheless, the reversibility of the cold denaturation might hint that there is a fine balance of the hydration of the hydrophobic core. As a result, weak hydration shell around the hydrophobic residues might be weak enough to allow displacement of water molecules leading to residual intermolecular hydrophobic interactions.

Cold denaturation might be a process that promotes LLPS, as it leads to a higher disorder of FUS structure and the exposure of charged residues that might be involved in self-assembly interactions. Moreover, as observed previously, RNA has a great impact on FUS phase separation, which suggests that both the RRM and ZnF motifs contribute to FUS LLPS process. As suggested by Maharana *et al*., since interactions between nucleic acids and FUS are rather weak, these motifs might be involved in intermolecular interactions and participate in FUS self-assembly. [219] Cold denaturation allows the exposure of RRM and ZnF charged residues that undergo electrostatic intermolecular interactions and promote FUS protein droplet formation. Since it is observed reversibility in the cold denaturation process, it is proposed that hydrophobic interactions might also play a role in the intermolecular interactions. As a result, FUS phase separation is higher at lower temperatures but is reverted at higher temperatures by the folding of the RRM and ZnF domains.

4. CONCLUSIONS AND FUTURE PERSPECTIVES

"I would rather have questions that can't be answered than answers that can't be questioned"

R. Feynman

4. Conclusions and future perspectives

The formation of cellular membraneless proteinaceous organelles, driven by LLPS, constitute a ubiquitous effective responsive strategy for biological compartmentalization, implicated in both cellular homeostasis and disease. In cellular stress, FUS protein self-assembles leading to the formation of transient stress granules that provide a microenvironment involved in RNA-related functions. These granules provide templates for protein deposits found in several neurodegenerative diseases. As a result, it is important to understand the process and conditions that drive FUS LLPS which can potentially drive protein aggregation.

The main goal of the work presented in this thesis was to contribute towards understanding the determinants and mechanisms that drive FUS LLPS process, using microplate assays and NMR techniques. Additionally, microscopic imaging was used to visualize FUS granules. Both non-labeled and ^{15}N-labeled FUS were successfully expressed and purified.

In summary, the influence of three main variable conditions on FUS LLPS were studied: temperature, pH and presence of distinct abundant cellular metabolites. Remarkably, FUS LLPS process exhibited extreme sensitivity to all conditions.

Temperature revealed to be an important condition to which FUS granule formation and stability is strongly dependent. FUS displayed a UCST phase separation behavior, undergoing reversible LLPS at low temperature.

FUS phase separation was significantly enhanced when the protein contained an overall neutral charge (at pH 9.40) and in the presence of charged metabolites such as NaCl, $CaCl_2$, $ZnCl_2$ and lysine-HCl. It is proposed that the reduction of the electric-double layer repulsion complemented with charge screening of the protein surface, effectively promoted FUS self-assembly. Interestingly, FUS granule formation was tightly controlled not only by the charged nature of the metabolite but also by its concentration. Above a certain optimal concentration that led to a maximum in phase separation, it was observed an inhibition of the LLPS process. These findings suggest that charge screening must be high enough to reduce repulsive interactions, but low enough to prevent hindering of crucial intermolecular electrostatic interactions. The charge dependence and regulation of FUS phase separation indicates that LLPS is modulated by intermolecular electrostatic interactions.

One another hand, stabilizing metabolites such as glucose and Na-glutamate progressively inhibited FUS phase separation. Induced preferential hydration by these stabilizing metabolites can lead to protein compaction and destabilization of hydrophobic interactions. These results suggest that FUS intrinsic disorder is crucial for self-assembly and that hydrophobic interactions might also play a crucial role in the LLPS process.

Through microscopy imaging, it was possible to visualize FUS droplets and to identify liquid-like properties such as wetting and fusion. In addition, it was observed irreversible protein aggregation at 1 mM FUS.

Through NMR spectroscopy, it was showed that FUS globular domains undergo reversible cold denaturation at a temperature in which the LLPS process is enhanced. Cold denaturation might promote LLPS by exposing the charged residues of the RRM and ZnF motif. Together with the phase separation assays results that demonstrated that both RNA and Zn^{2+} significantly enhanced FUS phase separation, it is proposed

that the RRM and ZnF domains mediate FUS phase separation at low temperature through intermolecular electrostatic interactions. Nonetheless, since cold denaturation is reversible, hydrophobic hydration might be weak enough to allow transient hydrophobic interactions.

Moreover, through NMR spectroscopy it was possible to demonstrate that FUS structure is retained upon phase separation. This indicated that phase separation is not a spontaneous process and indeed relies on the surrounding environment. In fact, FUS has to be already poised and structurally ready, just has in the case of cold denaturation, to phase separate.

In conclusion, in this work, it was demonstrated that FUS droplet formation and stability is highly responsive and tightly regulated by the surrounding conditions. Moreover, although the LC domains are usually remarked as imperative for protein self-assembly, in this work it was showed that globular domains might also mediate FUS granule formation. Interestingly, FUS globular domains undergo cold denaturation. This process might provide a pathway that allows accessibility of additional fundamental residues for intermolecular interactions, leading to promotion FUS self-assembly. Such finding might justify the UCST phase separation of FUS protein. Remarkably, FUS retains its overall structure, modulated by the external conditions, upon phase separation, giving additional insight on the crucial regulation of LLPS by the environment.

The work presented on this thesis paved a path towards the comprehension of the structural determinants, the interactions and conditions that drive LLPS of FUS protein. These findings might provide crucial towards unraveling the mechanisms that lead to stress granule formation and ultimately to protein co-deposition encountered in several neurodegenerative diseases. Such knowledge might lead to improved diagnosis and to the to the development of appropriate therapies.

Moreover, proteinaceous granules might have potentially as delivery systems in biotechnological and pharmaceutical areas, as they are extremely sensitive and responsive to external conditions.

As a future work, it is proposed the study of FUS phase separation in a wider range of temperature in order to establish the exact upper critical solution temperature, above which FUS granules are dissipated. Thermodynamic and kinetic assays would prove valuable towards the rationalization of the charged metabolites impact on the LLPS process. In addition, the study of FUS LLPS should be explore at physiological conditions, to understand the triggering events that lead to stress granule formation in the cellular context. The conditions studied in this work should be explored through the protein point of view, making use of NMR spectroscopy, fluorescence spectroscopy and microscopic imaging, to study the structure and dynamics of FUS in the different environments.

5. BIBLIOGRAPHIC REFERENCES

“Scientific knowledge advances haltingly and is stimulated by contention and doubt”

C. Lévi-Strauss

5. Bibliographic references

1 Ovadi, J. & Srere, P. A. Macromolecular compartmentation and channeling. *Int Rev Cytol* **192**, 255-280 (2000).

2 Hyman, A. A., Weber, C. A. & Jülicher, F. Liquid-Liquid Phase Separation in Biology. *Annual Review of Cell and Developmental Biology* **30**, 39-58, doi:10.1146/annurev-cellbio-100913-013325 (2014).

3 Shorter, J. Membraneless organelles: Phasing in and out. *Nature Chemistry* **8**, 528-530, doi:10.1038/nchem.2534 (2016).

4 Mitrea, D. M. & Kriwacki, R. W. Phase separation in biology; functional organization of a higher order. *Cell Communication and Signaling* **14**, 1-1, doi:10.1186/s12964-015-0125-7 (2016).

5 Stoeger, T., Battich, N. & Pelkmans, L. Passive Noise Filtering by Cellular Compartmentalization. *Cell* **164**, 1151-1161, doi:10.1016/j.cell.2016.02.005 (2016).

6 Farber, D. L., Yudanin, N. A. & Restifo, N. P. Human memory T cells: generation, compartmentalization and homeostasis. *Nat Rev Immunol* **14**, 24-35, doi:10.1038/nri3567 (2014).

7 Verkman, A. S. Solute and macromolecule diffusion in cellular aqueous compartments. *Trends in Biochemical Sciences* **27**, 27-33, doi:Doi 10.1016/S0968-0004(01)02003-5 (2002).

8 Heald, R. & Cohen-Fix, O. Morphology and function of membrane-bound organelles. *Curr Opin Cell Biol* **26**, 79-86, doi:10.1016/j.ceb.2013.10.006 (2014).

9 Shinoda, W. Permeability across lipid membranes. *Biochim Biophys Acta* **1858**, 2254-2265, doi:10.1016/j.bbamem.2016.03.032 (2016).

10 Shin, Y. & Brangwynne, C. P. Liquid phase condensation in cell physiology and disease. *Science* **357** (2017).

11 Brangwynne, C. P. *et al.* Germline P Granules Are Liquid Droplets That Localize by Controlled Dissolution/Condensation. *Science* **324**, 1729-1732, doi:10.1126/science.1172046 (2009).

12 Elbaum-Garfinkle, S. *et al.* The disordered P granule protein LAF-1 drives phase separation into droplets with tunable viscosity and dynamics. *Proceedings of the National Academy of Sciences of the United States of America* **112**, 7189-7194, doi:10.1073/pnas.1504822112 (2015).

13 Strome, S. & Wood, W. B. Generation of asymmetry and segregation of germ-line granules in early C. elegans embryos. *Cell* **35**, 15-25, doi:10.1016/0092-8674(83)90203-9 (1983).

14 Aizer, A. *et al.* Quantifying mRNA targeting to P-bodies in living human cells reveals their dual role in mRNA decay and storage. *Journal of Cell Science* **127**, 4443-4456, doi:10.1242/jcs.152975 (2014).

15 Yoon, J. H. & Parker, R. Coil-in-to snRNP assembly and Cajal bodies. *Nature Structural and Molecular Biology* **17**, 391-393, doi:10.1038/nsmb0410-391 (2010).

16 Li, L. *et al.* Dynamic Nature of Cleavage Bodies and Their Spatial Relationship to DDX1 Bodies, Cajal Bodies, and Gems. *Molecular biology of the cell* **17**, 1126-1140, doi:10.1091/mbc.E05 (2006).

17 Shav-Tal, Y. *et al.* Dynamic Sorting of Nuclear Components into Distinct Nucleolar Caps during Transcriptinal Inhibition. *Molecular biology of the cell* **16**, 2395-2413, doi:10.1091/mbc.E04 (2005).

18 Fox, A. H. *et al.* Paraspeckles: A novel nuclear domain. *Current Biology* **12**, 13-25, doi:10.1016/s0960-9822(01)00632-7 (2002).

19 Lamond, A. I. & Spector, D. L. Nuclear speckles: A model for nuclear organelles. *Nature Reviews Molecular Cell Biology* **4**, 605-612, doi:10.1038/nrm1172 (2003).

20 Li, B., Carey, M. & Workman, J. L. The Role of Chromatin during Transcription. *Cell* **128**, 707-719, doi:10.1016/j.cell.2007.01.015 (2007).

21 Nizami, Z., Deryusheva, S. & Gall, J. G. The Cajal body and histone locus body. *Cold Spring Harbor perspectives in biology* **2**, 1-12, doi:10.1101/cshperspect.a000653 (2010).

22 Biamonti, G. & Vourc'h, C. Nuclear stress bodies. *Cold Spring Harbor perspectives in biology* **2**, 1-12, doi:10.1101/cshperspect.a000695 (2010).

23 Harrigan, J. A. *et al.* Replication stress induces 53BP1-containing OPT domains in G1 cells. *Journal of Cell Biology* **193**, 97-108, doi:10.1083/jcb.201011083 (2011).

24 Pirrotta, V. & Li, H. B. A view of nuclear Polycomb bodies. *Current Opinion in Genetics and Development* **22**, 101-109, doi:10.1016/j.gde.2011.11.004 (2012).

25 Huang, S. Perinucleolar structures. *Journal of Structural Biology* **129**, 233-240, doi:DOI 10.1006/jsbi.2000.4247 (2000).

26 Maul, G. G., Negorev, D., Bell, P. & Ishov, A. M. Properties and assembly mechanisms of ND10, PML2 bodies, or PODs. *Journal of Structural Biology* **129**, 278-287, doi:10.1006/jsbi.2000.4239 (2000).

27 Decker, M. *et al.* Limiting amounts of centrosome material set centrosome size in C. elegans embryos. *Current Biology* **21**, 1259-1267, doi:10.1016/j.cub.2011.06.002 (2011).

28 Kiebler, M. A. & Bassell, G. J. Neuronal RNA Granules: Movers and Makers. *Neuron* **51**, 685-690, doi:10.1016/j.neuron.2006.08.021 (2006).

29 Decker, C. J., Teixeira, D. & Parker, R. Edc3p and a glutamine/asparagine-rich domain of Lsm4p function in processing body assembly in Saccharomyces cerevisiae. *Journal of Cell Biology* **179**, 437-449, doi:10.1083/jcb.200704147 (2007).

30 Buchan, J. R. & Parker, R. Eukaryotic Stress Granules: The Ins and Outs of Translation. *Molecular Cell* **36**, 932-941, doi:10.1016/j.molcel.2009.11.020 (2009).

31 Jourdain, A. A., Boehm, E., Maundrell, K. & Martinou, J. C. Mitochondrial RNA granules: Compartmentalizing mitochondrial gene expression. *Journal of Cell Biology* **212**, 611-614, doi:10.1083/jcb.201507125 (2016).

32 Anderson, P. & Kedersha, N. RNA granules: post-transcriptional and epigenetic modulators of gene expression. *Nature Reviews Molecular Cell Biology* **10**, 430-436, doi:10.1038/nrm2694 (2009).

33 Protter, D. S. W. & Parker, R. Principles and Properties of Stress Granules. *Trends in Cell Biology* **26**, 668-679, doi:10.1016/j.tcb.2016.05.004 (2016).

34 Courchaine, E. M., Lu, A. & Neugebauer, K. M. Droplet organelles? *The EMBO Journal* **35**, 1603-1612, doi:10.15252/embj.201593517 (2016).

35 Jain, S. *et al.* ATPase-Modulated Stress Granules Contain a Diverse Proteome and Substructure. *Cell* **164**, 487-498, doi:10.1016/J.CELL.2015.12.038 (2016).

36 Buchan, J. R. mRNP granules. *RNA Biology* **11**, 1019-1030, doi:10.4161/15476286.2014.972208 (2014).

37 Jain, S. *et al.* ATPase modulated stress granules contain a diverse proteome and substructure. *Cell* **164**, 487-498, doi:10.1016/j.cell.2015.12.038 (2016).

38 Wheeler, J. R., Matheny, T., Jain, S., Abrisch, R. & Parker, R. Distinct stages in stress granule assembly and disassembly. *Elife* **5**, doi:ARTN e18413
10.7554/eLife.18413 (2016).

39 Foty, R. A. & Steinberg, M. S. The differential adhesion hypothesis: a direct evaluation. *Developmental Biology* **278**, 255-263, doi:10.1016/J.YDBIO.2004.11.012 (2005).

40 Nott, T. J. *et al.* Phase Transition of a Disordered Nuage Protein Generates Environmentally Responsive Membraneless Organelles. *Molecular Cell* **57**, 936-947, doi:10.1016/j.molcel.2015.01.013 (2015).

41 Wek, R. C., Jiang, H. Y. & Anthony, T. G. Coping with stress: eIF2 kinases and translational control. *Biochemical Society Transactions* **34**, 7-11, doi:Doi 10.1042/Bst0340007 (2006).

42 Ohn, T., Kedersha, N., Hickman, T., Tisdale, S. & Anderson, P. A functional RNAi screen links O-GlcNAc modification of ribosomal proteins to stress granule and processing body assembly. *Nature Cell Biology* **10**, 1224-1231, doi:10.1038/ncb1783 (2008).

43 Thandapani, P., O'Connor, T. R., Bailey, T. L. & Richard, S. Defining the RGG/RG Motif. *Molecular Cell* **50**, 613-623, doi:10.1016/j.molcel.2013.05.021 (2013).

44 Onomoto, K. *et al.* Critical Role of an Antiviral Stress Granule Containing RIG-I and PKR in Viral Detection and Innate Immunity. *PLOS ONE* **7**, e43031-e43031 (2012).

45 Arimoto, K., Fukuda, H., Imajoh-Ohmi, S., Saito, H. & Takekawa, M. Formation of stress granules inhibits apoptosis by suppressing stress-responsive MAPK pathways. *Nature Cell Biology* **10**, 1324-1332, doi:10.1038/ncb1791 (2008).

46 Kim, W. J., Back, S. H., Kim, V., Ryu, I. & Jang, S. K. Sequestration of TRAF2 into Stress Granules Interrupts Tumor Necrosis Factor Signaling under Stress Conditions Sequestration of TRAF2 into Stress Granules Interrupts Tumor Necrosis Factor Signaling under Stress Conditions. *Molecular and cellular biology* **25**, 2450-2462, doi:10.1128/MCB.25.6.2450 (2005).

47 Adjibade, P. *et al.* Sorafenib, a multikinase inhibitor, induces formation of stress granules in hepatocarcinoma cells. *Oncotarget* **6**, 43927-43943, doi:10.18632/oncotarget.5980 (2015).

48 Kaehler, C., Isensee, J., Hucho, T., Lehrach, H. & Krobitsch, S. 5-Fluorouracil affects assembly of stress granules based on RNA incorporation. *Nucleic Acids Research* **42**, 6436-6447, doi:10.1093/nar/gku264 (2014).

49 Li, Y. R., King, O. D., Shorter, J. & Gitler, A. D. Stress granules as crucibles of ALS pathogenesis. *Journal of Cell Biology* **201**, 361-372, doi:10.1083/jcb.201302044 (2013).

50 Kwiatkowski, T. J. *et al.* Mutations in the FUS/TLS gene on chromosome 16 cause familial amyotrophic lateral sclerosis. *Science (New York, N.Y.)* **323**, 1205-1208, doi:10.1126/science.1166066 (2009).

51 Sun, Y. & Chakrabartty, A. Phase to Phase with TDP-43. *Biochemistry* **56**, 809-823, doi:10.1021/acs.biochem.6b01088 (2017).

52 Zhang, K. *et al.* The C9orf72 repeat expansion disrupts nucleocytoplasmic transport. *Nature* **525**, 56-56 (2015).

53 Ling, S. C., Polymenidou, M. & Cleveland, D. W. Converging mechanisms in als and FTD: Disrupted RNA and protein homeostasis. *Neuron* **79**, 416-438, doi:10.1016/j.neuron.2013.07.033 (2013).

54 Wolozin, B. Regulated protein aggregation: Stress granules and neurodegeneration. *Molecular Neurodegeneration* **7**, 1-1, doi:10.1186/1750-1326-7-56 (2012).

55 Dobson, C. M. Protein folding and misfolding. *Nature* **426**, 884-890, doi:10.1038/nature02261 (2003).

56 Jarrett, J. T. & Lansbury, P. T. Seeding “one-dimensional crystallization” of amyloid: A pathogenic mechanism in Alzheimer's disease and scrapie? *Cell* **73**, 1055-1058, doi:10.1016/0092-8674(93)90635-4 (1993).

57 Molliex, A. *et al.* Phase Separation by Low Complexity Domains Promotes Stress Granule Assembly and Drives Pathological Fibrillization Article Phase Separation by Low Complexity Domains Promotes Stress Granule Assembly and Drives Pathological Fibrillization. *Cell* **163**, 123-133, doi:10.1016/j.cell.2015.09.015 (2015).

58 Atkins, P. *The Laws of Thermodynamics*. (Oxford University Press, 2010).

59 Ambadipudi, S., Biernat, J., Riedel, D., Mandelkow, E. & Zweckstetter, M. Liquid–liquid phase separation of the microtubule-binding repeats of the Alzheimer-related protein Tau. *Nature Communications* **8**, 275-275, doi:10.1038/s41467-017-00480-0 (2017).

60 Raut, A. S. & Kalonia, D. S. Liquid-Liquid Phase Separation in a Dual Variable Domain Immunoglobulin Protein Solution: Effect of Formulation Factors and Protein-Protein Interactions. *Molecular Pharmaceutics* **12**, 3261-3271, doi:10.1021/acs.molpharmaceut.5b00256 (2015).

61 Atkins, P. & De Paula, J. *Physical Chemistry*. 9th edn, (Oxford University Press, 2010).

62 Beysens, D., Straub, J. & Turner, D. J. in *Fluid Sciences and Materials Science in Space: A European Perspective* (ed H. U. Walter) 221-256 (Springer Berlin Heidelberg, 1987).

63 Rubinstein, M. & Colby, R. H. *Polymer physics*. (Oxford University Press, 2003).

64 Brangwynne, Clifford P., Tompa, P. & Pappu, Rohit V. Polymer physics of intracellular phase transitions. *Nature Physics* **11**, 899-904, doi:10.1038/nphys3532 (2015).

65 Flory, P. J. Thermodynamics of High Polymer Solutions. *The Journal of Chemical Physics* **10**, 51-61, doi:10.1063/1.1723621 (1942).

66 Huggins, M. L. Solutions of Long Chain Compounds. *The Journal of Chemical Physics* **9**, 440-440, doi:10.1063/1.1750930 (1941).

67 Darling, A., Liu, Y., Oldfield, C. J. & Uversky, V. N. Intrinsically Disordered Proteome of Human Membrane-Less Organelles. *Proteomics* **1700193**, 1700193-1700193, doi:10.1002/pmic.201700193 (2017).

68 Uversky, V. N., Kuznetsova, I. M., Turoverov, K. K. & Zaslavsky, B. Intrinsically disordered proteins as crucial constituents of cellular aqueous two phase systems and coacervates. *FEBS Letters* **589**, 15-22, doi:10.1016/j.febslet.2014.11.028 (2015).

69 Das, R. K., Ruff, K. M. & Pappu, R. V. Relating sequence encoded information to form and function of intrinsically disordered proteins. *Current Opinion in Structural Biology* **32**, 102-112, doi:10.1016/j.sbi.2015.03.008 (2015).

70 Kwon, I. *et al.* Phosphorylation-Regulated Binding of RNA Polymerase II to Fibrous Polymers of Low-Complexity Domains. *Cell* **155**, 1049-1060, doi:10.1016/j.cell.2013.10.033 (2013).

71 Kyte, J. & Doolittle, R. F. A Simple Method for Displaying the Hydropathic Character of a Protein. *Journal of Molecular Biology* **157**, 105-132, doi:Doi 10.1016/0022-2836(82)90515-0 (1982).

72 Bandyopadhyay, D. & Mehler, E. L. Quantitative expression of protein heterogeneity: Response of amino acid side chains to their local environment. *Proteins* **72**, 646-659, doi:10.1002/prot.21958 (2008).

73 Zhu, C. Q. *et al.* Characterizing hydrophobicity of amino acid side chains in a protein environment via measuring contact angle of a water nanodroplet on planar peptide network. *Proceedings of the National Academy of Sciences of the United States of America* **113**, 12946-12951, doi:10.1073/pnas.1616138113 (2016).

74 Fauchere, J. L. & Pliska, V. Hydrophobic Parameters-Pi of Amino-Acid Side-Chains from the Partitioning of N-Acetyl-Amino-Acid Amides. *Eur J Med Chem* **18**, 369-375 (1983).

75 Lagier-Tourenne, C., Polymenidou, M. & Cleveland, D. W. TDP-43 and FUS/TLS: emerging roles in RNA processing and neurodegeneration. *Hum Mol Genet* **19**, R46-R64, doi:10.1093/hmg/ddq137 (2010).

76 Ling, S.-C., Polymenidou, M. & Cleveland, Don W. Converging Mechanisms in ALS and FTD: Disrupted RNA and Protein Homeostasis. *Neuron* **79**, 416-438, doi:10.1016/j.neuron.2013.07.033 (2013).

77 Schwartz, J. C., Cech, T. R. & Parker, R. R. Biochemical Properties and Biological Functions of FET Proteins. *Annu Rev Biochem* **84**, 355-379, doi:10.1146/annurev-biochem-060614-034325 (2015).

78 Masuda, A. *et al.* Position-specific binding of FUS to nascent RNA regulates mRNA length. *Genes Dev* **29**, 1045-1057, doi:10.1101/gad.255737.114 (2015).

79 Murakami, T. *et al.* ALS/FTD Mutation-Induced Phase Transition of FUS Liquid Droplets and Reversible Hydrogels into Irreversible Hydrogels Impairs RNP Granule Function. *Neuron* **88**, 678-690, doi:10.1016/j.neuron.2015.10.030 (2015).

80 Yoshizawa, T. *et al.* Nuclear Import Receptor Inhibits Phase Separation of FUS through Binding to Multiple Sites. *Cell* **173**, 693.e691-693.e622, doi:10.1016/j.cell.2018.03.003 (2018).

81 Liu, X. *et al.* The fused in sarcoma protein forms cytoplasmic aggregates in motor neurons derived from integration-free induced pluripotent stem cells generated from a patient with familial amyotrophic lateral sclerosis carrying the FUS-P525L mutation. *Neurogenetics* **16**, 223-231, doi:10.1007/s10048-015-0448-y (2015).

82 Rabbitts, T. H., Forster, A., Larson, R. & Nathan, P. Fusion of the dominant negative transcription regulator CHOP with a novel gene FUS by translocation t(12;16) in malignant liposarcoma. *Nat Genet* **4**, 175-180, doi:10.1038/ng0693-175 (1993).

83 Crozat, A., Aman, P., Mandahl, N. & Ron, D. Fusion of CHOP to a novel RNA-binding protein in human myxoid liposarcoma. *Nature* **363**, 640-644, doi:10.1038/363640a0 (1993).

84 Deng, H., Gao, K. & Jankovic, J. The role of FUS gene variants in neurodegenerative diseases. *Nat Rev Neurol* **10**, 337-348, doi:10.1038/nrneurol.2014.78 (2014).

85 Yang, S., Warraich, S. T., Nicholson, G. A. & Blair, I. P. Fused in sarcoma/translocated in liposarcoma: A multifunctional DNA/RNA binding protein. *International Journal of Biochemistry and Cell Biology* **42**, 1408-1411, doi:10.1016/j.biocel.2010.06.003 (2010).

86 Wang, X., Schwartz, J. C. & Cech, T. R. Nucleic acid-binding specificity of human FUS protein. *Nucleic Acids Research* **43**, 7535-7543, doi:10.1093/nar/gkv679 (2015).

87 Tan, A. Y. & Manley, J. L. The TET family of proteins: functions and roles in disease. *J Mol Cell Biol* **1**, 82-92, doi:10.1093/jmcb/mjp025 (2009).

88 Liu, X. *et al.* The RRM domain of human fused in sarcoma protein reveals a non-canonical nucleic acid binding site. *Biochimica et Biophysica Acta - Molecular Basis of Disease* **1832**, 375-385, doi:10.1016/j.bbadis.2012.11.012 (2013).

89 Hoell, J. I. *et al.* RNA targets of wild-type and mutant FET family proteins. *Nature Structural and Molecular Biology* **18**, 1428-1431, doi:10.1038/nsmb.2163 (2011).

90 Lu, Y., Lim, L. & Song, J. RRM domain of ALS/FTD-causing FUS characteristic of irreversible unfolding spontaneously self-assembles into amyloid fibrils. *Scientific Reports* **7**, 1043, doi:10.1038/s41598-017-01281-7 (2017).

91 Maris, C., Dominguez, C. & Allain, F. H. T. The RNA recognition motif, a plastic RNA-binding platform to regulate post-transcriptional gene expression. *FEBS Journal* **272**, 2118-2131, doi:10.1111/j.1742-4658.2005.04653.x (2005).

92 Iko, Y. *et al.* Domain architectures and characterization of an RNA-binding protein, TLS. *Journal of Biological Chemistry* **279**, 44834-44840, doi:10.1074/jbc.M408552200 (2004).

93 Hanakahi, L. A., Sun, H. & Maizels, N. High affinity interactions of nucleolin with G-G-paired rDNA. *Journal of Biological Chemistry* **274**, 15908-15912, doi:DOI 10.1074/jbc.274.22.15908 (1999).

94 Jarvelin, A. I., Noerenberg, M., Davis, I. & Castello, A. The new (dis)order in RNA regulation. *Cell Commun Signal* **14**, 9, doi:10.1186/s12964-016-0132-3 (2016).

95 Ozdilek, B. A. *et al.* Intrinsically disordered RGG/RG domains mediate degenerate specificity in RNA binding. *Nucleic Acids Research* **45**, 7984-7996, doi:10.1093/nar/gkx460 (2017).

96 Laity, J. H., Lee, B. M. & Wright, P. E. Zinc finger proteins: new insights into structural and functional diversity. *Current Opinion in Structural Biology* **11**, 39-46, doi:https://doi.org/10.1016/S0959-440X(00)00167-6 (2001).

97 Gamsjaeger, R., Liew, C., Loughlin, F., Crossley, M. & Mackay, J. Sticky fingers: zinc-fingers as protein-recognition motifs. *Trends in Biochemical Sciences* **32**, 63-70, doi:10.1016/j.tibs.2006.12.007 (2007).

98 Mastrocola, A. S., Kim, S. H., Trinh, A. T., Rodenkirch, L. A. & Tibbetts, R. S. The RNA-binding protein fused in sarcoma (FUS) functions downstream of poly(ADP-ribose) polymerase (PARP) in response to DNA damage. *Journal of Biological Chemistry* **288**, 24731-24741, doi:10.1074/jbc.M113.497974 (2013).

99 Luo, F. *et al.* Atomic structures of FUS LC domain segments reveal bases for reversible amyloid fibril formation. *Nature Structural and Molecular Biology* **25**, 341-346, doi:10.1038/s41594-018-0050-8 (2018).

100 Lin, Y., Currie, S. L. & Rosen, M. K. Intrinsically disordered sequences enable modulation of protein phase separation through distributed tyrosine motifs. *Journal of Biological Chemistry*, jbc.M117.800466-jbc.M800117.800466, doi:10.1074/jbc.M117.800466 (2017).

101 Schwartz, J. C., Wang, X., Podell, E. R. & Cech, T. R. RNA seeds higher-order assembly of FUS protein. *Cell Rep* **5**, 918-925, doi:10.1016/j.celrep.2013.11.017 (2013).

102 Burke, K. A. *et al.* Residue-by-residue view of in vitro FUS granules that bind the C-terminal domain of RNA polymerase II. *Molecular Cell Biology* **60**, 231-241, doi:10.1016/j.molcel.2015.09.006.Residue-by-residue (2016).

103 Dormann, D. & Haass, C. Fused in sarcoma (FUS): An oncogene goes awry in neurodegeneration. *Molecular and Cellular Neuroscience* **56**, 475-486, doi:10.1016/j.mcn.2013.03.006 (2013).

104 Sama, R. R. a. K., Ward, C. L. & Bosco, D. A. Functions of FUS/TLS from DNA repair to stress response: implications for ALS. *ASN neuro* **6**, doi:10.1177/1759091414544472 (2014).

105 Zinszner, H., Sok, J., Immanuel, D., Yin, Y. & Ron, D. TLS (FUS) binds RNA in vivo and engages in nucleo-cytoplasmic shuttling. *J Cell Sci* **110 (Pt 15)**, 1741-1750 (1997).

106 King, M. C., Lusk, C. P. & Blobel, G. Karyopherin-mediated import of integral inner nuclear membrane proteins. *Nature* **442**, 1003-1007, doi:10.1038/nature05075 (2006).

107 Manuscript, A. Nuclear import by Karyopherin- β s : recognition and inhibition. **1813**, 1593-1606, doi:10.1016/j.bbamcr.2010.10.014.Nuclear (2012).

108 Davidson, Y. S. *et al.* Nuclear carrier and RNA-binding proteins in frontotemporal lobar degeneration associated with fused in sarcoma (FUS) pathological changes. *Neuropathol Appl Neurobiol* **39**, 157-165, doi:10.1111/j.1365-2990.2012.01274.x (2013).

109 Chook, Y. M. & Blobel, G. Karyopherins and nuclear import. *Curr Opin Struct Biol* **11**, 703-715 (2001).

110 Zhang, Z. C. & Chook, Y. M. Structural and energetic basis of ALS-causing mutations in the atypical proline–tyrosine nuclear localization signal of the Fused in Sarcoma protein (FUS). *Proceedings of the National Academy of Sciences of the United States of America* **109**, 12017-12021, doi:10.1073/pnas.1207247109 (2012).

111 Lee, B. J. *et al.* Rules for nuclear localization sequence recognition by karyopherin beta 2. *Cell* **126**, 543-558, doi:10.1016/j.cell.2006.05.049 (2006).

112 Zhang, Z. C. & Chook, Y. M. Structural and energetic basis of ALS-causing mutations in the atypical proline-tyrosine nuclear localization signal of the Fused in Sarcoma protein (FUS). *Proc Natl Acad Sci U S A* **109**, 12017-12021, doi:10.1073/pnas.1207247109 (2012).

113 Dormann, D. *et al.* Arginine methylation next to the PY-NLS modulates Transportin binding and nuclear import of FUS. *EMBO Journal* **31**, 4258-4275, doi:10.1038/emboj.2012.261 (2012).

114 Fulda, S., Gorman, A. M., Hori, O. & Samali, A. Cellular Stress Responses: Cell Survival and Cell Death. *International Journal of Cell Biology* **2010**, 1-23, doi:10.1155/2010/214074 (2010).

115 Bentmann, E. *et al.* Requirements for stress granule recruitment of fused in sarcoma (FUS) and TAR DNA-binding protein of 43 kDa (TDP-43). *Journal of Biological Chemistry* **287**, 23079-23094, doi:10.1074/jbc.M111.328757 (2012).

116 Dormann, D. *et al.* ALS-associated fused in sarcoma (FUS) mutations disrupt Transportin-mediated nuclear import. *The EMBO Journal* **29**, 2841-2857, doi:10.1038/emboj.2010.143 (2010).

117 Bosco, D. A. *et al.* Mutant FUS proteins that cause amyotrophic lateral sclerosis incorporate into stress granules. *Hum Mol Genet* **19**, 4160-4175, doi:10.1093/hmg/ddq335 (2010).

118 Sama, R. R. K. *et al.* FUS/TLS assembles into stress granules and is a prosurvival factor during hyperosmolar stress. *Journal of Cellular Physiology* **228**, 2222-2231, doi:10.1002/jcp.24395 (2013).

119 Burke, K. A., Janke, A. M., Rhine, C. L. & Fawzi, N. L. Residue-by-Residue View of In Vitro FUS Granules that Bind the C-Terminal Domain of RNA Polymerase II. *Molecular Cell* **60**, 231-241, doi:10.1016/j.molcel.2015.09.006 (2015).

120 Patel, A. *et al.* A Liquid-to-Solid Phase Transition of the ALS Protein FUS Accelerated by Disease Mutation. *Cell* **162**, 1066-1077, doi:10.1016/j.cell.2015.07.047 (2015).

121 Dutertre, M., Lambert, S., Carreira, A., Amor-Guéret, M. & Vagner, S. DNA damage: RNA-binding proteins protect from near and far. *Trends in Biochemical Sciences* **39**, 141-149, doi:10.1016/j.tibs.2014.01.003 (2014).

122 Weissman, J. S. *et al.* Molecular Determinants and Genetic Modifiers of Aggregation and Toxicity for the ALS Disease Protein FUS/TLS. *Plos Biol* **9**, e1000614, doi:10.1371/journal.pbio.1000614 (2011).

123 Sun, Z. H. *et al.* Molecular Determinants and Genetic Modifiers of Aggregation and Toxicity for the ALS Disease Protein FUS/TLS. *Plos Biol* **9**, doi:ARTN e1000614
10.1371/journal.pbio.1000614 (2011).

124 Patel, A. *et al.* A Liquid-to-Solid Phase Transition of the ALS Protein FUS Accelerated by Disease Mutation. *Cell* **162**, 1066-1077 (2015).

125 Kiernan, M. C. *et al.* Amyotrophic lateral sclerosis. *The Lancet* **377**, 942-955, doi:10.1016/S0140-6736(10)61156-7 (2011).

126 Brown, R. H. & Al-Chalabi, A. Amyotrophic Lateral Sclerosis. *New England Journal of Medicine* **377**, 162-172, doi:10.1056/NEJMra1603471 (2017).

127 Talbot, K. Motor neuron disease: the bare essentials. *Practical Neurology* **9**, 303-309, doi:10.1136/jnnp.2009.188151 (2009).

128 Rabinovici, G. & Miller, B. *Frontotemporal lobar degeneration: epidemiology, pathophysiology, diagnosis and management*. Vol. 24 (2010).

129 Lomen-Hoerth, C., Langmore, S., Cotts, M. & Olney, R. K. The overlap of Amyotrophic Lateral Sclerosis and Frontotemporal Lobar Dementia. *Neurology* **58**, A412-A412 (2002).

130 Chio, A. *et al.* A two-stage genome-wide association study of sporadic amyotrophic lateral sclerosis. *Hum Mol Genet* **18**, 1524-1532, doi:10.1093/hmg/ddp059 (2009).

131 Beleza-Meireles, A. & Al-Chalabi, A. Genetic studies of amyotrophic lateral sclerosis: Controversies and perspectives. *Amyotroph Lateral Sc* **10**, 1-14, doi:Pii 907234608
10.1080/17482960802585469 (2009).

132 Kwiatkowski, T. J. & Vanderburg, C. R. Mutations in the FUS/TLS gene on chromosome 16 cause familial amyotrophic lateral sclerosis (vol 323, pg 1205, 2009). *Science* **324**, 465-465 (2009).

133 Shelkovnikova, T. a. Modelling FUSopathies: focus on protein aggregation. *Biochemical Society transactions* **41**, 1613-1617, doi:10.1042/BST20130212 (2013).

134 Snowden, J. S. *et al.* The most common type of FTLD-FUS (aFTLD-U) is associated with a distinct clinical form of frontotemporal dementia but is not related to mutations in the FUS gene. *Acta Neuropathologica* **122**, 99-110, doi:10.1007/s00401-011-0816-0 (2011).

135 Davidson, Y. S. *et al.* Nuclear carrier and RNA-binding proteins in frontotemporal lobar degeneration associated with fused in sarcoma (FUS) pathological changes. *Neuropath Appl Neuro* **39**, 157-165, doi:10.1111/j.1365-2990.2012.01274.x (2013).

136 Neumann, M. *et al.* FET proteins TAF15 and EWS are selective markers that distinguish FTLD with FUS pathology from amyotrophic lateral sclerosis with FUS mutations. *Brain* **134**, 2595-2609, doi:10.1093/brain/awr201 (2011).

137 Brelstaff, J. *et al.* Transportin1: a marker of FTLD-FUS. *Acta Neuropathologica* **122**, 591-600, doi:10.1007/s00401-011-0863-6 (2011).

138 Johnson, B. S. *et al.* TDP-43 Is Intrinsically Aggregation-prone, and Amyotrophic Lateral Sclerosis-linked Mutations Accelerate Aggregation and Increase Toxicity. *Journal of Biological Chemistry* **284**, 20329-20339, doi:10.1074/jbc.M109.010264 (2009).

139 Ayala, Y. M., Misteli, T. & Baralle, F. E. TDP-43 regulates retinoblastoma protein phosphorylation through the repression of cyclin-dependent kinase 6 expression. *Proceedings of the National Academy of Sciences* **105**, 3785-3789, doi:10.1073/pnas.0800546105 (2008).

140 Hicks, G. G. *et al.* Fus deficiency in mice results in defective B-lymphocyte development and activation, high levels of chromosomal instability and perinatal death. *Nature Genetics* **24**, 175-179, doi:10.1038/72842 (2000).

141 Couthouis, J. *et al.* Evaluating the role of the FUS/TLS-related gene EWSR1 in amyotrophic lateral sclerosis. *Hum Mol Genet* **21**, 2899-2911, doi:10.1093/hmg/dds116 (2012).

142 Couthouis, J. *et al.* A yeast functional screen predicts new candidate ALS disease genes. *Proceedings of the National Academy of Sciences of the United States of America* **108**, 20881-20890, doi:10.1073/pnas.1109434108 (2011).

143 Shang, Y. L. & Huang, E. J. Mechanisms of FUS mutations in familial amyotrophic lateral sclerosis. *Brain Res* **1647**, 65-78, doi:10.1016/j.brainres.2016.03.036 (2016).

144 Schägger, H. Tricine–SDS-PAGE. *Nature Protocols* **1**, 16-22, doi:10.1038/nprot.2006.4 (2006).

145 Gasteiger E, H. C. G. A. D. S. W. M. R. A. R. D. B. A. Protein Identification and Analysis Tools on the ExPASy Server. *The Proteomics Protocols Handbook*, 571-607 (2005).

146 Singh, S. M. & Panda, A. K. Solubilization and refolding of bacterial inclusion body proteins. *Journal of Bioscience and Bioengineering* **99**, 303-310, doi:10.1263/jbb.99.303 (2005).

147 Schindelin, J. *et al.* Fiji: an open-source platform for biological-image analysis. *Nature Methods* **9**, 676-682, doi:10.1038/nmeth.2019 (2012).

148 Bornhorst, J. A. & Falke, J. J. Purification of proteins using polyhistidine affinity tags. *Method Enzymol* **326**, 245-254 (2000).

149 Kapust, R. B. & Waugh, D. S. Escherichia coli maltose-binding protein is uncommonly effective at promoting the solubility of polypeptides to which it is fused. *Protein Sci* **8**, 1668-1674, doi:Doi 10.1110/Ps.8.8.1668 (1999).

150 Cummins, P. M., Rochfort, K. D. & O'Connor, B. F. Ion-Exchange Chromatography: Basic Principles and Application. *Methods Mol Biol* **1485**, 209-223, doi:10.1007/978-1-4939-6412-3_11 (2017).

151 Molliex, A. *et al.* Phase Separation by Low Complexity Domains Promotes Stress Granule Assembly and Drives Pathological Fibrillization Article Phase Separation by Low Complexity Domains Promotes Stress Granule Assembly and Drives Pathological Fibrillization. *Cell* **163**, 123-133, doi:10.1016/j.cell.2015.09.015 (2015).

152 Monahan, Z. *et al.* Phosphorylation of the FUS low-complexity domain disrupts phase separation, aggregation, and toxicity. *Embo Journal* **36**, 2951-2967, doi:10.15252/embj.201696394 (2017).

153 Bates, F. S. Polymer-Polymer Phase-Behavior. *Science* **251**, 898-905, doi:DOI 10.1126/science.251.4996.898 (1991).

154 Quiroz, F. G. & Chilkoti, A. Sequence heuristics to encode phase behaviour in intrinsically disordered protein polymers. *Nat Mater* **14**, 1164-+, doi:10.1038/Nmat4418 (2015).

155 Luby-Phelps, K. The physical chemistry of cytoplasm and its influence on cell function: an update. *Mol Biol Cell* **24**, 2593-2596, doi:10.1091/mbc.E12-08-0617 (2013).

156 Clegg, J. S. Properties and metabolism of the aqueous cytoplasm and its boundaries. *American Journal of Physiology-Regulatory, Integrative and Comparative Physiology* **246**, R133-R151, doi:10.1152/ajpregu.1984.246.2.R133 (1984).

157 Zimmerman, S. B. & Trach, S. O. Estimation of macromolecule concentrations and excluded volume effects for the cytoplasm of Escherichia coli. *J Mol Biol* **222**, 599-620 (1991).

158 Cheung, M. C. *et al.* Intracellular protein and nucleic acid measured in eight cell types using deep-ultraviolet mass mapping. *Cytometry Part A* **83A**, 540-551, doi:10.1002/cyto.a.22277 (2013).

159 Ellis, R. J. Macromolecular crowding: obvious but underappreciated. *Trends in Biochemical Sciences* **26**, 597-604, doi:10.1016/s0968-0004(01)01938-7 (2001).

160 Kuznetsova, I., Turoverov, K. & Uversky, V. What Macromolecular Crowding Can Do to a Protein. *International Journal of Molecular Sciences* **15**, 23090-23140, doi:10.3390/ijms151223090 (2014).

161 Kretsinger, R. H., Uversky, V. N. & Permyakov, E. A. *Encyclopedia of Metalloproteins*. 583 (Springer, 2013).

162 Lankalapalli, S. & Kolapalli, V. R. M. Polyelectrolyte complexes: A review of their applicability in drug delivery technology. *Indian J Pharm Sci* **71**, 481-487, doi:Doi 10.4103/0250-474x.58165 (2009).

163 Keating, C. D. Aqueous Phase Separation as a Possible Route to Compartmentalization of Biological Molecules. *Accounts Chem Res* **45**, 2114-2124, doi:10.1021/ar200294y (2012).

164 Derjaguin, B. & Landau, L. Theory of the stability of strongly charged lyophobic sols and of the adhesion of strongly charged particles in solutions of electrolytes. *Progress in Surface Science* **43**, 30-59, doi:10.1016/0079-6816(93)90013-l (1993).

165 Verwey, E. J. W. Theory of the Stability of Lyophobic Colloids. *J Phys Colloid Chem* **51**, 631-636, doi:DOI 10.1021/j150453a001 (1947).

166 Guo, D., Xie, G. X. & Luo, J. B. Mechanical properties of nanoparticles: basics and applications. *J Phys D Appl Phys* **47**, doi:Artn 013001
10.1088/0022-3727/47/1/013001 (2014).

167 Dumetz, A. C., Chockla, A. M., Kaler, E. W. & Lenhoff, A. M. Protein phase behavior in aqueous solutions: Crystallization, liquid-liquid phase separation, gels, and aggregates. *Biophysical Journal* **94**, 570-583, doi:10.1529/biophysj.107.116152 (2008).

168 Zhang, Z. J., Zhao, L., Li, Y. A. & Chu, M. A Modified Method to Calculate Critical Coagulation Concentration Based on DLVO Theory. *Math Probl Eng*, doi:Artn 317483
10.1155/2015/317483 (2015).

169 Po, H. N. & Senozan, N. M. The Henderson-Hasselbalch equation: Its history and limitations. *Journal of Chemical Education* **78**, 1499-1503, doi:DOI 10.1021/ed078p1499 (2001).

170 Bjellqvist, B., Basse, B., Olsen, E. & Celis, J. E. Reference points for comparisons of two-dimensional maps of proteins from different human cell types defined in a pH scale where isoelectric points correlate with polypeptide compositions. *Electrophoresis* **15**, 529-539 (1994).

171 Hofmeister, F. About the science of the effects of salts : About the water withdrawing effect of the salts. *Arch. Exp. Pathol. Pharmacol.* **24**, 247-260 (1888).

172 Zhang, Y. J. & Cremer, P. S. Interactions between macromolecules and ions: the Hofmeister series. *Curr Opin Chem Biol* **10**, 658-663, doi:10.1016/j.cbpa.2006.09.020 (2006).

173 Okur, H. I. *et al.* Beyond the Hofmeister Series: Ion-Specific Effects on Proteins and Their Biological Functions. *The Journal of Physical Chemistry B* **121**, 1997-2014, doi:10.1021/acs.jpcb.6b10797 (2017).

174 Burke, K. A. *et al.* Residue-by-residue view of in vitro FUS granules that bind the C-terminal domain of RNA polymerase II. *Molecular Cell Biology* **60**, 231-241, doi:10.1016/j.molcel.2015.09.006.Residue-by-residue (2016).

175 Roberts, D. *et al.* Specific Ion and Buffer Effects on Protein–Protein Interactions of a Monoclonal Antibody. *Molecular Pharmaceutics* **12**, 179-193, doi:10.1021/mp500533c (2015).

176 Shimizu, S., McLaren, W. M. & Matubayasi, N. The Hofmeister series and protein-salt interactions. *J Chem Phys* **124**, 234905, doi:10.1063/1.2206174 (2006).

177 Curtis, R. A., Montaser, A., Prausnitz, J. M. & Blanch, H. W. Protein-protein and protein-salt interactions in aqueous protein solutions containing concentrated electrolytes. *Biotechnol Bioeng* **58**, 451 (1998).

178 Record, M. T., Jr., Zhang, W. & Anderson, C. F. Analysis of effects of salts and uncharged solutes on protein and nucleic acid equilibria and processes: a practical guide to recognizing and interpreting polyelectrolyte effects, Hofmeister effects, and osmotic effects of salts. *Adv Protein Chem* **51**, 281-353 (1998).

179 Cacace, M. G., Landau, E. M. & Ramsden, J. J. The Hofmeister series: salt and solvent effects on interfacial phenomena. *Q Rev Biophys* **30**, 241-277 (1997).

180 Psychogios, N. *et al.* The human serum metabolome. *PLoS One* **6**, e16957, doi:10.1371/journal.pone.0016957 (2011).

181 Rodwell, V. W. *et al. Harper's illustrated biochemistry*. 416 (McGraw-Hill Education, 2015).

182 Arakawa, T. & Timasheff, S. N. Stabilization of Protein-Structure by Sugars. *Biochemistry* **21**, 6536-6544, doi:DOI 10.1021/bi00268a033 (1982).

183 Arakawa, T. & Timasheff, S. N. Stabilization of protein structure by sugars. *Biochemistry* **21**, 6536-6544 (1982).

184 Timasheff, S. N. The Control of Protein Stability and Association by Weak Interactions with Water: How Do Solvents Affect These Processes? *Annual Review of Biophysics and Biomolecular Structure* **22**, 67-97, doi:10.1146/annurev.bb.22.060193.000435 (1993).

185 Na, G. C., Butz, L. J., Bailey, D. G. & Carroll, R. J. In vitro collagen fibril assembly in glycerol solution: evidence for a helical cooperative mechanism involving microfibrils. *Biochemistry* **25**, 958-966 (1986).

186 Vagenende, V., Yap, M. G. S. & Trout, B. L. Mechanisms of Protein Stabilization and Prevention of Protein Aggregation by Glycerol. *Biochemistry* **48**, 11084-11096, doi:10.1021/bi900649t (2009).

187 Gennaro, R., Pozzan, T. & Romeo, D. Monitoring of cytosolic free Ca2+ in C5a-stimulated neutrophils: loss of receptor-modulated Ca2+ stores and Ca2+ uptake in granule-free cytoplasts. *Proceedings of the National Academy of Sciences of the United States of America* **81**, 1416-1420 (1984).

188 Valko, M., Jomova, K., Rhodes, C. J., Kuča, K. & Musílek, K. Redox- and non-redox-metal-induced formation of free radicals and their role in human disease. *Archives of Toxicology* **90**, 1-37, doi:10.1007/s00204-015-1579-5 (2015).

189 Kröncke, K.-D. & Klotz, L.-O. Zinc Fingers as Biologic Redox Switches? *Antioxidants & Redox Signaling* **11**, 1015-1027, doi:10.1089/ars.2008.2269 (2009).

190 Krezel, A. & Maret, W. Zinc-buffering capacity of a eukaryotic cell at physiological pZn. *J Biol Inorg Chem* **11**, 1049-1062, doi:10.1007/s00775-006-0150-5 (2006).

191 Pace, N. J. & Weerapana, E. Zinc-binding cysteines: diverse functions and structural motifs. *Biomolecules* **4**, 419-434, doi:10.3390/biom4020419 (2014).

192 Coleman, J. E. Zinc Proteins - Enzymes, Storage Proteins, Transcription Factors, and Replication Proteins. *Annual Review of Biochemistry* **61**, 897-946, doi:DOI 10.1146/annurev.bi.61.070192.004341 (1992).

193 Berridge, M. J., Lipp, P. & Bootman, M. D. The versatility and universality of calcium signalling. *Nat Rev Mol Cell Biol* **1**, 11-21, doi:10.1038/35036035 (2000).

194 Braunewell, K.-H. & Gundelfinger, E. D. Intracellular neuronal calcium sensor proteins: a family of EF-hand calcium-binding proteins in search of a function. *Cell and Tissue Research* **295**, 1-12, doi:10.1007/s004410051207 (1999).

195 Ikura, M., Osawa, M. & Ames, J. B. The role of calcium-binding proteins in the control of transcription: structure to function. *BioEssays* **24**, 625-636, doi:10.1002/bies.10105 (2002).

196 Baimbridge, K. G., Celio, M. R. & Rogers, J. H. Calcium-binding proteins in the nervous system. *Trends in Neurosciences* **15**, 303-308, doi:10.1016/0166-2236(92)90081-i (1992).

197 Yáñez, M., Gil-Longo, J. & Campos-Toimil, M. in *Calcium Signaling Advances in Experimental Medicine and Biology* Ch. Chapter 19, 461-482 (2012).

198 Takada, T. *et al.* Effect of pH Values on the Formation and Solubility of Zinc Compounds. *Bulletin of the Institute for Chemical Research, Kyoto University* **56**, 242-246 (1978).

199 Bulaj, G., Kortemme, T. & Goldenberg, D. P. Ionization-reactivity relationships for cysteine thiols in polypeptides. *Biochemistry* **37**, 8965-8972, doi:10.1021/bi973101r (1998).

200 Marino, S. M. & Gladyshev, V. N. Analysis and Functional Prediction of Reactive Cysteine Residues. *Journal of Biological Chemistry* **287**, 4419-4425, doi:10.1074/jbc.R111.275578 (2012).

201 Oteiza, P. I. Zinc and the modulation of redox homeostasis. *Free Radical Bio Med* **53**, 1748-1759, doi:10.1016/j.freeradbiomed.2012.08.568 (2012).

202 Bosco, D. A. *et al.* Mutant FUS proteins that cause amyotrophic lateral sclerosis incorporate into stress granules. *Hum Mol Genet* **19**, 4160-4175, doi:10.1093/hmg/ddq335 (2010).

203 Yin, X. *et al.* Downregulated AEG-1 together with inhibited PI3K/Akt pathway is associated with reduced viability of motor neurons in an ALS model. *Molecular and Cellular Neuroscience* **68**, 303-313, doi:10.1016/j.mcn.2015.08.009 (2015).

204 Kherb, J., Flores, S. C. & Cremer, P. S. Role of Carboxylate Side Chains in the Cation Hofmeister Series. *Journal of Physical Chemistry B* **116**, 7389-7397, doi:10.1021/jp212243c (2012).

205 Carafoli, E. Intracellular Calcium Homeostasis. *Annual Review of Biochemistry* **56**, 395-433, doi:DOI 10.1146/annurev.biochem.56.1.395 (1987).

206 Irving, H. & Williams, R. J. P. The Stability of Transition-Metal Complexes. *J Chem Soc*, 3192-3210, doi:DOI 10.1039/jr9530003192 (1953).

207 Mattson, M. P. Neurotransmitters in the Regulation of Neuronal Cytoarchitecture. *Brain Res Rev* **13**, 179-212, doi:Doi 10.1016/0165-0173(88)90020-3 (1988).

208 Marambaud, P., Dreses-Werringloer, U. & Vingtdeux, V. Calcium signaling in neurodegeneration. *Molecular Neurodegeneration* **4**, doi:Artn 20

10.1186/1750-1326-4-20 (2009).

209 Tradewell, M. L., Cooper, L. A., Minotti, S. & Durham, H. D. Calcium dysregulation, mitochondrial pathology and protein aggregation in a culture model of amyotrophic lateral sclerosis: Mechanistic relationship and differential sensitivity to intervention. *Neurobiol Dis* **42**, 265-275, doi:10.1016/j.nbd.2011.01.016 (2011).

210 Clark, V. L., Peterson, D. E. & Bernlohr, R. W. Changes in Free Amino Acid Production and Intracellular Amino Acid Pools of Bacillus licheniformis as a Function of Culture Age and Growth Media. *Journal of Bacteriology* **112**, 715-725 (1972).

211 Scimemi, A. & Beato, M. Determining the Neurotransmitter Concentration Profile at Active Synapses. *Molecular Neurobiology* **40**, 289-306, doi:10.1007/s12035-009-8087-7 (2009).

212 Bergström, J., Fürst, P., Norée, L. O. & Vinnars, E. Intracellular free amino acid concentration in human muscle tissue. *Journal of Applied Physiology* **36**, 693-697, doi:10.1152/jappl.1974.36.6.693 (1974).

213 Erecinska, M. & Silver, I. A. Metabolism and role of glutamate in mammalian brain. *Prog Neurobiol* **35**, 245-296 (1990).

214 Arakawa, T. & Timasheff, S. N. The mechanism of action of Na glutamate, lysine HCl, and piperazine-N,N'-bis(2-ethanesulfonic acid) in the stabilization of tubulin and microtubule formation. *J Biol Chem* **259**, 4979-4986 (1984).

215 Wilson, L. & Meza, I. The mechanism of action of colchicine. Colchicine binding properties of sea urchin sperm tail outer doublet tubulin. *J Cell Biol* **58**, 709-719 (1973).

216 Bosshard, H. R., Marti, D. N. & Jelesarov, I. Protein stabilization by salt bridges: Concepts, experimental approaches and clarification of some misunderstandings. *Journal of Molecular Recognition* **17**, 1-16, doi:10.1002/jmr.657 (2004).

217 Foran, E. & Trotti, D. Glutamate Transporters and the Excitotoxic Path to Motor Neuron Degeneration in Amyotrophic Lateral Sclerosis. *Antioxidants & Redox Signaling* **11**, 1587-U1586, doi:10.1089/ars.2009.2444 (2009).

218 Saha, S. *et al.* Polar Positioning of Phase-Separated Liquid Compartments in Cells Regulated by an mRNA Competition Mechanism. *Cell* **166**, 1572-+, doi:10.1016/j.cell.2016.08.006 (2016).

219 Maharana, S. *et al.* RNA buffers the phase separation behavior of prion-like RNA binding proteins. *Science*, eaar7366-eaar7366, doi:10.1126/science.aar7366 (2018).

220 Harvey Lodish, A. B., Paul Matsudaria, Chris A. Kaiser, Monty Krierger, Matthew P. Scott, Lawrence Zipursky, James Darnell. *Molecular Cell Biology*. 5th edn, 278 (2003).

221 Re, A., Joshi, T., Kulberkyte, E., Morris, Q. & Workman, C. T. in *RNA Sequence, Structure, and Function: Computational and Bioinformatic Methods Methods in Molecular Biology* Ch. Chapter 23, 491-521 (2014).

222 Jones, S., Daley, D. T. A., Luscombe, N. M., Berman, H. M. & Thornton, J. M. Protein–RNA interactions: a structural analysis. *Nucleic Acids Research* **29**, 943-954 (2001).

223 Chong, P. A., Vernon, R. M. & Forman-Kay, J. D. RGG/RG Motif Regions in RNA Binding and Phase Separation. *J Mol Biol*, doi:10.1016/j.jmb.2018.06.014 (2018).

224 Hall, T. M. T. Multiple modes of RNA recognition by zinc finger proteins. *Current Opinion in Structural Biology* **15**, 367-373, doi:10.1016/j.sbi.2005.04.004 (2005).

225 Roux, D. C. & Cooper-White, J. J. Dynamics of water spreading on a glass surface. *J Colloid Interface Sci* **277**, 424-436, doi:10.1016/j.jcis.2004.05.007 (2004).

226 Bertini, I., McGreevy, K. S. & Parigi, G. *NMR of Biomolecules: Towards Mechanistic Systems Biology*. 1st edn, (Wiley-Blackwell, 2011).

227 Felli, I. C. & Pierattelli, R. *Intrinsically Disordered Proteins Studied by NMR Spectroscopy*. (2015).

228 Felli, I. C. & Pierattelli, R. Novel methods based on 13C detection to study intrinsically disordered proteins. *Journal of Magnetic Resonance* **241**, 115-125, doi:10.1016/j.jmr.2013.10.020 (2014).

229 Baxter, N. J. & Williamson, M. P. Temperature dependence of 1H chemical shifts in proteins. *Journal of Biomolecular NMR* **9**, 359-369, doi:10.1023/a:1018334207887 (1997).

230 Okazaki, H. *et al.* Using 1HN amide temperature coefficients to define intrinsically disordered regions: An alternative NMR method. *Protein Sci*, doi:10.1002/pro.3485 (2018).

231 Ringe, D. & Petsko, G. A. Study of protein dynamics by X-ray diffraction. *Methods Enzymol* **131**, 389-433 (1986).

232 Privalov, P. L. Cold Denaturation of Proteins. *Crit Rev Biochem Mol* **25**, 281-305, doi:Doi 10.3109/10409239009090612 (1990).

233 Dias, C. L. *et al.* The hydrophobic effect and its role in cold denaturation. *Cryobiology* **60**, 91-99, doi:10.1016/j.cryobiol.2009.07.005 (2010).

234 Tsai, C. J., Maizel, J. V., Jr. & Nussinov, R. The hydrophobic effect: a new insight from cold denaturation and a two-state water structure. *Crit Rev Biochem Mol Biol* **37**, 55-69, doi:10.1080/10409230290771456 (2002).

235 Dyson, H. J., Wright, P. E. & Scheraga, H. A. The role of hydrophobic interactions in initiation and propagation of protein folding. *Proc Natl Acad Sci U S A* **103**, 13057-13061, doi:10.1073/pnas.0605504103 (2006).

236 Cavanagh, J. *Protein NMR spectroscopy : principles and practice*. 2nd edn, (Academic Press, 2007).

6. APPENDIX

“The truth of the story lies in the details”

P. Auster

6. Appendix

6.1 Supplementary materials and methods

Table A. I – Composition of a discontinuous 10% Tris-SDS-PAGE gel (quantity for one gel)

Reagents	Separating gel (10%)	Stacking gel (10%)
Water (mL)	1.75	1.95
3 M Tris-HCl/SDS pH 8.45 (mL)	2.50	0.77
30% acrylamide (µL)	2.50	0.40
Glycerol (µL)	750	-
10% APS (µL)	21	21
TEMED (µL)	7	7

APS – Ammonium persulfate (*NZYTech)*
TEMED – Tetramethylethylenediamine (*Riedel-de-Haën)*
Acrylamide (*Fluka)*

Table A. II – Composition of the Tris-tricine buffer for Tris-SDS-PAGE (per liter)

Reagents	Running buffer 10X (pH 8.3)	Anode buffer 10X (pH 8.8)
Tris-Base (g)	121.10	242
Tricine (g)	179.20	-
20% SDS (mL)	50	-
Water	until 1 L	until 1 L

Tricine (*Amresco*)
Dilution to 1X before use

Table A. III – Composition of the sample buffer for Tris-SDS-PAGE (per 50 mL)

Reagents	Sample buffer 4X
1 M Tris-HCl pH 6.8 (mL)	10 mL
Glycerol (mL)	24 mL
SDS (g)	8
DTT (g)	3.10
Coomassie Blue R250 (mg)	20
Water	until 50 mL

Coomassie Brilliant Blue R250 (*Panreac*)

Table A. IV – Staining and destaining solutions for visualization of protein bands in SDS-PAGE gels

Reagents	Staining solution	Destaining solution
Coomassie Blue R250 (% v/v)	0.1	-
Methanol (% v/v)	50	40
Glacial acetic acid (% v/v)	10	10

Methanol (*Sigma-Aldrich*)
Glacial acetic acid (*Panreac*)

6.2 Supplementary production of FUS protein

Table A. V – Molecular weight and extinction coefficient values of non-labeled and ^{15}N-labeled MBP-FUS and FUS

Protein	Molecular weight (kDa)	Extinction coefficient (M^{-1}/cm^{-1})
MBP-FUS	98.10	139720
^{15}N MBP-FUS	99.35	
FUS	53.42	70390
^{15}N FUS	54.15	

6.2.1 General Expression

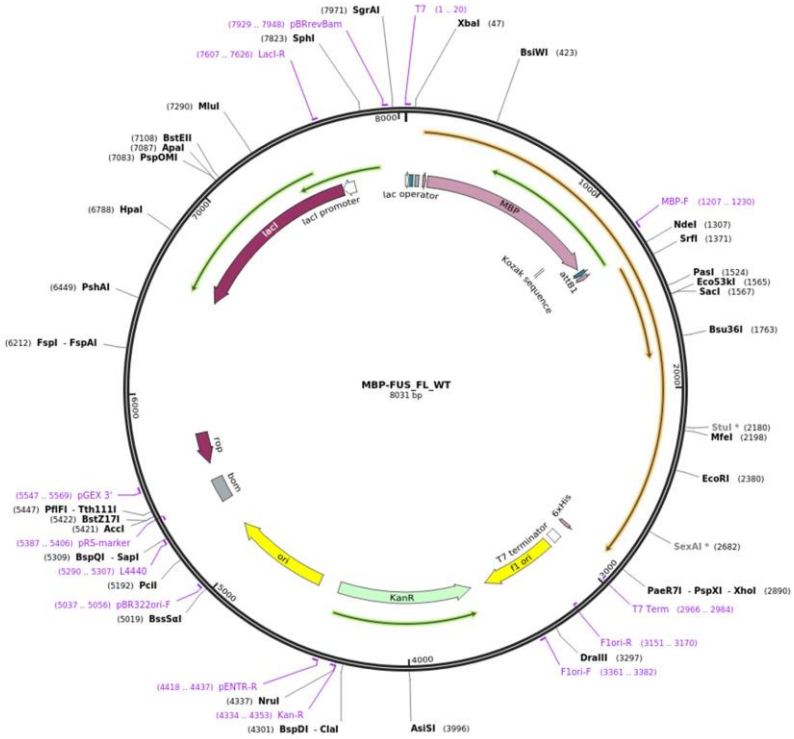

Figure A. 1 – Map of the MBP-FUS-FL-WT plasmid – Plasmid constructed to express full-length human WT-FUS including a His_6-MBP moiety and a TEV cleavage site (Addgene #98651).

Table A. VI – Composition of LB medium (per liter)

Reagents	LB medium
NaCl (g)	10
Tryptone (g)	10
Yeast extract (g)	5
Water	until 1L

Tryptone (*NZYTech*)
Yeast extract (*Cultimed*)
Autoclave before use.

Table A. VII – Composition of LB-agar

Reagents	LB-Agar
LB medium (mL)	100
Bacteriological agar (g)	1.50

Bacteriological agar (*NZYTech*)
Autoclave before use.
Cool until 55ºC before adding antibiotic.
Pour into Petri dishes (25 mL/100 mm)

Table A. VIII – Composition of M9 salts (per liter)

Reagents	M9 salts
$Na_2HPO_4.7H_2O$ (g)	70
KH_2PO_4 (g)	30
NaCl (g)	5
Water	until 1 L

KH_2PO_4 (*Panreac*)
Autoclave before use

Table A. IX – Composition of M9 minimal medium (per liter)

Reagents	M9 medium
M9 salts (autoclaved)	100 mL
2 M $MgSO_4$ (mL)	1
100 mM $CaCl_2$ (mL)	1
100 mM $FeSO_4$ (mL)	1
Thiamine-HCl (mg)	10
Glucose (g)	1
$^{15}NH_4Cl$ (g)	2
MEM vitamins (mL)	2.50
Water (autoclaved):	until 900 mL

$MgSO_4$ (*Panreac*)
$CaCl_2$ (*Merck*)
$FeSO_4$ (*Panreac*)
Thiamine-HCl (*Sigma-Aldrich*)
$^{15}NH_4Cl$ (*Cambridge Isotope Laboratories*)
MEM vitamins (*Sigma-Aldrich*)

6.2.2 Purification non-labeled FUS

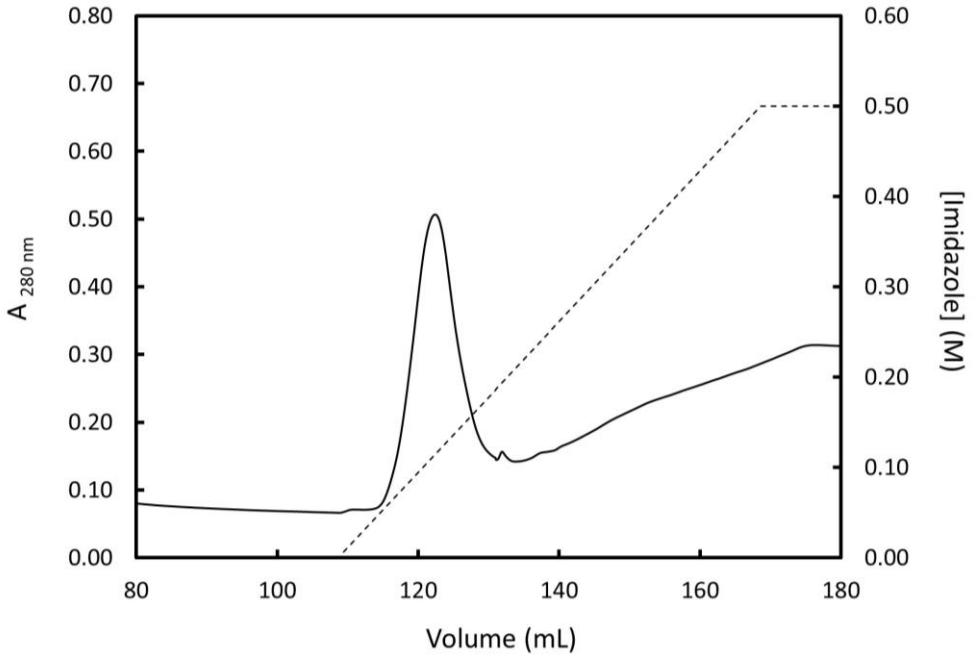

Figure A. 2 - First purification step of non-labeled FUS by Ni-NTA affinity chromatography – Elution profile for the first IMAC purification step of non-labeled FUS. Column equilibrated with 20 mM sodium phosphate buffer, 40 mM imidazole, 300 mM NaCl, 10% glycerol, 5 mM βME, 2 mM benzamidine and 2 protease inhibitor tablets, at pH 7.50. Primary and secondary y-axis correspond the to a variation in absorbance at 280 nm (solid line) and the imidazole gradient (dashed line), respectively. Protein eluted at 150 mM imidazole and fraction collected between 115 mL and 131 mL.

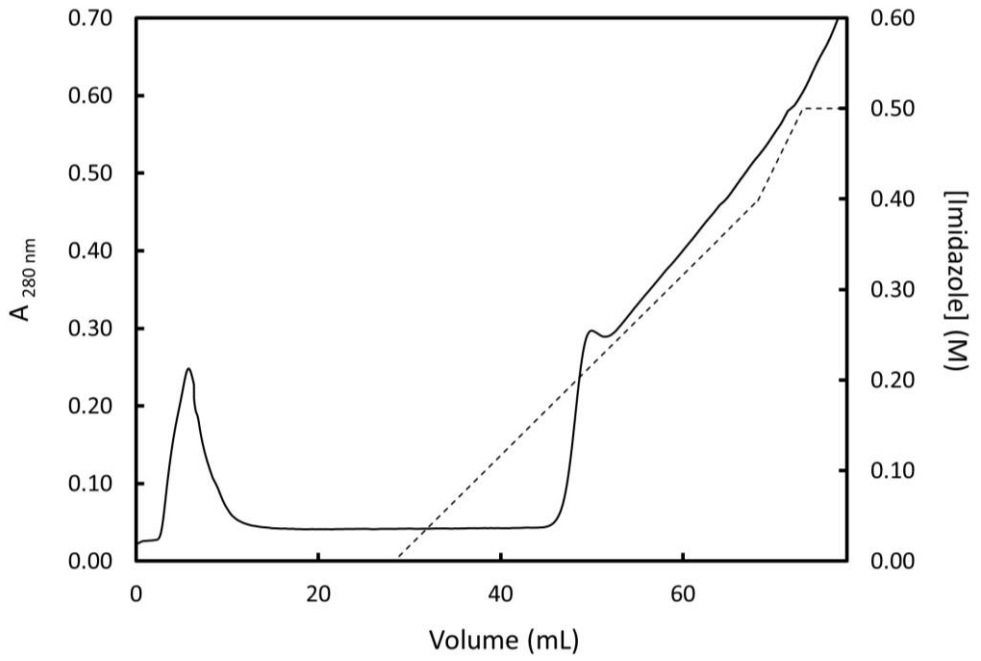

Figure A. 3 – Second purification step of non-labeled FUS by Ni-NTA affinity chromatography – Elution profile for the second IMAC purification step of non-labeled FUS. Column equilibrated with 20 mM sodium phosphate buffer, 40 mM imidazole, 300 mM NaCl, 10% glycerol, 5 mM βME, 2 mM benzamidine and 2 protease inhibitor tablets, at pH 7.50. Primary and secondary y-axis correspond to the variation in absorbance at 280 nm (solid line) and the imidazole gradient (dashed line), respectively. Protein eluted in the flow-through corresponding to the first peak in absorbance. Protein fraction collected between 2 mL and 12 mL. His_6-MBP moiety eluted at 240 mM imidazole.

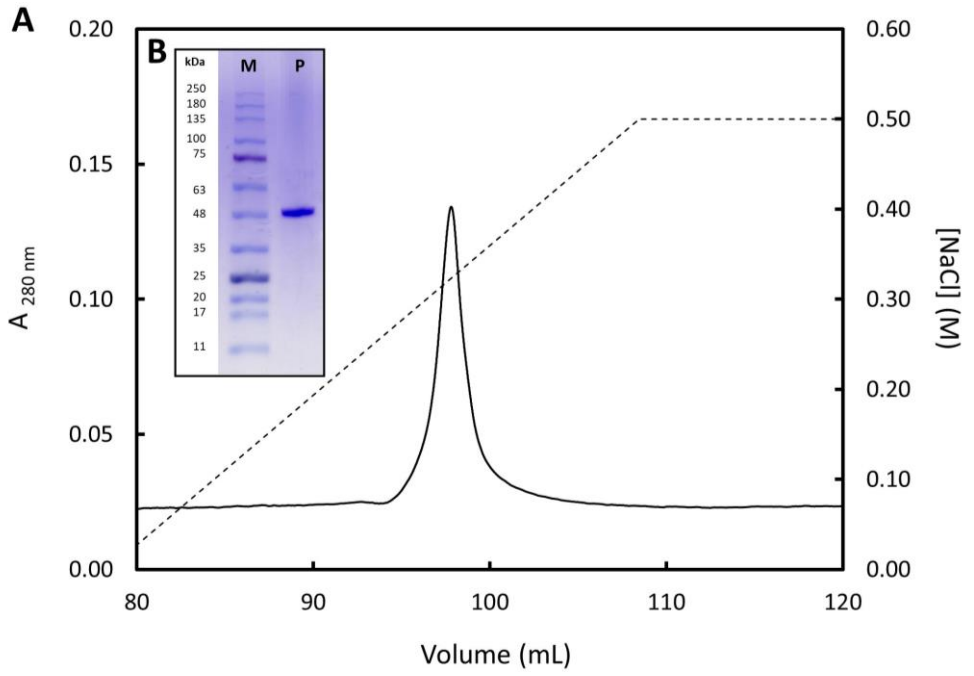

Figure A. 4 – Final purification step of non-labeled FUS by ion exchange chromatography – (A) Elution profile for the third and final IEX purification step of non-labeled FUS. Column equilibrated with 20 mM Tris-HCl, 10% glycerol and 5 mM βME, at pH 8.00. Primary and secondary y-axis correspond to the variation in absorbance at 280 nm (solid line) and the NaCl gradient (dashed line), respectively. Protein eluted at 320 mM NaCl and fraction collected between 95 mL and 103 mL. **(B)** Inset of the purity analysis by SDS-PAGE. Lane: M – Prestained protein marker, P – FUS after ion exchange chromatography. Corresponding MW of the protein marker on the left.